(2)

SCIENTIFIC FINAL REPORT ON

AIR FORCE OFFICE OF SCIENTIFIC RESEARCH

GRANT AFSOR-88-0127

(FEB.1, 1988 - JAN.31, 1991)

The Role of Hydromagnetic Waves in the Magnetosphere and the Ionosphere

S. P. Kuo

Principle Investigator

M. H. Whang

J. Huang

REPORT DOCUMENTATION PAGE

Form Approved
OMB No. 0704-0188

1. AGENCY USE ONLY (Leave blank)	2. REPORT DATE	3. REPORT TYPE AND DATES COVERED
		FINAL 01 Feb 88 TO 31 Jan 91

4. TITLE AND SUBTITLE
THE ROLE OF HYDROMAGNETIC WAVES IN THE MAGNETOSPHERE AND THE IONOSPHERE

5. FUNDING NUMBERS
G AFOSR-88-0127
PE 61102F
PR 2311
TA A1

6. AUTHOR(S)
Dr Specncer Kuo

7. PERFORMING ORGANIZATION NAME(S) AND ADDRESS(ES)
Polytechnic University
Dept of Electrical Engineering
and Computer Science
333 Jay Street
Brooklyn, NY 11201

8. PERFORMING ORGANIZATION REPORT NUMBER
AFOSR-TR- 92 0199

9. SPONSORING/MONITORING AGENCY NAME(S) AND ADDRESS(ES)
Dr Henry Radoski
AFOSR/NL
Building 410
Bolling AFB DC 20332-6448

10. SPONSORING/MONITORING AGENCY REPORT NUMBER

11. SUPPLEMENTARY NOTES

12a. DISTRIBUTION/AVAILABILITY STATEMENT
Approved for public release; distribution unlimited.

12b. DISTRIBUTION CODE

13. ABSTRACT (Maximum 200 words)
Four research areas were investigated: 1. the propagation and coupling of hydromagnetic waves in the magnetospere. The coupled hydromagnetic equations in the dipole model of the magnetosphere were solved numerically. A reconstruction of the long period waves in an actual geomagnetic storm was demonstrated. 2. non-linear wave-particle interactions in the magnetosphere. Anomalous cross-field diffusion of trapped energetic protons may result in proton precipitation in the equatorial region; 3 the filamentation instability of large amplitude hydromagnetic waves in the solar wind plasma. This work is relevant to observations of Alven waves and magnetosonic waves in space plasmas; 4. parametric excitation of whistler waves in the high latitude ionoosphere by a high frequency heater transmitting from the ground. It has been shown that whisler waves and Langmuir waves can be excited by ionospheric heaters. The instability which produces these waves offers a potential mechanism to generate large amplitude long period waves in the ionosphere.

14. SUBJECT TERMS			15. NUMBER OF PAGES
			16. PRICE CODE
17. SECURITY CLASSIFICATION OF REPORT (U)	18. SECURITY CLASSIFICATION OF THIS PAGE (U)	19. SECURITY CLASSIFICATION OF ABSTRACT (U)	20. LIMITATION OF ABSTRACT (U)

I. Introduction

This report only discusses work that has been carried out during the funding period from Feb.1, 1990 to Jan.31, 1991 supported under Grant No. AFOSR-88-0127. This grant has been awarded to the Polytechnic University since Feb.1,1988. The work accomplished during the early funding period has already been reported in the previous two years' progress reports.

The investigation covered by the Grant deals with the physical phenomena associated with waves in the plasmas of the ionosphere, magnetosphere, and solar wind. The focus of the study is to explore the role of the coupled hydromagnetic waves in the geomagnetic substorms of the magnetosphere.

During the past year, our work has achieved many interesting results, which have all been accepted for publication. Basically, the topics of investigation are divided into four general categories: (a) propagation and coupling of hydromagnetic waves in the magnetosphere. In this study, coupled hydromagnetic equations in the dipole model of the magnetosphere are solved numerically. As an example and practical application of this study, a reconstruction of the storm time Pc 5 waves of November 14-15, 1979 by our numerical solution is demonstrated; (b) nonlinear wave-particle interaction in the magnetosphere. Energetic protons in the radiation belts are trapped by the earth's dipole magnetic field. In the presence of large amplitude kinetic Alven waves, the trajectory of these protons may become chaotic and anomalous cross-field diffusion of protons may result as manifested by the proton precipitation in the equatorial region; (c) filamentation instability of large amplitude hydromagnetic waves in the solar wind plasma. Large-amplitude Alven waves and magnetosonic waves are frequently observed in the high speed streams of the solar wind. Their stability against a convective filamentation instability are investigated thoroughly. The relevance of the study with some observations in the space plasmas is also discussed; and (d) parametric excitation of whistler waves in high latitude ionosphere by the HF heater transmitted from the ground. Our study shows that whistler waves (VLF waves) together with Langmuir waves can be excited parametrically by the EISCAT's HF heater. The proposed instability process is a potential mechanism to generate strong artificial PC waves in the ionosphere.

Through the support of this grant, one graduate student has completed the requirements of the degree in August 1989. His Ph.D dissertation was included in the last year's progress report. A new graduate student Joe Huang had been recruited to continue the research work during the past one and half funding years.

II. Publications

The following publications include work supported by the present Grant, which was duly acknowledged:

1. S.P. Kuo, M.H. Whang and M.C. Lee, "Filamentation Instability of Large-Amplitude Alven Waves", J. Geophys. Res., 93(A9), 9621-9627, 1988.

2. M.C. Lee, K.M. Groves, C.P. Liao, D.R. Rivas and S.P. Kuo, "Combined Operation of Two Ground Transmitters for Enhanced Ionospheric Heating", J. Geomag. Geoelectr., 40, 1141-1145,1988.

3. K.M. Groves, M.C. Lee and S.P. Kuo, "Spectral Broadening of VLF Radio Signals Traversing the Ionosphere", J. Geophys. Res., 93(A12), 14683-14687, 1988.

4. S.P. Kuo, M.H. Whang and G. Schmidt, "Convective Filamentation Instability of Circularly Polarized Alven Wave", Phys. Fluids B, 32(4), 734-740, 1989.

5. S.P. Kuo and M.C. Lee, "Filamentation Instability of Magnetosonic Waves in the Solar Wind Environment", J. Geophys. Res., 94(A10), 13387-13395, 1989.

6. M.H. Whang and S.P. Kuo, "Coupling of Hydromagnetic Waves in the Dipole Model of the Magnetosphere", EOS, 69(16), 424, 1988.

7. S.P. Kuo and M.H. Whang, "Filamentation Instability of Large-Amplitude Alven Waves", EOS, 69(16), 459, 1988.

8. S.P. Kuo and M.C. Lee, "Parametric excitation of Whistler Waves by HF Heater", JATP, 51, 727-731, 1989.

9. M.H. Whang , "On the Coupling of Hydromagnetic Waves in the Magnetosphere", Ph.D. thesis, Polytechnic University.

10. S.P. Kuo and M.C. Lee, "Nonlinear Wave-Particle Interaction in the Magnetosphere", IV Int'l. Workshop on Nonlinear and Turbulent Processes in Physics, Kiev, USSR, Oct. 9-22, 1989; Nonlinear World, Vol. 2, 124-127,1989.

11. S.P. Kuo and M.H. Whang, "Convective Filamentation Instability of Compressional Alven Wave", EOS, 70(15),453,1989.

12. M.H. Whang and S.P. Kuo, "On the Coupling of Hydromagnetic Waves in the Magnetosphere", EOS, 70(15), 453,1989.

13. S.P. Kuo, A.Y. Ho and M.H. Whang, "Filamentation Instability of MHD Waves in Solar Wind Plasma ", EOS, 70(15),453,1989.

14. M.H. Whang and S.P. Kuo, "Numerical Analysis of Coupled Hydromagnetic Waves in Dipole Magnetic Field: A Reconstruction of the Storm time PC5 waves of November 14-15, 1989", EOS, 70(43), 1292, 1989.

15. S.P. Kuo, A.Y. Ho and M.C. Lee,"Temporal Evolution of HF-enhanced Plasma Lines", Geophys. Res. Lett., 17(12), 2209-2212, 1990.

16. S.P. Kuo, A.Y. Ho M.C. Lee and F.T. Djuth, "Temporal Evolution of HF-enhanced Plasma Lines", NATO AGARD Conf. Proc., No. 485,11B-1-11B-9, 1990.

17. M.C. Lee, W. J. Burke, H.C. Carlson, J. L. Heckscher, P. A. Kossey, E. J. Weber, and S. P. Kuo, "Planning for Coordinated Space and Ground-Based Ionospheric Modification Experiments", NATO AGARD Conf. Proc., No. 485, 25-1-25-8, 1990.

18. M.H. Whang S.P. Kuo and M.C. Lee, "Reconstruction of Global Micropulsations in the Magnetosphere", J. Plasma Phys., 45, 159-172, 1991.

III. Appendix

Reprints attached to this report include:

1. Filamentation Instability of Large-Amplitude Alven Waves.
2. Combined Operation of Two Ground Transmitters for Enhanced Ionospheric Heating.
3. Spectral Broadening of VLF Radio Signals Traversing the Ionosphere.
4. Convective Filamentation Instability of Circularly Polarized Alven Wave.
5. Filamentation Instability of Magnetosonic Waves in the Solar Wind Environment.
6. Parametric excitation of Whistler Waves by HF Heater.
7. Nonlinear Wave-Particle Interaction in the Magnetosphere.
8. Temporal Evolution of HF-enhanced Plasma Lines.
9. Reconstruction of Global Micropulsations in the Magnetosphere.

JOURNAL OF GEOPHYSICAL RESEARCH, VOL. 93, NO. A9, PAGES 9621-9627, SEPTEMBER 1, 1988

FILAMENTATION INSTABILITY OF LARGE-AMPLITUDE ALFVÉN WAVES

S. P. Kuo and M. H. Whang

Weber Research Institute, Polytechnic University, Farmingdale, New York

M. C. Lee

Massachusetts Institute of Technology, Cambridge

Abstract. An instability that leads to the filamentation of large-amplitude Alfvén waves and gives rise to purely growing density and magnetic field fluctuations is studied. The dispersion relation of the instability is derived, from which the threshold conditions and the growth rates of the instability are analyzed quantitatively for applications to the solar wind plasma. We have examined their dependence on the filamentation spectrum, the plasma β, and the pump frequency and intensity for both right-hand and left-hand circularly polarized Alfvén waves. The excitation of filamentation instability for certain cases of interest is discussed and compared with that of the parametric decay and modulation instability. The relevance of the proposed instability with some observations is discussed.

1. Introduction

A great deal of interest in the stability of the MHD system in the presence of finite amplitude Alfvén waves has arisen in recent years [Wong and Goldstein, 1986; Terasawa et al., 1986; Longtin and Sonnerup, 1986]. It is mainly stimulated by the frequent observations of large-amplitude hydromagnetic fluctuations in the solar wind at 1 AU [Belcher and Davis, 1971], in the high-speed streams of the solar wind [Abraham-Shrauner and Feldman, 1977], in the upstream Jovian bow shock [Goldstein et al., 1985], and in the interplanetary shocks and the terrestrial foreshock [Vinas et al., 1984; Smith et al., 1985]. These fluctuations are generally believed to be circularly polarized Alfvén waves propagating almost exactly field aligned. A class of parametric instabilities excited by the circularly polarized Alfvén pumps has thus been investigated. Two different instability processes are currently discussed in the literature. One leads to the parametric decay instability [Galeev and Oraevskii, 1963; Sagdeev and Galeev, 1969; Cohen and Dewar, 1974; Terasawa et al., 1986], and the other one gives rise to the modulation instability [Lashmore-Davies, 1976; Ionson and Ong, 1976; Goldstein, 1978; Derby, 1978; Longtin and Sonnerup, 1986]. Moreover, the modulation instability has also been analyzed in the region that describes the nonlinear evolution of the Alfvén waves propagating along a static magnetic field [Mio et al. 1976a, b; Mjølhus, 1976; Spangler and Sheerin, 1983]. A derivative nonlinear Schrodinger equation possessing soliton solutions is derived to govern the evolution of nonlinear Alfven waves. On the contrary, Ovenden et al. [1983] have shown that the evolution of nonlinear Alfven waves is governed by a set of three coupled equations which in turn are related to the nonlinear Schrodinger equation with known soliton solutions. The possible applications of Alfvén solitons to solar and astrophysical plasmas have been discussed by Ovenden et al. [1983] and Spangler and Sheerin [1983].

Sakai and Sonnerup [1983] investigated the effects of dispersion on the modulation instability excited by the circularly polarized Alfvén waves. Their analysis is restricted to the situations in which dispersive effects are weak and the wave number k of the sound wave is much smaller than the wave number k_o of the pump wave ($k \ll k_o$). These restrictions have been lifted in the more recent work by Wong and Goldstein [1986]. They study the dispersive effects on both the modulation and the decay instabilities in a unified manner over a wide range of physical parameters. In addition, the results show that the maximum growth rate of the modulation instability occurs as k is comparable to k_o. A new but weaker instability existing in a very narrow bandwidth near $k \approx k_o$ has also been revealed by their analysis.

In this paper, a filamentation instability which has not been considered by the previous workers is analyzed. It is known that a large-amplitude, initially uniform wave propagating in a plasma can break up into filaments because of the filamentation instability [Schmidt, 1979; Kuo and Schmidt; 1983]. This starts from small perturbations in the plasma density, and it results in a modulation of the plasma dielectric constant and wave distribution, which in turn increases the density perturbations. The purpose of the present paper is to show that the filamentation instability can be excited together with the parametric decay and modulation instabilities by the large-amplitude circularly polarized Alfvén waves in the solar wind. The threshold conditions and the growth rates of the instability will be determined and compared with those of the decay instability and the modulation instability. Some observations will be discussed for corroborating the predicted characteristic of the proposed instability.

The organization of the paper is as follows. In section 2 we derive the coupling equations for Alfvén sidebands and the purely growing magnetostatic mode. A dispersion relation is obtained in section 3 and analyzed for the threshold fields and the growth rates for various cases. The numerical results are also given in section 3. Finally presented in section 4 are a summary and brief discussion.

2. Coupling Equations

We investigate the propagation and filamentation of ducted, large-amplitude, circularly polarized Alfven waves in infinite, spatially uniform plasmas embedded in a constant magnetic field $\vec{B}_o = \hat{z}B_o$. The wave magnetic fields are represented by

$$\vec{B}_{p\pm} = (\hat{x} \pm i\hat{y})B_p e^{i(k_o z - \omega_o t)} + \text{c.c.} \qquad (1)$$

Paper number 8A9497.
0148-0227/88/008A-9497$05.00

where B_p is the unperturbed wave field intensity, assumed to be constant and a real quantity for simplicity; the plus and minus signs refer to the right- and left-hand circular polarizations, respectively; k_o and ω_o are the wave number and angular wave frequency, satisfying the dispersion relation $\omega_o^2 = (1+-\omega_o/\Omega_i)k_o^2 v_A^2$ wherein v_A and Ω_i are the Alfvén speed and the ion cyclotron frequency, respectively.

The zeroth-order velocity responses of electrons and ions to the Alfvén waves can be written as

$$\vec{v}_{pe\pm} = (1\pm\omega_0/\Omega_i)\vec{v}_{pi\pm} = -(\hat{x}\pm\hat{y})(\omega_0/k_0)(B_p/B_0)e^{i(k_0 z-\omega_0 t)} + \text{c.c.} \quad (2)$$

where the subscripts e and i refer to electrons and ions.

The process under consideration is the scattering of the unperturbed Alfvén waves into sidebands (propagating oblique to the z direction) by the simultaneously excited density perturbations associated with the purely growing magnetostatic modes. Let $\vec{k} = \hat{x}k$ be the filamentation wave vector, the density and magnetic field perturbations of the purely growing magentostatic modes have the expression

$$n_s = \tilde{n}_s e^{\gamma t}\cos kx \quad \text{and} \quad \vec{B}_s = \hat{z}\tilde{B}_s e^{\gamma t}\cos kx$$

where $\tilde{n}_s$ and $\tilde{B}_s$ are real amplitudes and γ is the growth rate; quasi-neutrality has been assumed. The basic equations that are linearized for analyzing the purely growing modes include the continuity equations, the momentum equations for both electrons and ions, and the Maxwell equations:

$$\gamma n_s + n_0\frac{\partial v_{sex}}{\partial x} = 0 = \gamma n_s + n_0\frac{\partial v_{six}}{\partial x} \quad (3)$$

$$\gamma m\vec{v}_{se} + \vec{F}_e = -\hat{x}(T_e/n_0)\frac{\partial n_s}{\partial x} - e(\vec{E}_s + \frac{1}{c}\vec{v}_{se}\times\hat{z}B_0)$$

and

$$\gamma M\vec{v}_{si} + \vec{F}_i = -\hat{x}(T_i/n_0)\frac{\partial n_s}{\partial x} + e(\vec{E}_s + \frac{1}{c}\vec{v}_{si}\times\hat{z}B_0) \quad (4)$$

$$\frac{\partial E_{sy}}{\partial x} = -(\gamma/c)B_s$$

and

$$\frac{\partial B_s}{\partial x} = (4\pi n_0 e/c)(v_{sey}-v_{siy}) \quad (5)$$

where n_o, T_{ej}, and m(M) are the unperturbed plasma density and the unperturbed electron (ion) temperature and mass, respectively; the $\vec{F}_{ej}$ are the nonlinear Lorentz forces experienced by electrons and ions that reduce to the ponderomotive forces in the unmagnetized plasma case. In terms of $\vec{v}_{pej\pm}$ and $\delta\vec{v}_{ej\pm}$ that represent the velocity responses of electrons and ions to the unperturbed Alfvén waves and the sidebands, respectively, the nonlinear Lorentz forces are given by [Kuo and Lee, 1983]

$$\vec{F}_{ej}/m_{ej} = \nabla(\vec{v}_{pej\pm}\cdot\delta\vec{v}^{*}_{ej\pm}) + i\epsilon_{ej}(\Omega_{ej}/\omega_0)\cdot(\delta\vec{v}^{*}_{ej\pm}\times[\nabla\times(\vec{v}_{pej\pm}\times\hat{z})] - \vec{v}_{pej\pm}\times[\nabla\times(\delta\vec{v}^{*}_{ej\pm}\times\hat{z})]) + \text{c.c.} \quad (6)$$

where the notations m_{ej}=m(M) and ϵ_{ej}=±1 are used. One can show in a self-consistent way that the nonlinear Lorentz forces act only in the x direction, i.e., $\vec{F}_{ej} = \hat{x}F_{ej}$.

We now substitute the expressions

$$\vec{v}_{sej} = (\hat{x}\tilde{v}_{sejx} + \hat{y}\tilde{v}_{sejy})e^{\gamma t}\sin kx$$

$$\tilde{v}_{sex} = \tilde{v}_{six} = \tilde{v}_{sx}$$

$$\vec{E}_s = \hat{y}\tilde{E}_{sy}e^{\gamma t}\sin kx$$

and $\vec{F}_{ej} = \hat{x}\tilde{F}_{ej}e^{\gamma t}\sin kx$

into (3)-(5). The relation

$$\tilde{B}_s/B_0 = [\omega_{pe}^2/(\omega_{pe}^2 + k^2c^2)]\tilde{n}_s/n_0$$

is obtained, and the resultant equation can be combined into a single coupled mode equation for the purely growing magnetostatic mode:

$$\{\gamma^2 + [k^2v_A^2/(1 + k^2v_A^2/\Omega_i\Omega_e)] + k^2c_s^2\}\tilde{n}_s/n_0 = (1/M)(\tilde{F}_e + \tilde{F}_i) \quad (7)$$

This equation gives the purely growing density perturbation as a function of the Alfvén waves and sidebands. Without the nonlinear Lorentz forces, (6) reduces to the linear dispersion relation of the magnetosonic eigenmode. The magnetostatic mode is, however, a nonlinearly driven mode.

The Alfvén sidebands are excited through the beating current density driven by the Alfvén pump wave fields on the density perturbation of the magnetostatic mode. The coupled mode equation for these sidebands can be derived from the following fluid equations for electrons and ions together with the Maxwell equations:

$$\frac{\partial\delta n_\pm}{\partial t} + \nabla\cdot(n_0\delta\vec{v}_{e\pm} + n_s\vec{v}_{pe\pm}) = 0 = \frac{\partial\delta n_\pm}{\partial t} + \nabla\cdot(n_0\delta\vec{v}_{i\pm} + n_s\vec{v}_{pi\pm}) \quad (8)$$

$$\delta\vec{E}_\pm + \frac{1}{c}\delta\vec{v}_{e\pm}\times\hat{z}B_0 = -(T_e/n_0e)\nabla\delta n_\pm \quad (9)$$

$$\frac{\partial\delta\vec{v}_{i\pm}}{\partial t} = -c_s^2\nabla(\delta n_\pm/n_0) + (e/Mc)(\delta\vec{v}_{i\pm} - \delta\vec{v}_{e\pm})\times\hat{z}B_0 \quad (9')$$

$$\nabla\times\delta\vec{E}_\pm = -\frac{1}{c}\frac{\partial\delta\vec{B}_\pm}{\partial t} \quad (10)$$

and

$$\nabla\times\delta\vec{B}_\pm = (4\pi n_0e/c)[(\delta\vec{v}_{i\pm} - \delta\vec{v}_{e\pm}) + (n_s/n_0)(\vec{v}_{pi\pm} - \vec{v}_{pe\pm})] \quad (11)$$

where $c_s^2 = (T_e + T_i)/m_i$.

We have neglected the nonlinear Lorentz forces $(\vec{v}\cdot\nabla\vec{v})$ in (9) and kept the beating currents $(n_s\vec{v}_{p\pm})$ in (8) and (11) as the driving sources of the Alfvén sidebands. The underlying reason is that the purely growing mode is more effective in producing density perturbations than velocity perturbations.

Following the functional dependence of the magnetostatic mode, we express the physical quantities of the sidebands as

$$\delta\vec{v}_{ei\pm} = [(\hat{x}\delta\tilde{v}_{ei\pm x} \pm i\hat{y}\delta\tilde{v}_{ei\pm y})\cos kx + i\hat{z}\delta\tilde{v}_{ei\pm z}\sin kx]e^{\gamma t}e^{i(k_0 z-\omega_0 t)} + \text{c.c.}$$

$$\delta n_{\pm} = i\delta\tilde{n}_{\pm}(\sin kx)e^{\gamma t}e^{i(k_0 z-\omega_0 t)} + \text{c.c.}$$

$$\delta\vec{B}_{\pm} = [(\hat{x}\pm i\alpha_{\pm}\hat{y})\cos kx - i\hat{z}(k/k_0)\sin kx]\delta\tilde{B}_{\pm}e^{\gamma t}e^{i(k_0 z-\omega_0 t)} + \text{c.c.} \quad (12)$$

where the upper sideband ($\vec{k}_+ = \vec{k}_0 + \vec{k}$, $\omega_+ = \omega_0 + i\gamma$) and lower sideband ($\vec{k}_- = \vec{k}_0 - \vec{k}$, $\omega_- = \omega_0 - (i\gamma)^*$) propagate together along the magnetic field and form a standing wave pattern across the magnetic field, $\alpha_\pm$ are unknown parameters defining the polarizations of the Alfvén sidebands and will be determined shortly; the expressions of $\delta\vec{E}_\pm$ can be obtained from the Faraday law.

Substituting (12) into (8)-(11) and eliminating $\delta\tilde{n}_\pm$ from (8) and (9), we first obtain

$$\delta\tilde{v}_{e\pm x} = -(\omega_0/k_0)\delta\tilde{B}_\pm/B_0$$

$$\delta\tilde{v}_{e\pm y} = -\alpha_\pm(\omega_0/k_0)\delta\tilde{B}_\pm/B_0$$

$$\delta\tilde{v}_{i\pm x} = [(k_0 v_A^2/\omega_0)(\tilde{n}_s/n_0)(B_p/B_0) - (k_0\Omega_i^2/k^2\omega_0)(\omega_0^2/k_0^2c_s^2-1)(1\mp\alpha_\pm\omega_0/\Omega_i) \cdot (\delta\tilde{B}_\pm/B_0)]/f$$

$$\delta\tilde{v}_{i\pm y} = \mp(\Omega_i/\omega_0)\{(k_0 v_A^2/\omega_0)(\tilde{n}_s/n_0)(B_p/B_0) + (\omega_0/\kappa_0)[1 + (k_0/k)^2(\Omega_i/\omega_0)(\omega_0^2/k_0^2c_s^2-1) \cdot (\pm\alpha_\pm - \omega_0/\Omega_i)](\delta\tilde{B}_\pm/B_0)\}/f$$

$$\delta\tilde{v}_{i\pm z} = -(k_0/k)(\Omega_i/\omega_0)^2[(1-\omega_0^2/\Omega_i^2)(k_0 v_A^2/\omega_0) \cdot (\tilde{n}_s/n_0)(B_p/B_0) + (\omega_0/k_0)(1\mp\alpha_\pm\omega_0/\Omega_i)(\delta\tilde{B}_\pm/B_0)]/f \quad (13)$$

where $f = 1 + (k_0/k)^2(\Omega_i/\omega_0)^2(1-\omega_0^2/\Omega_i^2)(\omega_0^2/k_0^2c_s^2-1)$.

The missing component $\delta\tilde{v}_{e\pm z}$ can be obtained from the z component of (11), it reads

$$\delta\tilde{v}_{e\pm z} = \delta\tilde{v}_{i\pm z} \pm \alpha_\pm(kv_A^2/\Omega_i)(\delta\tilde{B}_\pm/B_0) \quad (14)$$

These relations of (13) and (14) are then used in the remaining two equations, i.e., the x and y component of (11), leading to the determination of the parameter

$$\alpha_\pm = \{(1\pm\omega_0/\Omega_i)[1-(k_0/k)^2(\omega_0^2/k_0^2c_s^2-1)] + (f \pm \Omega_i/\omega_0)(k_0^2v_A^2/\Omega_i^2)(1 + k^2/k_z^2)\} / \{(1/f \pm \omega_0/\Omega_i)[1-(k_0/k)^2(\omega_0^2/k_0^2c_s^2-1)] + (1-\Omega_i^2/\omega_0^2f)[fk_0^2v_A^2/\Omega_i^2-(k_0/k)^2(\omega_0^2/k_0^2c_s^2-1)]\} \quad (15)$$

and that of the coupled mode equations for the Alfvén sidebands

$$\{1-(k_0/k)^2(\Omega_i/\omega_0)^2(1\mp\alpha_\pm\omega_0/\Omega_i)(\omega_0^2/k_0^2c_s^2-1)/f \mp\alpha_\pm(k_0^2v_A^2/\Omega_i\omega_0)\}(\delta\tilde{B}_\pm/B_0) = -(1/f \pm \omega_0/\Omega_i)(k_0^2v_A^2/\omega_0^2)(\tilde{n}_s/n_0)(B_p/B_0) \quad (16)$$

Equation (16) shows the sideband fields to be produced by the pump field and the purely growing density perturbation of the magnetostatic mode. Thus, equations (7) and (16) form a complete coupled set of equations describing the proposed instability process.

3. Dispersion Relation

With the aid of (2), (13), (14), and (6), the coupling term on the right-hand side of (7) can be expressed explicitly as

$$(\tilde{F}_e + \tilde{F}_i)/M = \pm 2k(\Omega_i/\omega_0)(k_0v_A^2/\Omega_i)^2 \cdot (\{1+k^2/k_0^2 \mp (\omega_0\Omega_i/k_0^2v_A^2) \cdot [\alpha_\pm + (m/M)(1+\alpha_\pm)(1\pm\omega_0/\Omega_i) - (1/f)(k_0/k)^2 \cdot (\Omega_i/\omega_0)^2(1\mp\alpha_\pm\omega_0/\Omega_i)]](\delta\tilde{B}_\pm/B_0) \mp (\Omega_i/\omega_0)\{(1\pm 2\omega_0/\Omega_i) - (k_0/k)^2(\Omega_i/\omega_0)^2(1-\omega_0^2/\Omega_i^2)/f\} \cdot (\tilde{n}_s/n_0)(B_p/B_0))(B_p/B_0) \quad (17)$$

Substituting (17) into (7) and combining the resultant with (16), we finally obtain the dispersion relation

$$\gamma^2 + k^2v_A^2/(1+k^2v_A^2/\Omega_i\Omega_i) + k^2c_s^2 \pm 2k^2(k_0v_A^2/\omega_0)^2 [(1\pm 2\omega_0/\Omega_i) - (k_0/k)^2(\Omega_i^2/\omega_0^2-1)/f](B_p/B_0)^2 = -2k^2(k_0v_A^2/\omega_0)^2(k_0^2v_A^2/\Omega_i^2)(1\pm\Omega_i/\omega_0 f) \{1+k^2/k_0^2 \mp (\omega_0\Omega_i/k_0^2v_A^2)[\alpha_\pm + (m/M)(1+\alpha_\pm)(1\pm\omega_0/\Omega_i) - (1/f)(k_0/k)^2(\Omega_i/\omega_0)^2(1\mp\alpha_\pm\omega_0/\Omega_i)]\}(B_p/B_0)^2 / \{1-(k_0/k)^2(\Omega_i/\omega_0)^2(1\mp\alpha_\pm\omega_0/\Omega_i) (\omega_0^2/k_0^2c_s^2-1)/f \mp\alpha_\pm k_0^2v_A^2/\omega_0\Omega_i\} \quad (18)$$

Equation (18) is a general expression of the dispersion relation for filamentation instability of ducted Alfvén waves. It will be analyzed in the following discussion to determine the threshold conditions and the growth rates of the instability.

In principle, (18) is a quadratic equation in γ and can be solved analytically. However, since the coefficients of (18) are complicated functions of the constant parameters $\beta = c_s^2/v_A^2$ and $K = K_0V_A/\Omega_i$ and the normalized variable parameter $K = k/k_0$ (the notations used by Wong and Goldstein [1986] are adopted). A numerical analysis of (18) with different parameters is desirable. In doing so, we vary K from 0 to 2 and examine the dependences of the threshold intensity and the growth rate on β and K for both right-hand (R-H) and left-hand (L-H) circularly polarized Alfvén waves. Presented in Figures 1-4 are the dependence of the normalized threshold intensity

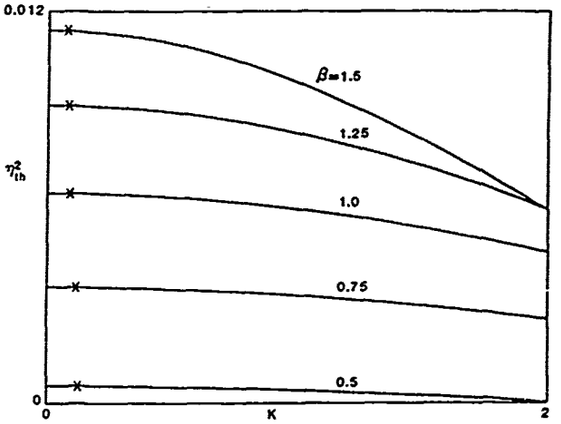

Fig. 1. Functional dependence of the threshold field intensity on K and β for low- frequency (κ = 0.01) R-H circularly polarized pump.

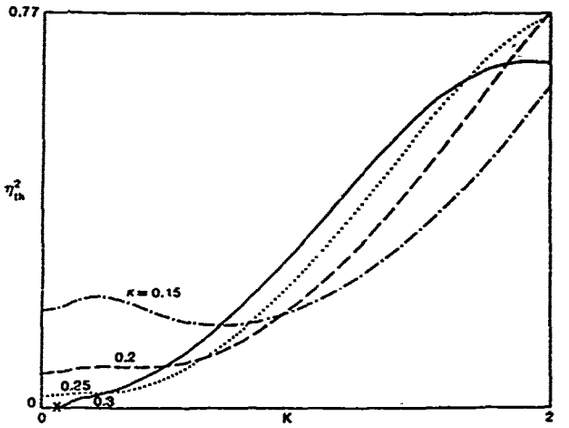

Fig. 3. Dependence of the threshold field intensity on K and κ for L-H circularly polarized pump in high β (= 1.5) plasma.

(η^2_{th}) on K; $\eta^2_{th} = (B_p/B_o)^2_{th}$ is obtained by setting γ = 0 in (18). Figures 1 and 2 correspond to the R-H circularly polarized waves. It is shown that the filamentation instability has a lower threshold level for a wave with a smaller frequency (i.e., smaller κ). In addition, the threshold of the instability also varies with β. For very low frequency waves ($\kappa \leq 0.05$) the threshold intensity increases with β. However, it becomes a decreasing function of β for $\kappa \geq 0.1$. This trend has been demonstrated in these two figures, wherein κ = 0.01 and 0.3 are used as the representative parametric values. We have excluded the threshold values in the neighborhood of X (marked on the curves) from the figures. This is because in that wave number region the nonlinear Lorentz forces on electrons and on ions are in opposite directions with comparable magnitude, so that the two terms proportional to $(B_p/B_o)^2$ in (18) tend to cancel to each other and thus the threshold becomes very high.

Figures 3 and 4 correspond to L-H circularly polarized waves. It is found that the instability can be excited only by waves with higher frequencies (e.g., $\kappa \geq$ 0.15) with reasonable thresholds. The dependence of the threshold on κ for β = 1.5 and that on β for κ = 0.3 are also shown in Figures 3 and 4, respectively. It appears that the instability prefers to be excited in the region K < 0.5. Otherwise, the threshold increases very fast with K. In the region K < 0.5, the threshold decreases with both κ and β until the instability becomes forbidden for the region of very small κ (e.g., the region below K = X marked in both Figures 3 and 4 for κ = 0.3 and β = 1.5).

We next present the growth rates of the instability. Shown in Figures 5 and 6 are the functional dependence of the growth rate γ on the wave field intensity η^2 of the R-H circularly polarized wave for low β (= 0.5) and high β (= 1.5) cases, where κ and K are considered to be constant parameters. In order to obtain adequate information for the dependencies of γ in these two cases, two representative values for each of the two parameters κ and K are chosen in the figure presentation: κ = 0.01 and 0.3 stand for the cases of the low-frequency and high-frequency waves, respectively. We then use K = 0.1 and 1 to characterize the regions of large-scale and small-scale filamentation instability, respectively. The

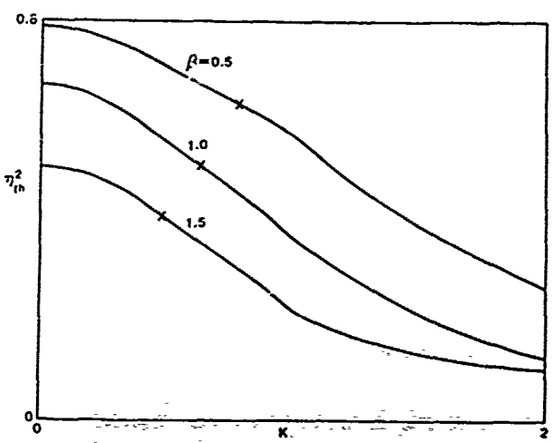

Fig. 2. Dependence of the threshold field intensity on K and β for high frequency (κ = 0.3) R-H circularly polarized pump.

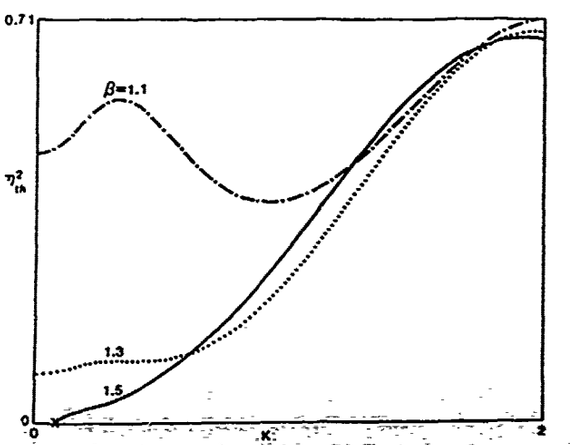

Fig. 4. Dependence of the threshold field intensity on K and β for high frequency (κ = 0.3) L-H circularly polarized pump.

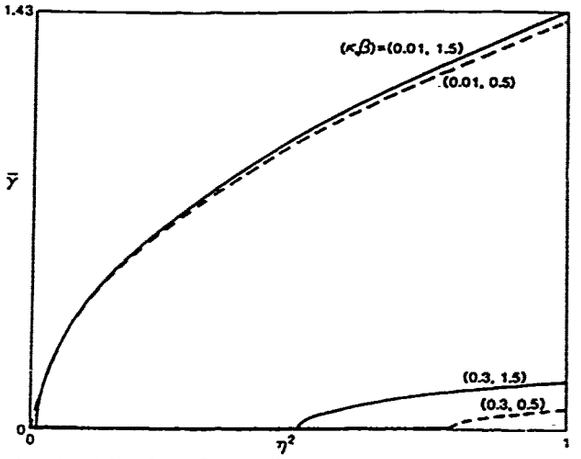

Fig. 5. The dependence of the normalized growth rate $\bar{\gamma} = \gamma/k_0V_A$ on the R-H circularly polarized pump intensity η^2, where K = 0.1 and (κ, β) as indicated are set in the evaluation.

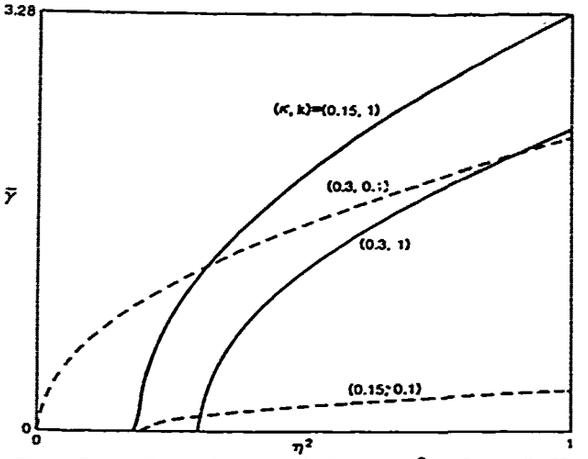

Fig. 7. Dependence of $\bar{\gamma}$ on η^2 of a L-H circularly polarized pump in a plasma with $\beta = 1.5$.

results show that, in general, the growth rate increases with β and K and decreases with κ. For the L-H circularly polarized wave case, the instability can be excited only by the high-frequency waves in the high β plasma. We therefore choose $\beta = 1.5$ and $\kappa = 0.15$ and 0.3 to evaluate the dependence of γ on η^2. Again K = 0.1 and 1 are considered, and the results are presented in Figure 7. In this case, the growth rate increases with κ for K = 0.1 and becomes a decreasing function of κ for K = 1.

4. Summary and Discussion

We have investigated the filamentation instabilities of large-amplitude, circularly polarized Alfvén waves propagating along the background magnetic field. The instabilities are excited via the scattering of the unperturbed Alfvén pumps (considered as a pump wave) into sidebands by the density perturbations that are associated with the simultaneously excited purely growing magnetostatic modes. A four-wave coupling process is then considered for the analysis of the instabilities. The theory developed is based on the two-fluid plasma model. In general, the fluid model is valid when the condition $k^2c_s^2/\Omega_i^2 = K^2\kappa^2\beta/2 \ll 1$ is satisfied. In the present work, the maximum value of the parameter $K^2\kappa^2\beta/2$ for K = 2, κ = 0.3, and β = 1.5 is 0.27, which reasonably justifies the use of the fluid model. For the more general consideration that includes the region $K^2\kappa\beta/2 \gtrsim 1$, however, a kinetic plasma model should be used.

The nonlinear source for the Alfvén sidebands is the beating current driven by the pump wave field on the density perturbation of the purely growing mode, whereas the nonlinear Lorentz force (which reduces to the ponderomotive force in the unmagnetized case) introduced by the spatial gradient of the resultant high-frequency wave field is the driving source for the nonoscillatory (i.e., the purely growing) mode. These nonlinear effects result in the coupling of the nonoscillatory mode with the Alfvén sidebands through the Alfven pump wave. A dispersion relation of the instabilities is thus derived by combining the coupled mode equations. Solving the dispersion relation, we have determined the threshold

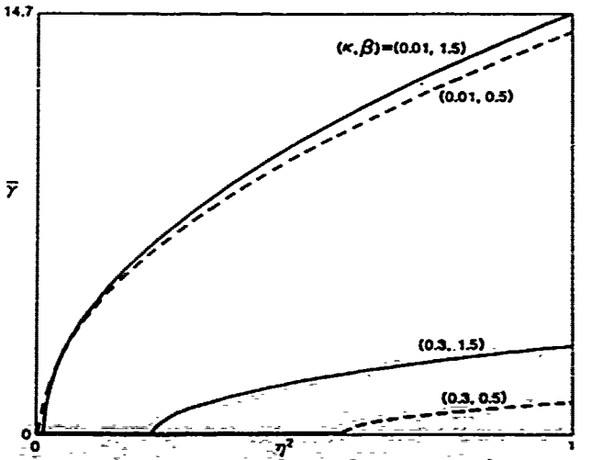

Fig. 6. Dependence of $\bar{\gamma}$ on η^2 of R-H circularly polarized pump for K = 1 and (κ, β) as indicated.

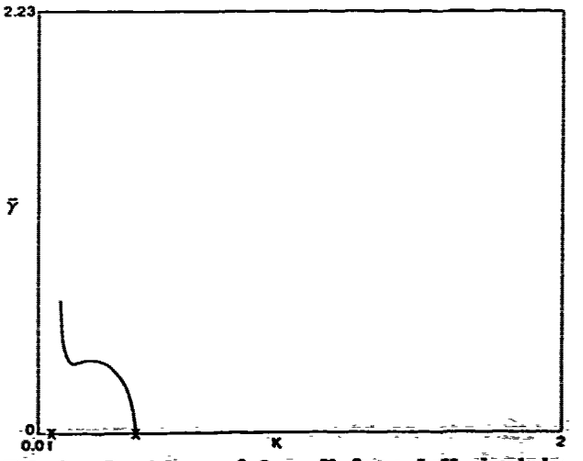

Fig. 8. Dependence of $\bar{\gamma}$ on K for a L-H circularly polarized pump with $\eta^2 = 0.05$ and $\kappa = 0.3$ in a plasma with $\beta = 1.5$.

fields and the growth rates for the cases of the R-H and L-H circularly polarized pump waves. We have also determined the functional dependencies of the threshold field η_{th} on the wave number K of the nonoscillatory mode, the β of the plasma, and the frequency κ of the pump (see Figures 1-4). The dependence of the growth rate γ on the pump intensity η^2 is examined for several sets of representative parameters (K,β,κ) (see Figures 5-7).

For the geophysical applications of the concerned instabilities, we follow the examples discussed by Wong and Goldstein [1986]. The finite amplitude Alfvén waves that were observed in the high-speed streams of the solar wind and discussed by Abraham-Shrauner and Feldman [1977] are the left-hand circularly polarized wave with $\kappa = 0.3$ and $\eta^2 = 0.05$. As shown by Wong and Goldstein [1986], these waves are stable to both the modulational and the decay instabilities for $\beta > 1$. From our analysis, however, it is found that these waves are unstable to the filamentation instability in the small K region. The growth rates of the instability evaluated for $\beta = 1.5$ are presented in Figure 8. We therefore predict the appearance of nonoscillatory, cross-field plasma density perturbations and magnetic field perturbations in the background solar wind plasma. However, these predicted cross-field density striations and magnetostatic structure probably have not been observed by Abraham-Shrauner and Feldman [1977]. The difficulty in the in situ measurements of the purely growing modes by satellites lies in the large velocity difference between the solar wind and the satellite. On the other hand, it should not be difficult for the satellites to observe the magnetic and density fluctuations of obliquely propagating sideband Alfvén waves. We have not drawn the supporting evidence from the literature yet.

Low-frequency, left-hand polarized finite amplitude Alfvén waves have also been observed in the upstream part of the Jovian bow shock [Goldstein et al., 1985]. It is shown from our analysis that this wave is filamentally stable. In fact, only the decay instability is very weakly unstable for the case $\kappa = 0.02$, $\eta^2 = 0.05$, and $\beta = 1.5$. Whereas the observation of right-hand polarized waves was not reported, it can be speculated from the linear dispersion relations of the Alfvén waves, because in such a low-frequency region the dispersion relations of right- and left-hand-polarized Alfvén waves are almost identical. If this is indeed so, the filamentation instability is found to be unstable against the right-hand pumps in the entire K region of interest. The functional dependence of the growth rate of the instability on K is presented in Figure 9. Again, this instability introduces nonoscillatory, cross-field density and magnetic fluctuations to the background plasma and thus can be attributed to the observed correlations in the magnetic and density fluctuations.

For the other cases of right-hand-polarized waves in interplanetary shocks and in the terrestrial foreshock [Vinas et al., 1984; Smith et al., 1985], the filamentation instability requires a threshold power higher than that used by Wong and Goldstein [1986] in each case.

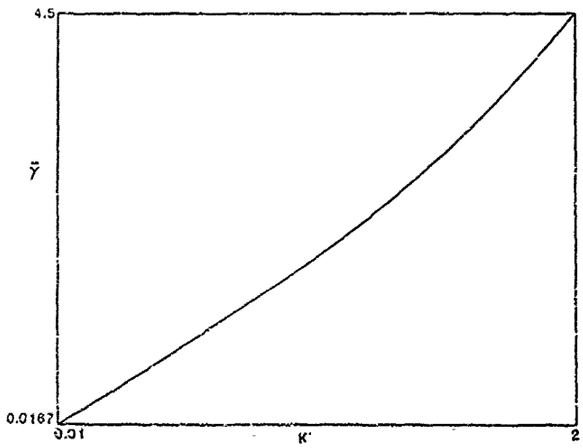

Fig. 9. Dependence of $\bar{\gamma}$ of K for a R-H circularly polarized pump with $\eta^2 = 0.05$ and $\kappa = 0.02$ in a plasma with $\beta = 1.5$.

Acknowledgments. This work was supported by the Air Force Office of Scientific Research, grant No. AFOSR-85-0133 and AFSOR-88-0127 at the Polytechnic University, and by the NASA contract NAG5-889, Lincoln Lab contract, and the RADC contract through southeastern Center for Electrical Engineering Education at the Massachusetts Institute of Technology. The numerical work was performed at the Pittsburgh Supercomputing Center of NSF.

The editor thanks L. Stenflo and another referee for their assistance in evaluating this paper.

References

Abraham-Shrauner, B., and W.C. Feldman, Nonlinear Alfvén waves in high-speed solar wind streams, J. Geophys. Res. 82, 618, 1977.

Belcher, J.W., and L. Davis, Large-amplitude Alfvén waves in the interplanetary medium, 2, J. Geophys. Res., 76, 3534, 1971.

Cohen, R., and R. Dewar, On the backscatter instability of solar wind Alfvén waves, J. Geophys. Res., 79, 4174, 1974.

Derby, N.F., Modulational instability of finite-amplitude circularly polarized Alfvén waves, Astrophys. J., 224, 1013, 1978.

Galeev, A.A., and V.N. Oraevskii, The stability of Alfvén waves, Sov. Phys. Dokl., Engl. Transl., 7, 988, 1963.

Goldstein, M.L., An instability of finite amplitude circularly polarized Alfvén waves, Astrophys, J., 219, 700, 1978.

Goldstein, M.L., H.K. Wong, A.F. Vinas, and C.W. Smith, Large-amplitude MHD waves upstream of the Jovian bow shock: Reinterpretation, J. Geophys. Res., 90, 302, 1985.

Ionson, J.A., and R.S.B. Ong, The long time behavior of a finite amplitude shear Alfvén wave in a warm plasma, Plasma Phys. Controlled Fusion, 809, 1976.

Kuo, S.P., and G. Schmidt, Filamentation instability in magneto plasmas, Phys. Fluids, 26, 2529, 1983.

Kuo, S.P., and M.C. Lee, Earth magnetic field fluctuations produced by filamentation instabilities of electromagnetic heater waves, Geophys. Res. Lett., 10, 979, 1983.

Lashmore-Davies, C.N., Modulation instability of a finite amplitude Alfvén wave, Phys. Fluids, 19, 587, 1976.

Longtin, M., and B.U.Ö.. Sonnerup, Modulational instability of circularly polarized Alfvén waves, J. Geophys. Res., 91, 6816, 1986.

Mio, J., T. Ogino, K. Minami, and S. Takeda, Modified nonlinear Schrodinger equation for Alfvén wave propagating along the magnetic field in cold plasmas, J. Phys. Soc., Jpn., 41, 265, 1976a.

Mio, J., T. Ogino, K. Minami, and S. Takeda, Modulational instability and cnvelope-solitons for nonlinear Alfvén waves propagating along the magnetic field in plasmas, J. Phys. Soc. Jpn., 41, 667, 1976b.

Mjølhus, E., On the modulational instability of hydromagnetic waves parallel to the magnetic field, J. Plasma Phys., 16, 321, 1976.

Ovenden, C.R., H.A. Shah, and S.J. Schwartz, Alfvén solitons in the solar wind, J. Geophys. Res, 88, 6095, 1983.

Sagdeev, R.Z., and A.A. Galeev, in Nonlinear Plasma Theory, edited by T. O'Neil and D. Book, W.A. Benjamin, New York, 1969.

Sakai, J., and B.U.O. Sonnerup, Modulational instability of finite amplitude dispersive Alfvén waves, J. Geophys Res., 88, 9069, 1983.

Schmidt, G., Physics of High Temperature Plasma, 2nd ed., Academic, San Diego, 1979.

Smith, C.W., M.L. Goldstein, S.P. Gary, and C.T. Russell, Beam driven ion-cyclotron harmonic waves resonances in the terrestrial foreshock, J. Geophys. Res., 90, 1429, 1985.

Spangler, S.R., and J.P. Sheerin, Alfvén wave collapse and the stability of a relativistic electron beam in a magnetized astrophysical plasma, Astrophys. J., 272, 273, 1983.

Terasawa, T., M. Hoshino, J.I. Sakai, and T. Hada, Decay instability of finite-amplitude circularly polarized Alfvén waves: A numerical simulation of stimulated Brillouin scattering, J. Geophys. Res., 91, 4171, 1986.

Vinas, A.F., M.l. Goldstein, and M.H. Acuna, Spectral analysis of magnetohydrodynamic fluctuations near interplanetary shocks, J. Geophys. Res., 89, 6813, 1984.

Wong, H.K., and M.L. Goldstein, Parametric instabilities of circularly polarized Alfvén waves including dispersion, J. Geophys. Res., 91, 5617, 1986.

S. P. Kuo and M. H. Whang, Polytechnic University, EE/CS and Weber Research Institute, Long Island Center, Route 110, Farmingdale, NY11735.

M. C. Lee, Massachusetts Institute of Technology, Cambridge, MA 02139.

(Received January 14, 1988;
revised April 15, 1988;
accepted April 19,1988.)

J. Geomag. Geoelectr., 40, 1141–1145, 1988

Combined Operation of Two Ground Transmitters for Enhanced Ionospheric Heating

M. C. LEE[1], K. M. GROVES[1], C. P. LIAO[1], D. R. RIVAS[1], and S. P. KLO[2]

[1]*Massachusetts Institute of Technology, Cambridge, Massachusetts 02139, U.S.A.*
[2]*Polytechnic University, Farmingdale, New York 11735, U.S.A.*

(Received April 8, 1988; Accepted June 3, 1988)

The combined operation of an HF or MF ground transmitter and a VLF transmitter for enhanced ionospheric heating is discussed. The HF or MF transmitter, operated in a pulsed mode, can preferentially produce short-scale density striations that can render the nonlinear mode conversion of the subsequently launched VLF waves into lower hybrid waves. In addition to the mode conversion process, the VLF waves, if intense enough, can also excite meter-scale density striations and lower hybrid waves via parametric instabilities. Intensified density striations and enhanced airglow are expected, and they can be detected by incoherent backscatter radars and photometers, respectively. The feasibility and planning of the proposed experiments are addressed.

1. Introduction

An experimental scheme is discussed for enhanced ionospheric heating by the combined operation of two powerful ground transmitters. One is an HF or MF heater wave, and the other is a VLF heater wave. The proposed scenario is as follows.

The ionosphere is illuminated by an HF or MF wave first and, then, a VLF wave subsequently (see Fig. 1). It has been known both theoretically and experimentally that short-scale (i.e., less than a few meters) ionospheric irregularities can be excited within seconds by HF heater waves, while it takes tens of seconds or longer for large-scale (say, hundreds of meters and longer) ionospheric irregularities to be generated (see, e.g., GUREVICH, 1978; FEJER, 1979; FREY *et al.*, 1984; COSTER *et al.*, 1985). As shown in Section 2 of this paper, short-scale ionospheric density striations can effectively cause the nonlinear scattering of VLF waves into lower hybrid waves. Hence, we only need to operate the HF or MF heater in pulsed mode to assure the excitation of meter-scale ionospheric irregularities. During the vertical ionospheric heating, the HF heater wave frequencies should be less than the f_0F_2 for overdense heating of the ionospheric F region. When a MF heater is used, the wave frequency is required to match the local electron gyrofrequency in the ionosphere to produce short-scale ionospheric irregularities via electron cyclotron heating (LEE *et al.*, 1986).

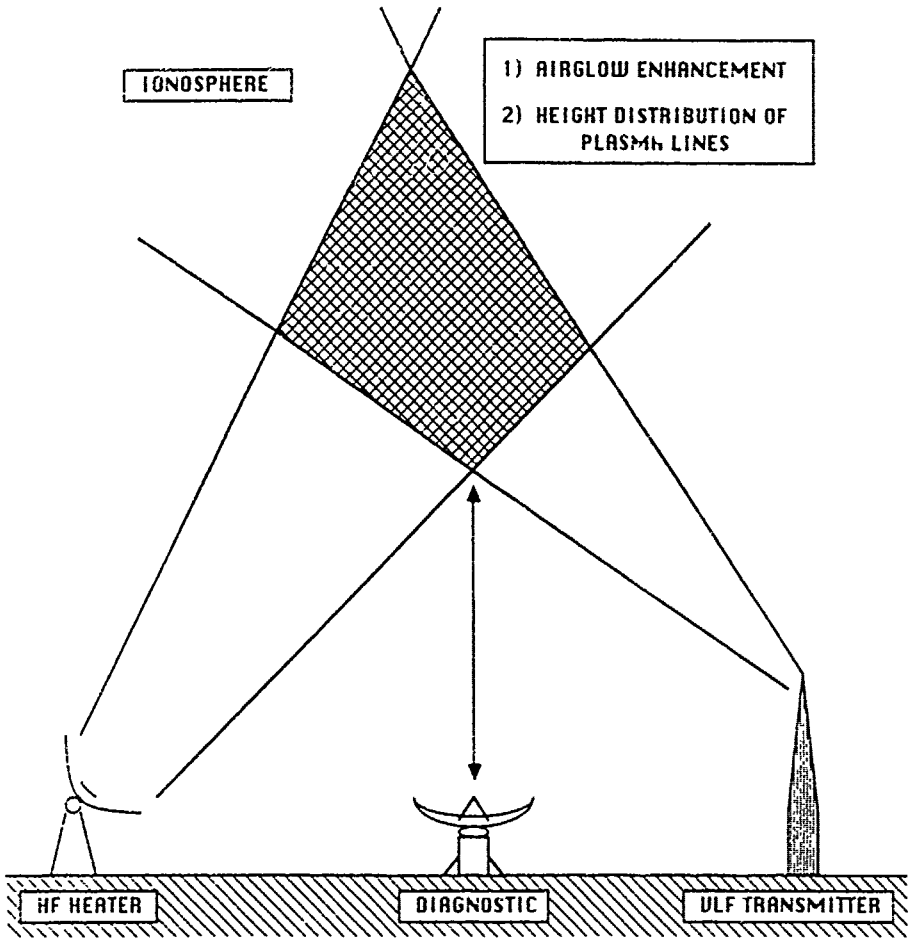

Fig. 1. The proposed experiment for enhanced ionospheric heating. Illumination of the ionosphere by a HF or MF ground transmitter first, and then a VLF ground transmitter subsequently.

In addition to the nonlinear scattering process, the VLF waves, if intense enough, can also excite lower hybrid waves and ionospheric irregularities via parametric instabilities (LEE and KUO, 1984). The suggested diagnoses for the expected ionospheric effects shall be discussed in Section 3. In principal, the two different processes producing the lower hybrid waves can be experimentally distinguished.

2 Heater Wave-Induced Ionospheric Effects

2.1 *Mode conversion via nonlinear scattering process*

Various plasma instabilities can be excited by HF heater waves during overdense ionospheric heating. In seconds, short-scale ionospheric density striations can be generated concomitantly with Langmuir waves, upper hybrid waves etc. However, it requires tens of seconds for the generation of large-scale ionospheric irregularities by self-focusing instability or thermal filamentation instability. Large-scale irregularities can give rise to phase and amplitude scintillation of beacon satellite signals. These wave interference patterns may not be associated with significant attenuation of the radio signals. By contrast, the short-scale irregularities are able to cause anomalous absorption of the radio signals via the nonlinear scattering process described below that converts electromagnetic wave energy into electrostatic wave energy (eventually, plasma kinetic energy) in the ionosphere.

For simplicity, a ducted whistler (VLF) wave propagating along the z direction is assumed, viz.,

$$\boldsymbol{E}_i = (\hat{x} - i\hat{y})E \exp[i(k_i z - \omega_i t)]. \tag{1}$$

Further, short-scale ionospheric irregularities induced by an HF or MF heater wave are represented by

$$\delta n = \delta \hat{n} \exp(ikx). \tag{2}$$

Solving the wave equation, we can show that the ionospheric irregularities scatter nonlinearly the circularly polarized (whistler) wave into an elliptically polarized wave. In other words, a linearly polarized component of the scattered wave is introduced by the EM wave-induced field-aligned ionospheric irregularities.

The scattered whistler (VLF) wave field can be expressed as

$$\boldsymbol{E} = \{(\hat{x} - i\hat{y})E_{cs} - i\hat{E}_{ls}\}\exp[i(k_s z - \omega_s t)], \tag{3}$$

where $E_{cs} = E_s(\delta n / N_0)$ representing the wave field intensity of the circularly polarized component while $\hat{E}_{ls}$ represents that of the linearly polarized component. N_0 is the unperturbed plasma density. It is found that E_{cs} and $\hat{E}_{ls}$ are related by

$$E_{cs} = 2\left(\frac{\lambda}{\lambda_s}\right)^2 \hat{E}_{ls}, \tag{4}$$

where $\lambda = 2\pi/k$ and $\lambda_s = 2\pi/k_s$ are the scale size of ionospheric irregularities and the wavelength of the whistler wave, respectively. If a VLF wave at the frequency of 10 kHz is injected, and the ionospheric conditions are assumed to be f_c (electron cyclotron frequency)=1.3 MHz and f_p (electron plasma frequency)=6 MHz, the

whistler wavelength in the ionosphere is found to be about 500 meters. According to Eq. (4), E_p dominates over E_s provided that $\lambda \ll \lambda_\perp$. Hence, meter-scale irregularities produced by HF or MF heater wave can effectively render the nonlinear mode conversion of a VLF (whistler) wave into a lower hybrid wave. The parallel and perpendicular wave vectors of the lower hybrid wave are identical to the wave vector of the ducted whistler wave and that of the field-aligned ionospheric irregularities, respectively.

2.2 *VLF wave-excited parametric instabilities*

While, in principle, the nonlinear scattering process occurs at any field intensity of the incident VLF wave, parametric instabilities can be triggered by intense enough VLF waves as suggested in LEE and KUO (1984). Short-scale ionospheric irregularities associated with zero-frequency modes can be excited simultaneously with lower hybrid waves by the VLF waves. Therefore, the HF or MF heater wave-induced short-scale ionospheric irregularities can be further strengthened by the VLF heater waves.

3 Diagnoses of Expected Ionospheric Effects

It is generally believed that spread F echos in ionograms and scintillation phenomena are caused by large-scale (say, hundreds of meters) ionospheric irregularities. The generation of large-scale ionospheric density irregularities, therefore, can be sensed by ionosondes and scintillation measurements of radio stars or beacon satellite signals. By contrast, the presence of field-aligned short-scale (a few meters and less) irregularities can be detected by backscatter radars.

Backscatter radar measurements can also be made for detecting the excited lower hybrid waves when the radar's beam angle is 90° with respect to the earth's magnetic field. The recorded incoherent backscatter radar spectrum should look like a double-humped ion spectrum peaking at the lower hybrid wave frequency. Since lower hybrid waves can accelerate electrons effectively along the geomagnetic field, airglow enhancement due to the impact excitation of neutrals by energetic electrons can be expected. Measurements of airglow at 6300 Å (red), 5577 Å (green), and even shorter wavelengths may possibly be observed. In addition, the technique described in CARLSON *et al.* (1982) for finding the height distribution of enhanced plasma lines is capable of distinguishing further the electron acceleration by Langmuir waves and/or upper hybrid waves, and lower hybrid waves that are produced, respectively, by HF and VLF heater waves.

There are several ionospheric heating facilities operated at the frequencies of a few MHz in the HF or MF band in the U.S.A., Europe, and the U.S.S.R. VLF transmitters have been used at different locations for the study of wave-particle interactions in the magnetosphere. However, it may not be possible to use the existing HF (or MF) and VLF transmitters for the proposed experiments. Since VLF waves in a narrow frequency band can be generated by lightning storms, the experiments can be carried out with available ionospheric heating facilities during

lightning storms. It is not necessary to have lightning storms occurring nearby. If lightning occurs at the conjugate location in the opposite hemisphere, the lightning-induced VLF waves can propagate in ducted whistler wave modes and bounce back and forth for several cycles before they die out.

This work was supported by NASA contract NAG5-1055, Lincoln Lab grant (under the Air Force Contract to Lincoln Lab # F19628-80-C-0002) and the RADC contract through Southeastern Center for Electrical Engineering Education at the Massachusetts Institute of Technology, and by the NSF grant ATM-8713217 and the AFOSR contract AFOSR 88-0127 at the Polytechnic University. Part of this work was presented in the International Symposium on Modification of the Ionosphere by Powerful Radio Waves, Suzdal' Moscow, U.S.S.R., September 9–12, 1986.

REFERENCES

CARLSON, H. C., V. B. WICKWAR, and G. P. MANTAS, Observation of fluxes of suprathermal electron accelerated by HF excited instabilities, *J. Atmos. Terr. Phys.*, **44**, 1089–1100, 1982.

COSTER, A. J., F. T. DJUTH, R. J. JONES, and W. E. GORDON, The temporal evolution of 3-meter striations in the modified ionosphere, *J. Geophys. Res.*, **90**, 2807–2818, 1985.

FEJER, J. A., Ionospheric modification and parametric instabilities, *Rev. Geophys. Space Phys.*, **17**, 135–153, 1979.

FREY, A., P. STUBBE, and H. KOPKA, First experimental evidence of HF produced electron density irregularities in the polar ionosphere, diagnosed by UHF radio star scintillations, *Geophys. Res. Lett.*, **11**, 523–526, 1984.

GUREVICH, A. V., *Nonlinear Phenomena in the Ionosphere* (Physics and Chemistry in Space 10), 370 pp., Springer-Verlag, 1978.

LEE, M. C., and S. P. KUO, Production of lower hybrid waves and field-aligned density striations by whistlers, *J. Geophys. Res.*, **89**, 10873–10880, 1984.

LEE, M. C., J. A. KONG, and S. P. KUO, On the resonant ionospheric heating at the electron gyrofrequency, *Proc. Int. Symp. Modif. Ionos. Powerful Radio Waves*, Suzdal', Moscow, U.S.S.R., September 9–12, 1986.

JOURNAL OF GEOPHYSICAL RESEARCH, VOL. 93, NO. A12, PAGES 14,683–14,687, DECEMBER 1, 1988

Spectral Broadening of VLF Radio Signals Traversing the Ionosphere

K. M. GROVES AND M. C. LEE

Plasma Fusion Center, Massachusetts Institute of Technology, Cambridge

S. P. KUO

Weber Research Institute, Polytechnic University, Farmingdale, New York

Nearly monochromatic signals at 13.6 kHz ±1 Hz injected from a ground-based VLF transmitter can experience a bandwidth expansion as high as 1% (~ 100 Hz) of the incident wave frequency as they traverse the ionosphere and reach satellite altitudes in the range of 600–3800 km (Bell et al., 1983). The off-carrier components, having electrostatic nature, are believed to be induced lower hybrid wave modes. We investigate two different source mechanisms that can potentially result in the observed spectral broadening of injected monochromatic VLF waves. One is the nonlinear scattering of VLF signals by ionospheric density fluctuations that renders the nonlinear mode conversion of VLF waves into lower hybrid waves. These electrostatic modes result when the injected VLF waves are scattered by ionospheric density fluctuations with scale lengths less than $\sqrt{2}\,\pi(c/\omega_{pe})(\Omega_e/\omega_o)^{1/2} \sim 2$ km in the upper ionosphere, where c, ω_{pe}, Ω_e, and ω_o are the speed of light in vacuum, the plasma frequency, the electron cyclotron frequency, and the VLF wave frequency, respectively. In the absence of ionospheric irregularities, a second mechanism that involves a parametric instability can excite the lower hybrid waves (Lee and Kuo, 1984). This process tends to produce a spectrally broadened transmitted pulse with peaks at a discrete set of frequencies on both sides of the nominal carrier frequency. By contrast, the nonlinear scattering mechanism generates single-peaked spectra centered at the carrier frequency. Both types of spectra were observed in the experiments. Therefore, the two suggested source mechanisms contribute additively to the observed spectral broadening of injected VLF waves.

1. INTRODUCTION

Nearly monochromatic signals at 13.6 kHz ± 1 Hz injected from a ground-based VLF transmitter were recently observed to experience bandwidth expansion as they traversed the ionosphere and reached the satellite altitudes in the range of 600–3800 km [*Bell et al.*, 1983]. This expansion of bandwidth, which results in a proportional increase in signal-to-noise ratio, may be as large as 1% (~ 100 Hz) of the carrier frequency, and the off-carrier components are thought to be electrostatic in nature [*Inan and Bell*, 1985]. They occur only in the presence of impulsive VLF hiss and/or a lower hybrid resonance (LHR) noise band with an irregular cutoff frequency, and only for signals whose frequencies exceed the LHR frequency at the satellite location. Based on these observed characteristics of the spectrally broadened transmitter signals, one may suspect the off-carrier components to be either electrostatic whistler wave modes or lower hybrid wave modes.

The linear scattering source mechanism producing quasi-electrostatic whistler wave modes was first suggested by *Bell et al.* [1983], who hypothesized the creation of the required ionospheric density fluctuations by precipitating, low-energy (< 1 keV) electrons. Such precipitation events have been accompanied by both VLF hiss and irregular LHR noise bands [*McEwen and Barrington*, 1967; *Laaspere et al.*, 1971; *Gurnett and Frank*, 1972]. *Bell et al.* [1983] then speculate that the broadening of the transmitted pulse spectrum results from the scattering of the initial signals from the precipitation-induced density fluctuations and the subsequent coupling into quasi-electrostatic whistler wave modes of short wavelength. The Doppler shift associated with these short-wavelength modes is estimated to be large enough to produce the bandwidth expansion of the signals measured on a moving satellite.

However, we interpret the off-carrier components of the spectrally broadened transmitter signals to be lower hybrid wave modes. The main reason is that the lower hybrid wave modes (eigenmodes of ionospheric plasmas) experience less spatial attenuation than the quasi-electrostatic whistler wave modes (quasi-modes of ionospheric plasmas) during propagation from the source regions to the satellite location. Two source mechanisms are proposed, whereby the transmitted VLF waves can potentially produce the lower hybrid waves. One mechanism comparable to that of *Bell et al.* [1983], termed "nonlinear scattering process," occurs in the presence of ionospheric density irregularities. The other one, by contrast, does not require the presence of ionospheric irregularities. It is a parametric instability that, excited by intense enough VLF waves, can generate lower hybrid waves and ionospheric irregularities concomitantly [*Lee and Kuo*, 1984].

The first mechanism, presented in section 2, differs from that of Bell et al. The newly proposed nonlinear process is a scattering of the whistler mode VLF signals by preexisting density fluctuations that render a mode conversion to lower hybrid waves, instead of a linear process that couples energy into the quasi-electrostatic branch of the whistler mode. We formulate a theory of VLF wave scattering off

Paper number 88JA03332.
0148-0227/88/88JA-03332$05.00

ionospheric irregularities, showing how this process depends upon the local fractional density fluctuations, the ratio of their scale lengths to the VLF wavelength, etc. The scattering of VLF waves by ionospheric density fluctuations generally causes elliptically polarized modes. The induced elliptically polarized modes, however, may be predominantly electrostatic under certain ionospheric conditions.

The second mechanism, described in section 3, produces a spectrally broadened signal via a parametric instability [*Lee and Kuo*, 1984]. The injected VLF wave, if intense enough, parametrically excites a magnetic field-aligned purely growing mode together with two sidebands of lower hybrid waves. The parametric excitation process requires the frequency and wave vector matching relations to be satisfied. The two lower hybrid wave sidebands are characterized by their wave vectors which are the sum and difference of the wave vectors of the whistler pump and the purely growing mode, respectively.

The lower hybrid waves generated by either of the two proposed mechanisms can have wavelengths much shorter than that of the incident VLF waves. In other words, much greater wave numbers are introduced by the suggested source mechanisms for the injected VLF waves that, essentially, become electrostatic modes. These electrostatic plasma modes with large wave numbers, detected by satellites moving across the geomagnetic field, give rise to Doppler shifts that were observed as the broadened spectra (i.e., off-carrier components) of the injected VLF waves. The preliminary results were presented in *Lee et al.* [1986].

2. NONLINEAR WAVE SCATTERING

Theory

A monochromatic VLF wave transmitted from a ground-based station into space has been observed to change from linear into circular polarization (i.e., whistler mode). If a ducted whistler wave mode, propagating exactly along the geomagnetic field, is considered for simplicity, the wave electric field may be represented as

$$\mathbf{E} = E_o(\hat{\mathbf{x}} + i\hat{\mathbf{y}})\exp[i(k_o z - \omega_o t)] \tag{1}$$

where the z axis has been taken along the geomagnetic field lines; ω_o is the transmitted wave frequency, and $\mathbf{k}_o$ the associated wave vector, assumed to be along the z axis as illustrated in Figure 1*a*. Propagating into the ionosphere with no irregular structure, the whistler wave satisfies the electromagnetic wave equation

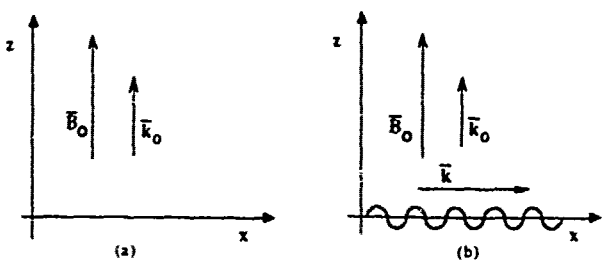

Fig. 1. Geometry of wave propagation for (*a*) uniform ionosphere and (*b*) ionosphere with irregularities.

$$\nabla^2\mathbf{E}_o - \frac{1}{c^2}\frac{\partial^2}{\partial t^2}\mathbf{E}_o = \mu_o\frac{\partial}{\partial t}\mathbf{j}_o \tag{2}$$

where $\mathbf{j}_o$ is the uniform oscillatory current driven by the incident wave field in the ionospheric plasma,

$$\mathbf{j}_o = \frac{ie^2N_o\mathbf{E}_o}{m(\omega_o - \Omega_e)}$$

and e, N_o, m, and Ω_e are the electron charge, uniform background plasma density, electron mass, and the unsigned electron cyclotron frequency, respectively. In the presence of field-aligned ionospheric density irregularities, the scattered wave, allowing for electrostatic modes, can be described by

$$\nabla(\nabla\cdot\mathbf{E}_s) - \nabla^2\mathbf{E}_s + \frac{1}{c^2}\frac{\partial^2}{\partial t^2}\mathbf{E}_s = -\mu_o\frac{\partial}{\partial t}\delta\mathbf{j}_s \tag{3}$$

where $\delta\mathbf{j}_s$ is the nonuniform current induced by the interaction of the whistler wave field with the density irregularities. We take the x axis along the direction of the density irregularities which are assumed to be of the form

$$\delta n = \delta\tilde{n}\exp[ikx] \tag{4}$$

depicted graphically in Figure 1*b*. The nonuniform current $\delta\mathbf{j}_s$ can then be expressed as

$$\delta\mathbf{j}_s = -e(N_o\delta\mathbf{v} + \frac{\delta n}{N_o}\mathbf{j}_o) \tag{5}$$

where $\delta\mathbf{v}$ is the induced velocity perturbation. The scattered wave field has the general form of

$$\mathbf{E}_s = [\hat{\mathbf{x}}E_x + i\hat{\mathbf{y}}E_y]\exp[i(k_o z - \omega_o t)] \tag{6}$$

Solving the wave equation together with the electron momentum equation, the scattered wave field is found to be elliptically polarized,

$$\mathbf{E}_s = E_o(\delta n/N_o)[\hat{\mathbf{x}} + (\hat{\mathbf{x}} + i\hat{\mathbf{y}})\alpha]\exp[i(k_o z - \omega_o t)] \tag{7}$$

where α is proportional to the amplitude of the circularly polarized component of the wave defined by

$$\alpha = -\frac{2\omega_{pe}^2\omega_o}{k^2c^2(\omega_o - \Omega_e)} \tag{8}$$

where ω_{pe} and c are the electron plasma frequency and the speed of light in vacuum, respectively, and k is the wave number of the density perturbation defined by (4). Rewriting the scattered field in terms of the ionospheric irregularity scale length, $\lambda = 2\pi/k$, we find

$$\mathbf{E}_s = E_o\exp[ikx](\delta\tilde{n}/N_o)\exp[i(k_o z - \omega_o t)] \times [\underbrace{\hat{\mathbf{x}}}_{LP} + \underbrace{(\hat{\mathbf{x}} + i\hat{\mathbf{y}})\frac{\lambda^2}{\lambda_c^2}}_{CP}] \tag{9}$$

where

$$\lambda_c = \sqrt{2}\pi(c/\omega_{pe})(\Omega_e/\omega_o)^{1/2} \approx 4.4/k_o \tag{10}$$

The scattered field is composed of a linearly polarized (LP) part and a circularly polarized (CP) part as indicated in (9). If the ratio $(\lambda^2/\lambda_c^2) \ll 1$ (i.e., $|\mathbf{k}| \gg |\mathbf{k}_o|$), the scattered wave is dominated by the linearly polarized component which, corresponding to a lower hybrid mode, oscillates in the direction of the irregularity wave vector $\mathbf{k}$; hence, the wave is electrostatic in nature and exhibits a broadened, enlarged wave vector spectrum relative to the incident wave. The

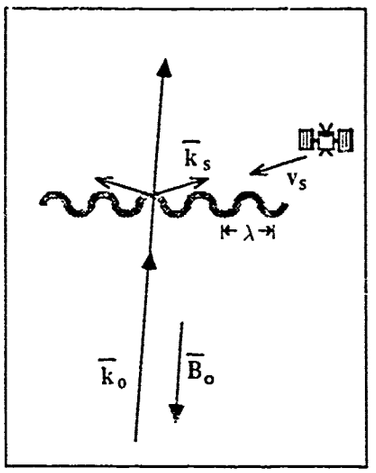

Fig. 2. Schematic of Doppler shift phenomena.

Doppler shift frequency measured by a moving satellite will be enlarged as elaborated in the next section.

Analysis

The condition found above for effective nonlinear scattering into electrostatic modes requires $\lambda \ll \lambda_c$. Typical plasma parameters for the upper ionosphere/lower magnetosphere region of interest are $\omega_{pe}/2\pi = 0.7$ MHz and $\Omega_e/2\pi = 0.6$ MHz. Assuming an incident frequency of $\omega_o/2\pi = 13.6$ kHz, we calculate $\lambda_c \approx 2$ km. The magnitude of the bandwidth expansion of the scattered VLF wave measured by a moving satellite due to the Doppler shift effect is given by

$$\Delta f = \frac{\mathbf{k}_s \cdot \mathbf{v}_s}{2\pi} \simeq \frac{v_s cos\theta}{\lambda} \approx \frac{v_s}{\lambda} \tag{11}$$

where $\mathbf{v}_s$ is the velocity of a satellite moving across the Earth's magnetic field as shown in Figure 2, and $\mathbf{k}_s = k\hat{\mathbf{x}} + k_o\hat{\mathbf{z}}$. Given $v_s \simeq 8$ km/s and $\Delta f \simeq 100$ Hz, we find $\lambda \simeq 80$ m $\ll \lambda_c \simeq 2$ km, so the condition for nonlinear scattering is well satisfied. Thus we have found that ionospheric irregularities with scale lengths of several tens of meters can produce Doppler shifts of the observed magnitude. Since $k(\lambda) \gg (\ll) k_o(\lambda_o)$, the simplification made in the formulation of the theory, namely, the assumption that the ducted whistlers propagate exactly along the Earth's magnetic field, is justified. Under this condition, even if the ducted whistlers have nonzero wave normal angles, the formulation of nonlinear scattering mechanism will not be significantly modified.

Ionospheric irregularities can occur naturally. There are many mechanisms that can generate field-aligned ionospheric irregularities [e.g., *Fejer and Kelley*, 1980]. Particle precipitation invoked by *Bell et al.* [1983] can produce irregularities with a broad range of scale lengths in a region near the F layer peak, about 300 km above the Earth's surface. The F region irregularities, as Bell et al. suggested, provide a favorable ionospheric condition for the linear scattering of the VLF waves and the subsequent coupling into quasi-electrostatic whistler wave modes. However, the amplitude of such a quasi-mode wave decreases with distance as it propagates upward to the satellite altitudes of 600–3800 km. This arises from the fact that the electrostatic whistlers are not eigenmodes but quasi-modes of ionospheric plasmas. Therefore, during the ionospheric propagation of quasi-electrostatic whistlers, the ionospheric plasmas do not respond in phase to these quasi-modes. This phase mixing (or phase mismatching) can attenuate the waves significantly during their propagation from the source region to the satellite location.

By contrast, our proposed nonlinear scattering mechanism can produce lower hybrid waves which are eigenmodes of ionospheric plasmas, experiencing less spatial attenuation than the quasi-electrostatic whistler modes during propagation. This mechanism is effective provided that field-aligned ionospheric irregularities exist and that the VLF wave frequency is greater than the local LHR (lower hybrid resonance) frequency. The characteristics of the nonlinear scattering mechanism, then, explain the observed facts that the spectral broadening phenomenon occurs only in the presence of impulsive VLF hiss and/or a LHR noise band with an irregular cutoff frequency, and only for signals whose frequencies exceed the LHR frequency at the satellite location.

3. Parametric Excitation of Lower Hybrid Waves

In this section we discuss the proposed second mechanism responsible for the observed VLF spectral broadening. While the nonlinear scattering mechanism does not work in the absence of ionospheric irregularities, lower hybrid wave modes can be excited parametrically by the VLF waves in the ionosphere. The parametric excitation of lower hybrid waves by the injected VLF waves has been suggested by us [*Lee and Kuo*, 1984] with the following scenario.

Propagating from the neutral atmosphere into the ionosphere, the incident VLF wave can be considered to be a ducted whistler mode with $\mathbf{k}_o = k_o\hat{\mathbf{z}}$ along the geomagnetic field lines, taken to be the z axis of a Cartesian system of coordinates. Assuming the space-time dependence of the perturbations to be $\exp[i(\mathbf{k}\cdot\mathbf{r} - \omega t)]$, the proposed parametric instability can be described by the following wave frequency and wave vector matching relations:

$$\omega_{1+} - \omega_s = \omega_o = \omega_{1-} + \omega_s \tag{12a}$$

$$\mathbf{k}_{1+} - \hat{\mathbf{x}}k_s = \hat{\mathbf{z}}k_o = \mathbf{k}_{1-} + \hat{\mathbf{x}}k_s \tag{12b}$$

where the subscripts minus/plus and s represent the Stokes/anti-Stokes components of the high-frequency lower hybrid sidebands and the field-aligned zero-frequency mode, respectively. By the definition of (12a), the Stokes and anti-Stokes components refer to the lower hybrid sidebands whose wave frequencies are downshifted and upshifted, respectively, by ω_s with respect to the whistler wave frequency (ω_o). For a purely growing mode (i.e., $\mathrm{Re}(\omega_s)=0$), the Stokes and anti-Stokes components of lower hybrid waves are characterized by their wave vectors, shown in (12b), which are the difference and sum of the wave vectors of the whistler and the purely growing mode, respectively. Both the Stokes and the anti-Stokes components of lower hybrid waves have to be considered in this two-dimensional instability process, since $|\mathbf{k}_s| \gg |\mathbf{k}_o|$ and the concomitantly excited low-frequency mode is a purely growing mode. Thus, $|\mathbf{k}_{1+}| \sim |\mathbf{k}_{1-}| \sim |\mathbf{k}_s|$; it is found that the lower hybrid waves have wave vectors large enough to yield the observed spectral broadening due to the Doppler effect.

It should be pointed out that a four-wave rather than a

simpler three-wave interaction process [*Berger and Perkins*, 1976; *Riggin and Kelley*, 1982] is proposed by *Lee and Kuo* [1984]. While the proposed parametric instability has a broad range of VLF (whistler) wave frequency ω_o, the three-wave interaction process [*Berger and Perkins*, 1976] is restricted to a very narrow frequency band, namely, $\omega_{LH} < \omega_o < \sqrt{2}\omega_{LH}$, where ω_{LH} is the lower hybrid resonance frequency. Further, the excited low-frequency mode in the work of *Lee and Kuo* [1984] is a zero-frequency mode. This four-wave interaction mechanism is found to require much lower thresholds than the three-wave interaction mechanism to excite lower hybrid waves in the ionosphere. Based on this proposed four-wave interaction process, we can interpret the observations of the VLF wave-excited lower hybrid waves in the ionosphere indicated in the experiments of the Franco-Soviet ARCAD 3 satellite [*Berthelier et al.*, 1982] and others [e.g., *Chmyrev et al.*, 1976].

At this point, we should comment on the effectiveness of the parametric instability in causing the observed VLF spectral broadening phenomenon. Although the production of lower hybrid waves by the parametric instability does not require the presence of naturally occurring ionospheric irregularities, this mechanism needs a threshold to operate. The thresholds in terms of whistler (VLF) wave electric fields can be calculated from equation (22*b*) of *Lee and Kuo* [1984]:

$$E_m = 0.86(k_s^2 v_{te}^3/\Omega_e)(m/e)|\eta|^{-1/2} \times \left[1 + \left(1 + \frac{4\Omega_e^2\nu_e^2\eta^2}{k_s^4 v_{te}^4}\right)^{1/2}\right]^{1/2} \quad (13)$$

where k, v_{te}, ν_e, and Ω_e are the wave number of field-aligned ionospheric irregularities, the electron thermal velocity, the electron-ion collision frequency, and the electron cyclotron frequency; η is defined by $[1+(M/m)(k_o/k)^2]/[1-(M/m)(k_o/k)^2(\Omega_e/\omega_{pe})^2]$ where M/m, k_o, and ω_{pe} are the ratio of oxygen ion (O^+) mass to electron mass, the wave number of the incident whistler wave, and the electron plasma frequency, respectively. It should be noted that the parametric wave number k is determined by the dispersion relation for the lower hybrid waves, $\omega_o = \omega_{LH}[1+(M/m)(k_o/k_s)^2]^{1/2}$, where ω_{LH} is the lower hybrid resonance frequency defined by $\omega_{LH} = \omega_{pi}/(1+\omega_{pe}^2/\Omega_e^2)^{1/2}$. If we choose the following model parameters: $v_{te} = 1.3 \times 10^6$ (m/s), $\omega_{pe}/2\pi = 0.7$ MHz (i.e., $N_o = 6 \times 10^9$ m^{-3}), $\nu_e = 10$ Hz, $\Omega_e/2\pi = 0.6$ MHz, the threshold field E_m is found to be 18 μV/m. According to *Inan and Bell* [1985], the measured power flux of transmitted VLF signals is 2×10^{-13} W/m^2 at the satellite location; namely, the measured field intensity of whistlers is 12 μV/m, which is of the same order of magnitude as the threshold of the parametric instability. The measured power flux (field intensity) of whistler (VLF) waves in the lower ionosphere is 2×10^{-9} W/m^2 (1.2 mV/m), which is also of the same order of magnitude as the instability thresholds calculated by *Lee and Kuo* [1984]. Therefore, it is possible for the instability to be excited though the VLF transmitters are operated in pulsed mode with a typical duration of seconds.

It is interesting to note that the proposed two source mechanisms are expected to produce broadened VLF spectra with different shapes. The parametric instability will preferentially excite lower hybrid waves with the scale length ($\lambda = 2\pi/k$) of $\sim$ 90 m at the satellite location. This likely generates a two-humped spectrum suppressed at the carrier frequency (f_o) relative to the sidebands peaking at approximately $f_o \pm 100$ Hz, whereas the nonlinear scattering mechanism simply broadens the bandwidth of the injected VLF waves, producing single-peaked spectra. This can be clearly seen from equation (9), showing that the scattered field intensity E_s is the incident field intensity E_o multiplied by the fractional plasma density fluctuation ($\delta n/N_o < 1$). This naturally leads to the broadened VLF spectrum peaking at the carrier frequency. These two types of broadened VLF spectra have indeed been observed. Nevertheless, the single-peaked spectra were much more frequently seen than the double-humped spectra (H. G. James, personal communications, 1988). The characteristics of our proposed two source mechanisms agree well with the observations. Hence, the observations of VLF spectral broadening offer additional evidence supporting the excitation of lower hybrid waves by VLF waves in the ionosphere as suggested by *Lee and Kuo* [1984].

4. Summary and Conclusion

In summary, we have investigated two possible source mechanisms that may be responsible for the observed spectral broadening of injected VLF waves. In the presence of ionospheric irregularities with various scale lengths as short as several tens of meters, the nonlinear scattering of the VLF waves off these density irregularities can produce electrostatic modes with larger wave vectors which give rise to the apparent spectral broadening through the Doppler shift observed by the moving satellites. The amplitude of the electrostatic modes depends linearly on the amplitude of the ionospheric irregularities. The broadening produced through this mechanism is of the same magnitude as the observed values. This mechanism produces single-peaked broadened spectra of VLF waves, which were most frequently observed in the experiments. There are many natural sources that can generate ionospheric irregularities with a broad range of scale lengths, providing favorable ionospheric conditions for the operation of the nonlinear scattering process.

In the absence of ionospheric irregularities, the spectral broadening of the incident wave packet may also stem from the second mechanism, which involves the parametric excitation of lower hybrid waves [*Lee and Kuo*, 1984]. This mechanism requires a threshold that can be exceeded by the employed navigation transmitters. These excited lower hybrid waves have much shorter (larger) wavelengths (wave numbers) than those of the injected VLF waves. The broadening introduced by this mechanism is characterized by the fact that it produces wave frequency spectra that exhibit suppressed field intensity at the carrier frequency and enhanced intensity at a discrete set of frequencies on either side of the carrier frequency. Such spectra are less frequently observed than those produced by the nonlinear scattering mechanism. The lower hybrid waves excited by this mechanism have enlarged wave vectors; the apparent broadening due to the Doppler effect is comparable to that calculated for the first mechanism.

We conclude that the two suggested mechanisms can contribute additively to the observed spectral broadening of injected VLF waves reported by *Bell et al.* [1983] and others. This spectral broadening phenomenon provides additional

evidence to support the mechanism suggested by *Lee and Kuo* [1984] for the excitation of lower hybrid waves by injected VLF (whistler) waves.

Acknowledgments. This work was supported by NASA contract NAG 5-1055, Lincoln Laboratory grant (under the Air Force contract to Lincoln Laboratory F19628-80-C-0002), and the RADC contract through Southeastern Center for Electrical Engineering Education, and the AFOSR grant AFOSR-88-0217 at the Massachusetts Institute of Technology, and by NSF grant ATM-8713217 and AFOSR contract AFOSR 88-0127 at the Polytechnic University. The earlier work by *Lee et al.* [1986] was supported by AFGL contract F19628-83-K-0024. We greatly appreciate the two referees' constructive comments.

The Editor thanks C. L. Siefring and another referee for their assistance in evaluating this paper.

REFERENCES

Bell, T. F., H. G. James, U. S. Inan, and J. P. Katsufrakis, The apparent spectral broadening of VLF transmitter signals during transionospheric propagation, *J. Geophys. Res., 88*, 4813, 1983.

Berger, R. L., and F. W. Perkins, On threshold of parametric instabilities near the lower hybrid frequency, *Phys. Fluids, 19*, 406, 1976.

Berthelier, J. J., et al., Measurements of the VLF electric and magnetic components of waves and dc electric field on board the AUREOL-3 spacecraft: The TBF-ONCH experiment, *Ann. Geophys., 38*, 643, 1982.

Chmyrev, V. M., V. K. Roldugin, I. A. Zhulin, M. M. Mogilevskii, V. I. Di, V. K. Koshelevskii, V. A. Bushmarin, and O. M. Raspopov, Artificial injection of very low frequency waves into the ionosphere and the magnetosphere of the Earth, *JETP Lett., 23*, 409, 1976.

Fejer, B. G., and M. C. Kelley, Ionospheric irregularities, *Rev. Geophys., 18*, 401, 1980.

Gurnett, D. A., and L. A. Frank, VLF hiss and related plasma observations in the polar magnetosphere, *J. Geophys. Res., 77*, 172, 1972.

Inan, U. S., and T. F. Bell, Spectral broadening of VLF transmitter signals observed on DE 1: A quasi-electrostatic phenomenon?, *J. Geophys. Res., 90*, 1771, 1985.

Laaspere, T., W. C. Johnson, and L. C. Semprebon, Observations of auroral hiss, LHR noise and other phenomena in the frequency range 20 Hz–540 kHz on OGO 6, *J. Geophys. Res., 76*, 4477, 1971.

Lee, M. C., and S. P. Kuo, Production of lower hybrid waves and field-aligned density striations by whistlers, *J. Geophys. Res., 89*, 10873, 1984.

Lee, M. C., J. F. Kiang, and S. P. Kuo, On the causes of spectral broadening of injected VLF waves (abstract), *EoS Trans. AGU, 67*, 317, 1986.

McEwen, D. J., and R. E. Barrington, Some characteristics of the lower hybrid resonance noise bands observed by the Alouette I satellite, *Can. J. Phys., 45*, 13, 1967.

Riggin, D., and M. C. Kelley, The possible production of lower hybrid parametric instabilities by VLF ground transmitters and by natural emissions, *J. Geophys. Res., 87*, 2545, 1982.

K. M. Groves and M. C. Lee, Plasma Fusion Center, NW 16-234, Massachusetts Institute of Technology, Cambridge, MA 02139.

S. P. Kuo, Weber Research Institute, Polytechnic University, Farmingdale, NY 11735.

(Received October 13, 1987;
revised July 19, 1988;
accepted July 27, 1988.)

Convective filamentation instability of circularly polarized Alfvén waves

S. P. Kuo and M. H. Whang
Department of Electrical Engineering/Computer Science, Weber Research Institute, Polytechnic University, Route 110, Farmingdale, New York 11735

G. Schmidt
Department of Physics, Stevens Institute of Technology, Hoboken, New Jersey 07030

(Received 17 October 1988; accepted 7 December 1988)

A convective instability that leads to the filamentation of large-amplitude Alfvén waves and generates nonoscillatory spatially growing density fluctuations is investigated by using a two-fluid plasma model. Based on linear perturbation analysis for a four-wave parametric coupling process, the dispersion relations of the instability for both a right- and left-hand circularly polarized Alfvén pump are derived. They are then solved numerically for the dependences of the threshold fields and growth rates on the wavenumber k of the nonoscillatory mode, the beta of the plasma, and the frequency of the pumps, for both right- and left-hand circularly polarized Alfvén pumps. The relevance of the proposed instability with some observations in the space plasmas is discussed.

I. INTRODUCTION

Large-amplitude Alfvén waves are frequently observed in the high-speed streams of the solar wind,[1] in the upstream Jovian bow shocks,[2] and in the interplanetary shocks and the terrestrial foreshock.[3,4] Moreover, the presence of such waves in front of supernova shocks is believed to play an important role in cosmic ray acceleration.[5–7] Therefore the stability of finite amplitude Alfvén waves is of great interest, not only in basic plasma physics, but also for their applications to space plasma physics[8–11] and astrophysics.[12,13]

Various processes of parametric instabilities excited by the Alfvén pumps have been investigated. In general, circularly polarized pumps propagating along the background magnetic field are considered. Within the one-dimensional regime, two instability processes have been studied extensively. One leads to the parametric decay instability ($k > k_0$),[14,15] and the other one gives rise to the modulation instability ($k \ll k_0$),[16–19] where k_0 and k are the wavenumbers of the pump and decay mode, respectively. In both processes, the decay modes and sidebands all propagate in, parallel to the Alfvén pump.

The modulation instability has also been analyzed in the region that describes the nonlinear evolution of the Alfvén waves propagating along a static magnetic field. It is shown that this evolution can be governed by a single "derivative nonlinear Schrödinger equation,"[20–22] or more generally, by a set of three coupled equations,[23] which in turn are related to the nonlinear Schrödinger equation with known soliton solutions. The possible applications of Alfvén solitons to solar and astrophysical plasmas have been discussed by Ovenden *et al.*[23] and Spangler and Sheerin.[22]

When the decay modes and sidebands are allowed to propagate in multidimensional space, new decay channels for the parametric instabilities are also present.[24–26] Though the effect of multidimensional space on the nonlinear property of the Alfvén waves is generally thought to be important, its understanding is still far from satisfactory, mainly because of the complexity involved in the analysis. Recently, an absolute filamentation instability process has been considered by Kuo *et al.*[11] Based on the two-fluid plasma model, a four-wave parametric coupling process is analyzed for the temporal growing instabilities, which are excited, via the scattering of the Alfvén pumps into obliquely propagating Alfvén sidebands by the density perturbations that are associated with the simultaneously excited purely growing and magnetic field-aligned nonoscillatory magnetostatic modes. The excited Alfvén sidebands are then added to the pumps and lead to the filamentation of the Alfvén pumps. The nonlinear source for the Alfvén sidebands is the beating current driven by the pump wave fields on the density perturbation of the purely growing mode, whereas the driving forces for the purely growing nonoscillatory density perturbations are the nonlinear Lorentz forces, which reduce to the ponderomotive forces in the unmagnetized case and are perpendicular to the background magnetic field.

In this paper, a convective filamentation instability process,[27] in contrast to the previous work,[11] is studied. Since the excited instabilities grow in space (not in time) along the propagation direction of the pumps, the nonoscillatory density perturbations are not magnetically field aligned anymore. Consequently, the nonlinear Lorentz forces introduced by the spatial gradient of the resultant Alfvén wave intensity also become not field aligned. The axial components of the forces can drive density perturbations more effectively than the transverse components, which have to move charged particles across the magnetic field lines. From this aspect, the convective instability process considered in this work is expected to be characteristically different from the absolute filamentation instability process presented in the previous work.[11]

In Sec. II the coupling equations for Alfvén sidebands and the purely growing mode are derived. A dispersion relation is obtained in Sec. III. It is analyzed for the threshold

 0899-8221/89/040734-07$01.90

fields and the growth rates for various cases. The numerical results are also presented in Sec. III. Finally, presented in Sec. IV are the summary and discussion.

II. COUPLING EQUATIONS

Monochromatic circularly polarized Alfvén waves propagating along a constant magnetic field $\mathbf{B}_0$ in z directions are represented by

$$\mathbf{B}_{p\pm} = (\hat{x} \pm i\hat{y}) B_{p\pm} e^{i(k_0 z - \omega_0 t)} + \text{c.c.}, \tag{1}$$

where $B_{p\pm}$ are the unperturbed wave magnetic field intensity, assumed to be constant and real quantities for simplicity; the $\pm$ signs refer to the right- and left-hand circular polarizations, respectively; k_0 and ω_0 are the wavenumber and angular wave frequency, satisfying the dispersion relation $\omega_0^2 = (1 \pm \omega_0/\Omega_i) k_0^2 v_A^2$, wherein v_A and Ω_i are the Alfvén speed and the ion cyclotron frequency, respectively.

The quiver velocities of electrons and ions introduced by such wave fields can be expressed as

$$\mathbf{v}_{pe\pm} = \left(1 \pm \frac{\omega_0}{\Omega_i}\right) \mathbf{v}_{pi\pm} = -(\hat{x} \pm i\hat{y}) \frac{\omega_0}{k_0} \frac{E_{p\pm}}{B_0} e^{i(k_0 z - \omega_0 t)} + \text{c.c.}, \tag{2}$$

where the subscripts e and i refer to electrons and ions.

In the following analysis of nonlinear wave–plasma interaction, the plasma is assumed to be collisionless and spatially uniform. The process under investigation is the convective filamentation instability of Alfvén pumps. The pumps are scattered into obliquely propagating sidebands by the simultaneously induced nonoscillatory density perturbations responding to the presence of the nonuniform radiation pressure of total Alfvén wave field. It is a linearized version of the self-focusing process for a large-amplitude and large cross-sectional wave beam propagating in a nonlinear medium.

The Alfvén sidebands are excited through the beating current density driven by the Alfvén pump wave fields in the density perturbation n_s, induced by the self-consistent radiation pressure. The coupled mode equations for these sidebands can be derived from the following fluid equations for electrons and ions together with the Maxwell equations:

$$\frac{\partial}{\partial t} \delta n_\pm + \nabla \cdot (n_0 \, \delta \mathbf{v}_{e\pm} + n_s \mathbf{v}_{pe\pm}) = 0 = \frac{\partial}{\partial t} \delta n_\pm + \nabla \cdot (n_0 \, \delta \mathbf{v}_{i\pm} + n_s \mathbf{v}_{pi\pm}), \tag{3}$$

$$\frac{\partial}{\partial t} \delta \mathbf{B}_\pm = B_0 \nabla \times (\delta \mathbf{v}_{e\pm} \times \hat{z}), \tag{4}$$

$$\frac{\partial}{\partial t} \delta \mathbf{v}_{i\pm} = -c_s^2 \nabla \frac{\delta n_\pm}{n_0} + \Omega_i (\delta \mathbf{v}_{i\pm} - \delta \mathbf{v}_{e\pm}) \times \hat{z}, \tag{5}$$

and

$$\nabla \times \delta \mathbf{B}_\pm = (4\pi n_0 e/c)[(\delta \mathbf{v}_{i\pm} - \delta \mathbf{v}_{e\pm}) + (n_s/n_0)(\mathbf{v}_{pi\pm} - \mathbf{v}_{pe\pm})], \tag{6}$$

where $c_s = [(T_e + T_i)/m_i]^{1/2}$ is the ion acoustic speed.

Let $\mathbf{k} = \hat{x}k$ be the filamentation wave vector, κ be the spatial growth rate along the z axis, and $(\mathbf{k}_{1,2}, \omega_{1,2})$ represent the lower and upper sidebands. In general, the upper sideband $(\mathbf{k}_2 = \mathbf{k}_0 + \mathbf{k} - i\kappa\hat{z},\ \omega_2 = \omega_0)$ and lower sideband $(\mathbf{k}_1 = \mathbf{k}_0 - \mathbf{k} - i\kappa\hat{z},\ \omega_1 = \omega_0)$ propagate together along the magnetic field and form a standing wave pattern across the magnetic field. Consequently, the self-consistent radiation pressure and the induced nonoscillatory density perturbation should also retain a similar standing wave pattern across the magnetic field. Without losing the generality, we may first prescribe the functional form of the nonoscillatory density perturbation to be

$$n_s = \tilde{n}_s e^{\kappa z} \cos kx, \tag{7}$$

where $\tilde{n}_s$ is a real amplitude; quasineutrality has been assumed. Following such a functional dependence for the nonoscillatory density perturbation, the physical quantities of the sidebands can be expressed accordingly as

$$\begin{aligned}
\delta \mathbf{v}_{ei\pm} &= [(\hat{x}\, \delta \bar{v}_{ei\pm x} \pm i\hat{y}\, \delta \bar{v}_{ei\pm y}) \cos kx + i\hat{z}\, \delta \bar{v}_{ei\pm z} \sin kx] e^{\kappa z} e^{i(k_0 z - \omega_0 t)} + \text{c.c.}, \\
\delta n_\pm &= i\, \delta \tilde{n}_\pm \sin kx e^{\kappa z} e^{i(k_0 z - \omega_0 t)} + \text{c.c.}, \\
\delta \mathbf{B}_\pm &= [(\hat{x} \pm i\alpha_\pm \hat{y}) \cos kx - i\hat{z}(k/\bar{k}_0) \sin kx] \times \delta \tilde{B}_\pm e^{\kappa z} e^{i(k_0 z - \omega_0 t)} + \text{c.c.},
\end{aligned} \tag{8}$$

where $\alpha_\pm$ are unknown parameters defining the polarization of the Alfvén sidebands and will be determined shortly; the notation $\bar{k}_0 = k_0 - i\kappa$ is used to simplify the expression.

Substituting (7) and (8) into (3)–(6), and eliminating $\delta \tilde{n}_\pm$ from (3) and (5), we first obtain

$$\begin{aligned}
\delta \bar{v}_{e\pm x} &= -(\omega_0/\bar{k}_0) \delta \tilde{B}_\pm / B_0, \\
\delta \bar{v}_{e\pm y} &= -\alpha_\pm (\omega_0/\bar{k}_0) \delta \tilde{B}_\pm / B_0, \\
\delta \bar{v}_{i\pm x} &= [(k_0 v_A^2/\omega_0)(\tilde{n}_s/n_0)(B_{p\pm}/B_0) - (\bar{k}_0 \Omega_i^2/k^2 \omega_0)(\omega_0^2/\bar{k}_0^2 c_s^2 - 1) \times (1 \mp \alpha_\pm \omega_0/\Omega_i)(\delta \tilde{B}_\pm / B_0)]/f, \\
\delta \bar{v}_{i\pm y} &= \mp (\Omega_i/\omega_0)\{(k_0 v_A^2/\omega_0)(\tilde{n}_s/n_0)(B_{p\pm}/B_0) + (\omega_0/\bar{k}_0)[1 + (\bar{k}_0/k)^2(\Omega_i/\omega_0) \times (\omega_0^2/\bar{k}_0^2 c_s^2 - 1)(\pm \alpha_\pm - \omega_0/\Omega_i)] \times (\delta \tilde{B}_\pm / B_0)\}/f, \\
\delta \bar{v}_{i\pm z} &= -(\bar{k}_0/k)(\Omega_i/\omega_0)^2 [(1 - \omega_0^2/\Omega_i^2) \times (k_0 v_A^2/\omega_0)(\tilde{n}_s/n_0)(B_{p\pm}/B_0) + (\omega_0/\bar{k}_0)(1 \mp \alpha_\pm \omega_0/\Omega_i)(\delta \tilde{B}_\pm / B_0)]/f, \\
\delta \bar{v}_{e\pm z} &= \delta \bar{v}_{i\pm z} \pm \alpha_\pm (k v_A^2/\Omega_i)(\delta \tilde{B}_\pm / B_0),
\end{aligned} \tag{9}$$

where $f = 1 + (\bar{k}_0/k)^2(\Omega_i/\omega_0)^2(1 - \omega_0^2/\Omega_i^2)(\omega_0^2/\bar{k}_0^2 c_s^2 - 1)$.

The x and y components of (6) are the two remaining equations. Incorporating the relations of (9) in those two remaining equations leads to the determination of the parameter

$$\alpha_{\pm} = \{(1 \pm \omega_0/\Omega_i)[1 - (\bar{k}_0/k)^2(\omega_0^2/\bar{k}_0^2 c_s^2 - 1)] + (f \pm \Omega_i/\omega_0)(\bar{k}_0^2 v_A^2/\Omega_i^2) \times (1 + k^2/\bar{k}_0^2)\}/\{(1/f \pm \omega_0/\Omega_i) \times [1 - (\bar{k}_0/k)^2(\omega_0^2/\bar{k}_0^2 c_s^2 - 1)] + (1 - \Omega_i^2/\omega_0^2 f) \times [f\bar{k}_0^2 v_A^2/\Omega_i^2 - (\bar{k}_0/k)^2(\omega_0^2/\bar{k}_0^2 c_s^2 - 1)]\} \quad (10)$$

and that of a single mode equation for the combined Alfvén sidebands

$$\{1 - (\bar{k}_0/k)^2(\Omega_i/\omega_0)^2(1 \mp \alpha_{\pm}\omega_0/\Omega_i)(\omega_0^2/\bar{k}_0^2 c_s^2 - 1) f \mp \alpha_{\pm}(\bar{k}_0^2 v_A^2/\Omega_i\omega_0)\}(\delta\bar{B}_{\pm}/B_0) = -(1/f \pm \omega_0/\Omega_i)(\bar{k}_0 k_0 v_A^2/\omega_0^2) \times (\tilde{n}_s/n_0)(B_{p\pm}/B_0). \quad (11)$$

Equation (11) shows that the sideband fields are produced by scattering the pump off the density perturbation induced by the radiation pressure force. From the z component of the one-fluid momentum transfer equation, the density perturbation induced by the radiation pressure force is governed by

$$c_s^2 \frac{\partial}{\partial z}\frac{n_s}{n_0} = -\frac{F_{ez} + F_{iz}}{M_i}, \quad (12)$$

where F_{ez} and F_{iz} are the radiation pressure forces on electrons and ions, respectively, and are given by

$$\frac{F_{e,iz}}{m_{e,i}} = \frac{\partial}{\partial z}\left[\mathbf{v}_{pe,i\pm} \cdot \delta\mathbf{v}^*_{e,i\pm} - i\epsilon_{e,i}\left(\frac{\Omega_{e,i}}{\omega_0}\right) \times (\hat{z} \cdot \mathbf{v}_{pe,i\pm} \times \delta\mathbf{v}^*_{e,i\pm})\right] + \text{c.c.}, \quad (13)$$

where $\epsilon_{e,i} = \pm 1$.

Substituting (2), (7), (8), and (9) into (13), yields

$$\frac{\tilde{n}_s}{n_0} = \left[\frac{\bar{k}_0^*}{k_0}\left(\alpha^*_{\pm} + 1 + \frac{k^2}{\bar{k}_0^{*2}}\right)\frac{\delta\bar{B}^*_{\pm}}{B_0} + \text{c.c.}\right] \times \frac{B_{p\pm}/B_0}{[c_s^2/v_A^2 + 4(B_{p\pm}/B_0)^2]}. \quad (14)$$

This equation gives the nonoscillatory density perturbations as a function of the pump and sidebands. Thus Eqs. (11) and (14) form a complete coupled set of equations describing the convective filamentation instability of circularly polarized Alfvén waves.

III. DISPERSION RELATION

Substituting (14) into (11), one equation relating $\delta\bar{B}_{\pm}$ to its complex conjugate $\delta\bar{B}^*_{\pm}$ is obtained. This equation, together with its complex conjugate, leads to a dispersion relation as

$$|\{1 - (\bar{k}_0/k)^2(\Omega_i/\omega_0)^2(1 \mp \alpha_{\pm}\omega_0/\Omega_i) \times (\omega_0^2/\bar{k}_0^2 c_s^2 - 1)/f \mp \alpha_{\pm}(\bar{k}_0^2 v_A^2/\Omega_i\omega_0) + (1/f \pm \omega_0/\Omega_i)(\bar{k}_0^2 v_A^2/\omega_0^2)(\alpha_{\pm} + 1 + k^2/\bar{k}_0^2) \times (B_{p\pm}/B_0)^2/[c_s^2/v_A^2 + 4(B_{p\pm}/B_0)^2]\}|^2 = |\{(1/f \pm \omega_0/\Omega_i)(|\bar{k}_0|^2 v_A^2/\omega_0^2)(\alpha^*_{\pm} + 1 + k^2/\bar{k}_0^{*2}) \times (B_{p\pm}/B_0)^2/[c_s^2/v_A^2 + 4(B_{p\pm}/B_0)^2]\}|^2. \quad (15)$$

This is a general expression of the dispersion relation for the convective filamentation instability of circularly polarized Alfvén waves. It is analyzed in the following to determine the threshold conditions and the growth rate of the instability.

We first determine the threshold conditions. Let $\kappa = 0$, i.e., $\bar{k}_0 = k_0$. Equation (15) is then solved to obtain the threshold intensity to be

$$(B_{p\pm}/B_0)^2_{\text{th}} = -(\beta/2)A_{\pm}/(B_{\pm} + 2A_{\pm}), \quad (16)$$

where $\beta = c_s^2/v_A^2$ is the ratio of the plasma kinetic pressure to the background magnetic pressure;

$$A_{\pm} = 1 - (k_0/k)^2(\Omega_i/\omega_0)^2(1 \mp \alpha_{0\pm}\omega_0/\Omega_i) \times (\omega_0^2/k_0^2 c_s^2 - 1)/f_0 \mp \alpha_{0\pm}(k_0^2 v_A^2/\Omega_i\omega_0);$$

$$B_{\pm} = (1/f_0 \pm \omega_0/\Omega_i)(k_0^2 v_A^2/\omega_0^2)(\alpha_{0\pm} + 1 + k^2/k_0^2);$$

$$\alpha_{0\pm} = \alpha_{\pm}|_{\bar{k}_0 = k_0} \text{ and } f_0 = f|_{\bar{k}_0 = k_0}.$$

From (16), $A_{\pm}/(B_{\pm} + 2A_{\pm}) < 0$ is the additional criterion of the instability. This criterion limits the regions of k of the instability. It can be manifested by a simple example. Considering a special case that $\beta = (1 \pm \omega_0/\Omega_i)$, it sets $\omega_0^2/k_0^2 c_s^2 - 1 = 0$. Thus, $f_0 = 1$,

$$\alpha_{0\pm} = \pm\tfrac{1}{2}(\Omega_i/\omega_0)[1 \pm (\omega_0/\Omega_i)(2 + k^2/k_0^2)],$$

$$A_{\pm} = (1/2\beta)[1 \mp (\omega_0/\Omega_i)(k^2/k_0^2)],$$

and

$$B_{\pm} = (2 + 3k^2/2k_0^2) \pm \tfrac{1}{2}(\Omega_i/\omega_0).$$

Now, we have to analyze separately the criterion for each pump polarization.

A. Right-hand (RH) circular polarization (+)

Here $B_+ + 2A_+ = (2 + 1/\beta + \frac{1}{2}\Omega_i/\omega_0) + [\frac{3}{2} - (1/\beta)(\omega_0/\Omega_i)](k^2/k_0^2)$; since $\beta > 1$ and $\omega_0/\Omega_i < 1$, $B_+ + 2A_+ > 0$ for all k. Hence the criterion reduced to $A_+ < 0$, which leads to the condition $k^2/k_0^2 > \Omega_i/\omega_0$ for the instability.

B. Left-hand (LH) circular polarization (−)

Since $A_- > 0$, it requires that

$$B_- + 2A_- = [2 - \tfrac{1}{2}(\Omega_i/\omega_0) + 1/\beta] + [\tfrac{3}{2} + (1/\beta)(\omega_0/\Omega_i)](k^2/k_0^2) < 0.$$

The region of k of the instability is then derived to be

$$k^2/k_0^2 < [\tfrac{1}{2}(\Omega_i/\omega_0) - 2 - 1/\beta]/[\tfrac{3}{2} + (1/\beta)(\omega_0/\Omega_i)],$$

providing that $\omega_0/\Omega_i < 2/(7 + \sqrt{33}) \sim 0.157$.

For the general case, i.e., arbitrary values of β, the unstable region of k imposed by the criterion can be determined numerically.

In the RH case, $A_+(k,\beta,\omega_0)$ has a zero at $k = k_2(\beta,\Omega_0)$, and $A_+ < 0$ for $k > k_2$, and $A_+ > 0$ for $k < k_2$. It is shown that $B_+ + 2A_+ > 0$ for all k in the region $\beta > 1 + \omega_0/\Omega_i$. However, $B_+ + 2A_+$ also has a zero at $k = k_1(\beta,\omega_0)$ for $\beta \leq 1 + \omega_0/\Omega_i$ and thus, $B_+ + 2A_+$ becomes negative in the region $k < k_1$. The dependences of $\bar{k}_1$ and $\bar{k}_2$ on β for two cases of $\bar{\omega}_0 = 0.3$ and 0.01 are presented in Fig. 1, where

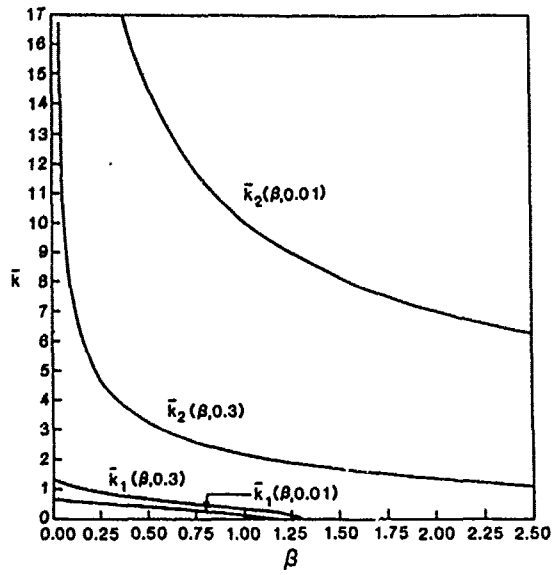

FIG. 1. Boundary curves $\bar{k}_1(\beta,\bar{\omega}_0)$ and $\bar{k}_2(\beta,\bar{\omega}_0)$ divide $\bar{k}$-β space into three regions, where $\bar{k} = k/k_0$. Instability is forbidden in the region between two curves. Two cases for $\bar{\omega}_0 = 0.3$ and 0.01 are presented for the RH circularly polarized pump.

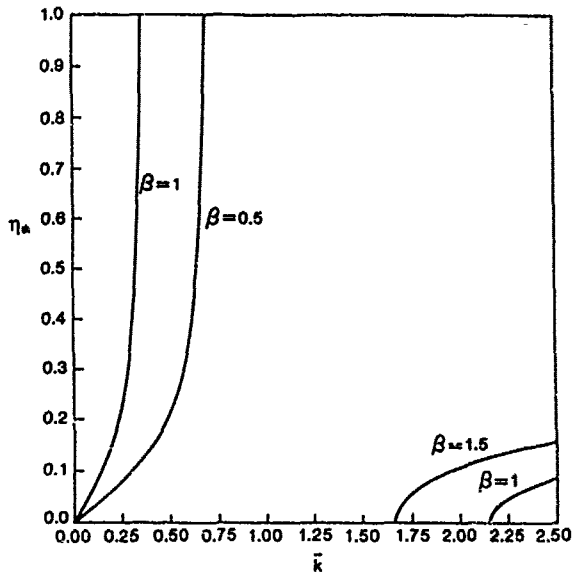

FIG. 3. The dependence of the threshold field on wavenumber $\bar{k}$ and plasma β for RH pump having frequency $\bar{\omega}_0 = 0.3$.

$\bar{k}_1 = k_1/k_0$, $\bar{k}_2 = k_2/k_0$, and $\bar{\omega}_0 = \omega_0/\Omega_1$ are normalized quantities. These two curves $\bar{k}_1$ and $\bar{k}_2$ divide the k-β space into three regions and $A_+/(B_+ + 2A_+) > 0$ in the central region. Therefore there are two instability regions $0 < k < k_1$ and $k > k_2$ for $\beta < 1 + \bar{\omega}_0$, and only one instability region $k > k_2$ for $\beta > 1 + \bar{\omega}_0$. In other words, both large and small scale filamentation instability can be excited by the RH Alfvén pump in low beta plasma, while only small scale instability exists in very high beta plasma.

In the LH case, A_- is always positive. However, the sign of $B_- + 2A_-$ depends on k, β, and $\bar{\omega}_0$. For large $\bar{\omega}_0$ (e.g., $\bar{\omega}_0 = 0.3$), $B_- + 2A_-$ has only a single zero at $k = k_1(\beta,\omega_0)$ for $\beta < \beta_1$ and $B_- + 2A_- < 0$ for $0 < k < k_1$; as $\bar{\omega}_0$ becomes very small (e.g., $\bar{\omega}_0 = 0.01$), two zeros of $B_- + 2A_-$ are present at $k = k_3$ and k_1, respectively, where $k_3 < k_1$ and k_3 exists only for β larger than a constant value β_3. Again, $B_- + 2A_- < 0$ for $(0,k_3) < k < k_1$. These boundary curves defined by $\bar{k}_1$ and $\bar{k}_3$ are shown in Fig. 2 for two cases of $\bar{\omega}_0 = 0.01$ and 0.3. It shows that, for $\bar{\omega}_0 = 0.01$, $\bar{k}_1$ exists in the entire β region and $\bar{k}_3$ exists only for $\beta > 0.99 = \beta_3$; however, only $\bar{k}_1$ exists in the region $\beta < 0.7$ for $\bar{\omega}_0 = 0.3$. In any event, instability exists only in the region below the $\bar{k}_1$ curve and above the $\bar{k}_3$ curve or the zero line.

Presented in Figs. 3–6 are the dependence of the normalized threshold field $\eta_{th} = (B_{p\pm}/B_0)_{th}$, defined by (16) on

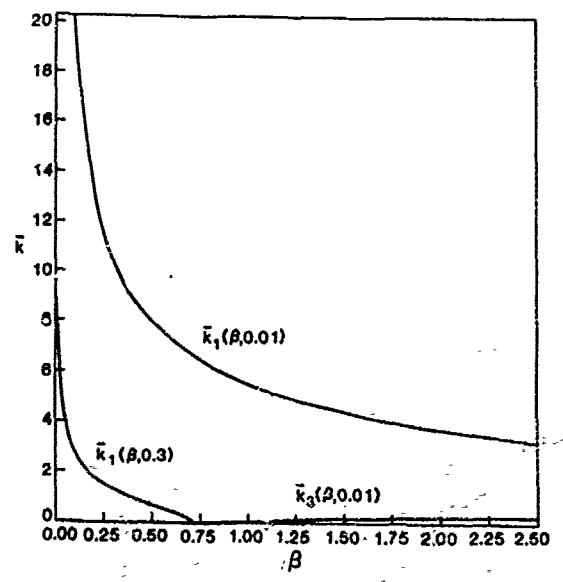

FIG. 2. For the LH pump case, the instability region in $\bar{k}$-β space is confined between either $\bar{k}_1(\beta,\bar{\omega}_0)$ and $\bar{k}_3(\beta,\bar{\omega}_0)$ curves or the $\bar{k}_1$ curve and $\bar{k} = 0$ line.

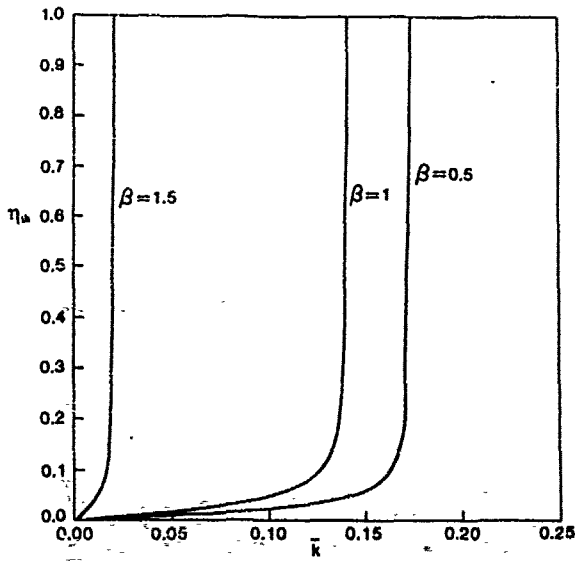

FIG. 4. Threshold field η_{th} vs $\bar{k}$ and β for a very low frequency, $\bar{\omega}_0 = 0.01$, RH pump. The dependence in very large $\bar{k}$ (> 8) region is not presented.

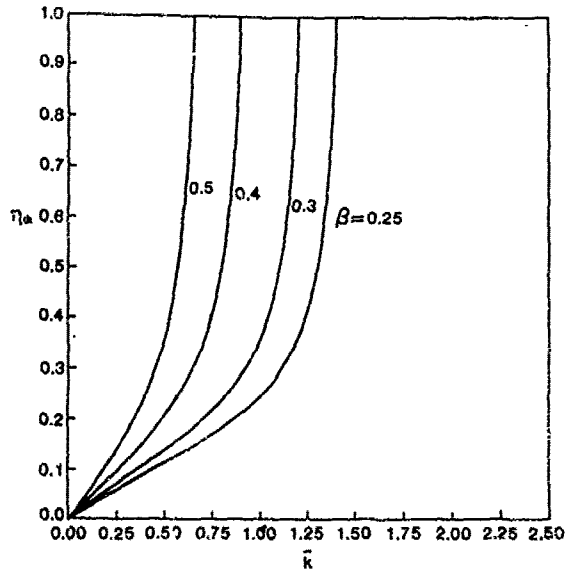

FIG. 5. Threshold versus $\bar{k}$ in four different beta plasmas for the case of a LH pump with frequency $\bar{\omega}_0 = 0.3$.

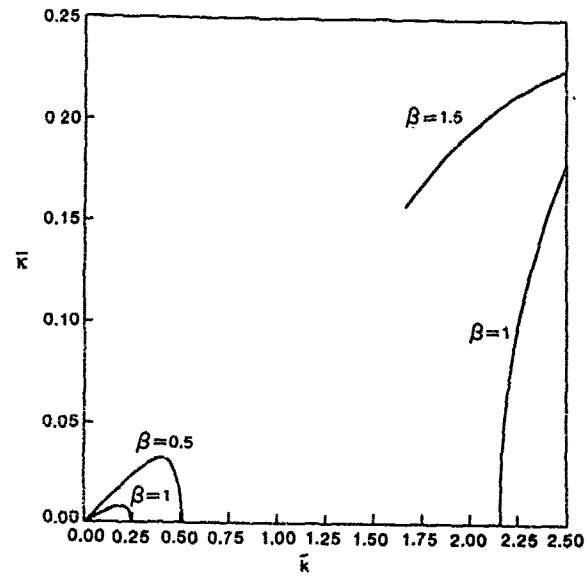

FIG. 7. The dependence of the spatial growth rate $\bar{\kappa}$ on $\bar{k}$ and β for the $\bar{\omega}_0 = 0.3$ RH pump having intensity $\eta^2 = 0.05$, where $\bar{\kappa} = \kappa/k_0$.

$\bar{k} = k/k_0$, where $\bar{k}$ is limited to the range of 2.5 so that the finite Larmor radius effect is still small and thus does not invalidate the fluid model of the present work. Figures 3 and 4 are the results of RH circularly polarized pump for $\bar{\omega}_0 = 0.3$ and 0.01 cases, respectively. In each case, three values of $\beta = 0.5$, 1.0, and 1.5 are considered. The results show that the threshold field increases with β and k in each instability region. Moreover, the threshold field increases very fast with k in the lower $\bar{k}$ region (i.e., $0 < \bar{k} < k_1$) and becomes infinite at $\bar{k} = \bar{k}_1$.

Figures 5 and 6 correspond to LH pump wave. Again, $\bar{\omega}_0 = 0.3$ and 0.01 are used, respectively, as the representative parametric values. For the high frequency pump case, $\bar{\omega}_0 = 0.3$, instability can only be excited in the relatively low β plasma, $\beta < 0.7$. As $\bar{\omega}_0$ reduces to 0.01, instability exists in all β ranges of interest. The results show that the threshold field also increases with β and k and in general, decreases with $\bar{\omega}_0$. It becomes infinite at $\bar{k} = \bar{k}_1$ and $\bar{k} = \bar{k}_3$ (Fig. 6 for $\beta = 1$ and 1.5 cases).

We next present the growth rate of the instability. Assuming that the pump intensity $\eta^2 = (B_{w\pm}/B_0)^2 = 0.05$, (15) is then solved for the spatial growth rate κ. Shown in Figs. 7–10 are the functional dependences of the normalized growth rate $\bar{\kappa} = \kappa/k_0$ on $\bar{k}$ and β for $\bar{\omega}_0 = 0.3$ and 0.01 and for RH and LH pump cases, respectively. For the RH pump (Figs. 7 and 8), the growth rate of small-scale instability ($\bar{k} > 1$) appears to increase with β, while the growth rate of large-scale instability ($\bar{k} < 1$) decreases with β. In general,

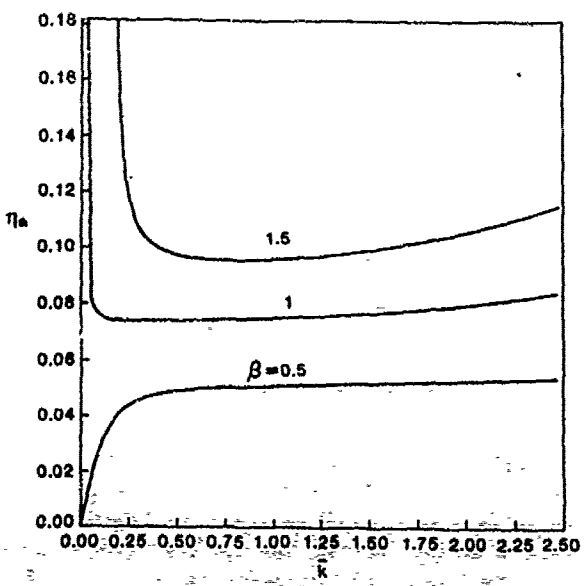

FIG. 6. Threshold versus $\bar{k}$ and β for the $\bar{\omega}_0 = 0.01$ LH pump.

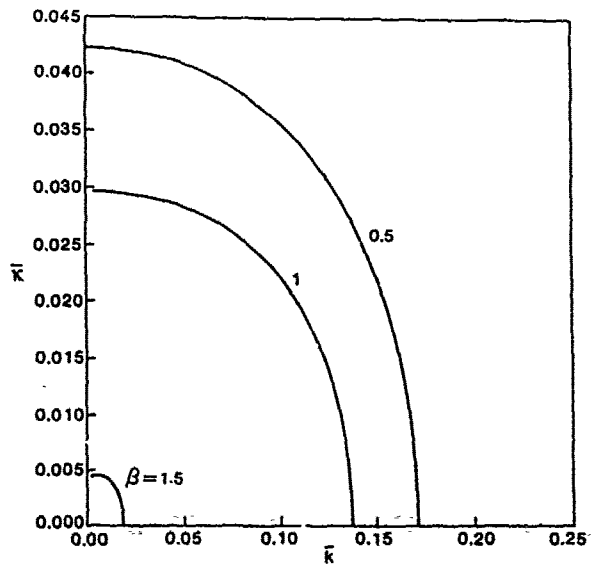

FIG. 8. Growth rate versus $\bar{k}$ and β for the $\bar{\omega}_0 = 0.01$ and $\eta^2 = 0.05$ RH pump.

the growth rate of small-scale instability is found to be larger than that of large-scale instability. Figures 9 and 10 correspond to the LH pump and $\bar{\omega}_0 = 0.3$ and 0.01, respectively. In the high-frequency pump case, the growth rate always has a peak in the unstable band. The peak growth rate tends to decrease with β, except in the region near $\beta = 0.5$, the peak growth rate increases again and then decreases to zero at $\beta = 0.7$. For the low-frequency case, the dependence becomes quite irregular. This is because there is an extra forbidden region $0 < k < k_3$ for $\beta > \beta_3 = 0.99$ (for the $\bar{\omega}_0 = 0.01$ case). In general, the growth rate decreases with β for $\beta < 0.99$ and increases with β for $\beta > 0.99$. The growth rate also has a finite jump near $k = k_3$ for the $\beta > 0.99$ case. This is because the threshold approaches quickly to infinite at $k = k_3$.

IV. SUMMARY AND DISCUSSION

The convective filamentation instabilities of large-amplitude, circularly polarized Alfvén waves propagating along the background magnetic field have been studied. Similar to the absolute filamentation instability process,[11] the convective instabilities are also excited via the scattering of the unperturbed Alfvén pumps into sidebands by the simultaneously excited purely growing density perturbations. The nonlinear source for the Alfvén sidebands is also the same. It is the beating current driven by the pump wave field on the density perturbation of the purely growing mode. However, the characteristic features of the two instability processes are quite different. The absolute instability grows in time, while the convective instability grows spatially along the path of the pump. The purely growing density perturbation is associated with the magnetostatic mode for the absolute instability, it becomes an electrostatic mode in the convective case. The nonlinear forces generated to drive the purely growing modes are also different. The magnetostatic mode is driven by a transverse nonlinear Lorentz force, while the electrostatic mode is driven by an axially directed nonlinear Lorentz force. Consequently, the dispersion relations and the results of threshold field and growth rate are all different for each instability process. Solving the dispersion relation (15), we have determined the threshold fields and growth rates of the convective filamentation instabilities for the cases of the RH and LH circularly polarized pump waves. We have also determined the functional dependences of the threshold field η_{th} on the wavenumber $\bar{k}$ of the nonoscillatory mode, the β of the plasma, and the frequency $\bar{\omega}_0$ of the pump (see Figs. 3–6). Similar dependences for the spatial growth rate $\bar{\kappa} = \kappa/k_0$ for pump intensity $\eta^2 = 0.05$ have been examined and presented in Figs. 7–10.

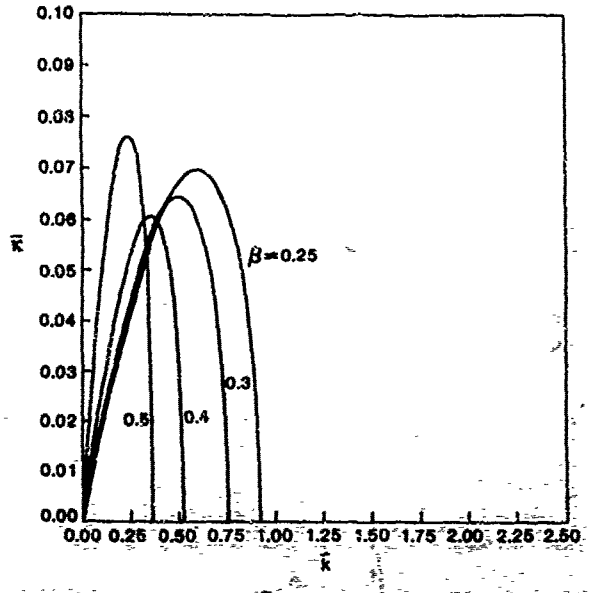

FIG. 9. Growth rate versus $\bar{k}$ and β for the $\bar{\omega}_0 = 0.3$ and $\eta^2 = 0.05$ LH pump.

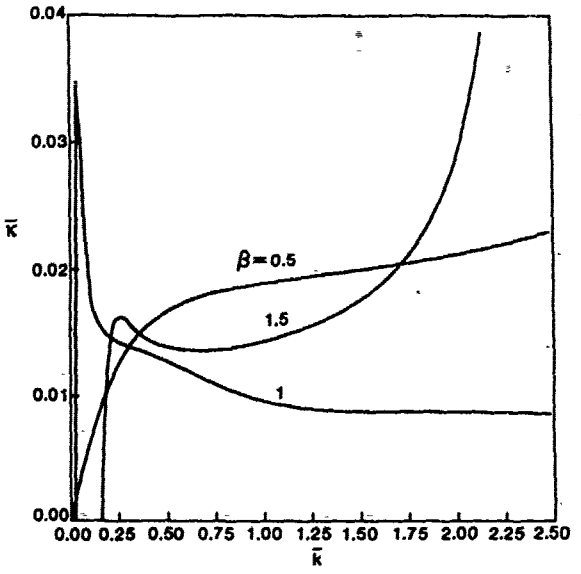

FIG. 10. Growth rate versus $\bar{k}$ and β for the $\bar{\omega}_0 = 0.01$ and $\eta^2 = 0.05$ LH pump.

We now apply the results of the proposed instability process to explain some of the observations associated with large-amplitude, low-frequency Alfvénic fluctuations appearing in the solar wind, in the upstream regions of planetary bow shock, and in the interplanetary shock. For the high-frequency pump case, e.g., $\bar{\omega}_0 = 0.3$, instability can be excited by both the RH and LH pump in low β (< 0.7) plasmas, however, only the RH pump is unstable in the high β (> 1) plasmas. The finite amplitude Alfvén waves that were observed in the high-speed streams of the solar wind and discussed by Abraham-Shrauner and Feldman are the left-hand circularly polarized waves with $\bar{\omega}_0 = 0.3$ and $\eta^2 = 0.05$. The results of Fig. 9 indicate that these waves are stable to the proposed instability for $\beta > 0.7$ and become unstable for $\beta < 0.7$. The high-frequency, right-hand polarized waves have been observed in the interplanetary shocks and in the terrestrial foreshock. Figure 7 shows that these waves are unstable in general and the excited instability has larger growth rate in high beta plasma and larger $\bar{k}$ (> 1) region.

Low-frequency, left-hand circularly polarized Alfvén waves have been observed in the upstream part of the Jovian bow shock. As shown in Fig. 10, these waves are unstable in both small beta and large beta plasma. The k spectrum of the

instability is also very broad. Though the observed frequency is about $\bar{\omega}_0 = 0.02$, the results of Fig. 10 for $\bar{\omega}_0 = 0.01$ are qualitatively the same and hence, no additional figure is presented. The proposed instability is also found unstable against the low-frequency RH pump in the very small $\bar{k}$ region. As shown in Fig. 8, the instability prefers to be excited in the low beta plasma. The existence of RH waves can be speculated, because in such a low-frequency region the dispersion relations of right- and left-hand circularly polarized Alfvén waves are almost identical.

In general, the instability conditions for the RH pump and the LH pump are different, even in the low-frequency region where Alfvén modes become approximately degenerate. This is because the sidebands in both cases are elliptically polarized and shear mode in nature, while the pumps are circularly polarized in the opposite sense. Thus the induced nonlinear Lorentz forces on electrons and ions are different for differently polarized pumps. Consequently, different instability conditions are required by differently polarized pumps.

ACKNOWLEDGMENTS

The computations were carried out at the Pittsburgh Supercomputing Center of the National Science Foundation.

This work was supported by the Air Force Office of Scientific Research, Air Force Systems Command, under Grant No. AFOSR-88-0127 and Grant No. AFOSR-85-0316.

[1]B. Abraham-Shrauner and W. C. Feldman, J. Geophys. Res. **82**, 618 (1977).
[2]M. L. Goldstein, H. K. Wong, A. F. Vinas, and C. W. Smith, J. Geophys. Res. **90**, 302 (1985).
[3]A. F. Vinas, M. L. Goldstein, and M. H. Acuna, J. Geophys. Res. **89**, 6813 (1984).
[4]C. W. Smith, M. L. Goldstein, S. P. Gary, and C. T. Russel, J. Geophys. Res. **90**, 1429 (1985).
[5]W. I. Axford, E. Leer, and G. Skadron, in *Proceedings of the 15th International Cosmic Ray Conference* (Bulgarian Academy of Sciences, Plovdiv, 1977), Vol. 2, p. 273.
[6]R. Blandford and D. Eicher, Phys. Rep. 154, **1**, 1 (1987).
[7]C. F. Kennel, in *Proceedings of the International Rosenbluth Symposium* (University of Texas, Austin, 1987).
[8]H. K. Wong and M. L. Goldstein, J. Geophys. Res. **91**, 5617 (1986).
[9]T. Terasawa, M. Hosbino, J. I. Sakai, and T. Hada, J. Geophys. Res. **91**, 4171 (1986).
[10]M. Longtin and B. U. O. Sunnerup, J. Geophys. Res. **91**, 6816 (1986).
[11]S. P. Kuo, M. H. Whang, and M. C. Lee, J. Geophys. Res. **93**, 9, 9621 (1988).
[12]S. R. Spangler, Astrophys. J. **299**, 122 (1985).
[13]B. T. Tsurutani and G. J. Smith, Geophys. Res. Lett. **13**, 259, 263 (1986).
[14]A. A. Galeev and V. N. Oraevskii, Sov. Phys. Dokl. **7**, 988 (1963).
[15]R. Cohen and R. Dewar, J. Geophys. Res. **79**, 4170 (1974).
[16]C. N. Lashmore-Davies, Phys. Fluids **19**, 587 (1976).
[17]M. L. Goldstein, Astrophys. J. **219**, 700 (1978).
[18]N. F. Derby, Astrophys. J. **22**, 1013 (1978).
[19]J. Sakai and B. U. O. Sonnerup, J. Geophys. Res. **88**, 9069 (1983).
[20]J. Mio, T. Ogino, K. Minami, and S. Takeda, J. Phys. Soc. Jpn. **41**, 265, 667 (1976).
[21]E. Mjoljus, J. Plasma Phys. **16**, 321 (1976).
[22]S. R. Spangler and J. P. Sheerin, Astrophys. J. **272**, 273 (1983).
[23]C. R. Ovenden, H. A. Shah, and S. J. Schwartz, J. Geophys. Res. **88**, 6095 (1983).
[24]S. P. Kuo and G. Schmidt, Phys. Fluids **26**, 2529 (1983).
[25]S. P. Kuo and M. C. Lee, Geophys. Res. Lett. **10**, 978 (1983).
[26]M. C. Lee and S. P. Kuo, J. Geophys. Res. **89**, 2289 (1984).
[27]L. Stenflo and P. K. Shukla, J. Geophys. Res. **93**, 4115 (1988).

JOURNAL OF GEOPHYSICAL RESEARCH, VOL. 94, NO. A10, PAGES 13,387-13,395, OCTOBER 1, 1989

FILAMENTATION INSTABILITY OF MAGNETOSONIC WAVES IN THE SOLAR WIND ENVIRONMENT

S. P. Kuo
Weber Research Institute, Polytechnic University, Farmingdale, New York

M.C. Lee
Massachusetts Institute of Technology, Cambridge

Abstract. Intense magnetosonic waves, originally propagating at the right angle with the interplanetary magnetic field, can excite a purely growing mode along the interplanetary magnetic field together with two symmetric magnetosonic sidebands propagating obliquely across the magnetic field. This instability process leads to the filamentation of the magnetosonic pump waves. These two excited magnetosonic sideband modes propagate together perpendicularly across the magnetic field and, meanwhile, form a standing wave pattern along the magnetic field. The thresholds of this filamentation instability can be exceeded in the solar wind environment. It is predicted that the density fluctuations produced by the filamentation instability along the interplanetary magnetic field have wavelengths greater than, at least, a few Earth radii. The polarization of the obliquely propagating magnetosonic waves excited by the filamentation instability is determined by the characteristics of the magnetosonic pump waves and the environmental plasmas.

Introduction

Recently, there has been a considerable effort in the study of the stability of Alfven waves in the space plasmas. It is attributed to the frequent appearance, as detected by the space crafts, of large-amplitude Alfven waves in the high-speed streams of the solar wind [Abraham-Shranner and Feldman, 1977], in the upstream Jovian bow shocks [Goldstein et al., 1985], and in the interplanetary shocks [Vinas et al., 1984]. In general, these waves appear to be circular polarization and propagating along the background magnetic field. Moreover, the ISEE 1 and 2 spacecrafts have detected both magnetosonic waves and Alfven waves propagating upstream into the solar wind with phase velocities much less than the solar wind velocity. Hence, these waves are blown backward over the spacecraft and, consequently, an apparent change in polarization of waves occurs. Intrinsically right (left) hand polarized waves are seen to have an apparent left (right) handed polarization in spacecraft records [Hoppe and Russell, 1983].

The parametric decay instability and modulation instability of large-amplitude, circularly polarized Alfven waves propagating in the solar wind along the magnetic field have been analyzed extensively by Lashmore-Davies [1976], Goldstein [1978], Derby [1978], Wong and Goldstein [1986], Longtin and Sonnerup [1986], and Terasawa et al [1986]. The filamentation instability, competing with these instabilities, can break up the large-amplitude Alfven waves and induce not only plasma density fluctuations but magnetostatic fluctuations [Kuo et al., 1988]. Starting from small perturbations in plasma density, the filamentation instability gives rise to a modulation of the plasma dielectric constant and then wave distribution that, in turn, enhances the density perturbations.

The modulation instability has also been analyzed in the region that describes the nonlinear evolution of the Alfven wave propagating along a background magnetic field. It is shown that this evolution can be governed by a single "derivative nonlinear Schrodinger equation" [Mjolhus, 1976; Spangler, 1986; Hada et al, 1989]. The possible applications of Alfven solitons to solar and astrophysical plasmas have been discussed by Ovenden et al [1983] and Spangler [1985].

While significant research has been directed to the Alfven waves, the magnetosonic waves have received much less attention. The magnetosonic waves are hybrid and elliptically polarized modes that can propagate obliquely across the magnetic field. They become decoupled from the Alfven waves when the direction of their propagation is exactly perpendicular to the ambient magnetic field. The purpose of the present work is to investigate the filamentation instability of the magnetosonic waves that propagate perpendicularly across the magnetic field. This instability excited obliquely propagating magnetosonic sideband modes. The concomitantly excited nonoscillatory (purely growing) modes have their wave normal parallel to the magnetic field. By contrast, the purely growing modes excited by the filamentation instability of Alfven waves are magnetic field-aligned [Kuo et al., 1988, 1989]. Hence, the characteristics of the filamentation instability under consideration are distinctively different from those of the instability discussed in our previous work [Kuo et al., 1988, 1989].

This paper is organized as follows. The coupled mode equations are derived in section 2. They show how the magnetosonic sidebands and the purely growing modes are parametrically coupled through the magnetosonic pump wave. In section 3 the dispersion relation is obtained and analyzed to derive the threshold conditions and the growth rates of the filamentation instability. The relevance of the present work to some observations is discussed. Finally presented in section 4 are summary and conclusions.

Filamentation Instability of Magnetosonic Waves

Consider a magnetosonic wave propagating perpendicularly across the interplanetary magnetic field $\vec{B}_0=\hat{z}B_0$. Its wave magnetic field is represented by

$$\vec{B}_p = \hat{z}B_p\exp[i(k_0x-\omega_0t)] + \text{c.c.} \qquad (1)$$

where the unperturbed wave field intensity B_p is assumed to be constant and a real quantity for simplicity. The wave number k_0 and the angular frequency ω_0 are related by the dispersion relation $\omega_0^2=k_0^2(v_A^2+c_s^2)$, wherein v_A and c_s are the Alfven speed and the ion acoustic speed, respectively. The velocity

Paper number 89JA00987.
0148-0227/89/89JA-00987$05.00

responses of electrons and ions to the magnetosonic pump wave can be written as

$$\vec{v}_{pz} = [\hat{x}+i(k_0^2 v_A^2/\omega_0\Omega_i)\hat{y}](\omega_0/k_0)(B_p/B_0)\exp[i(k_0 x-\omega_0 t)] + \text{c.c.}$$
$$\vec{v}_{pi} = \hat{x}(\omega_0/k_0)(B_p/B_0)\exp[i(k_0 x-\omega_0 t)] + \text{c.c.} \qquad (2)$$

In the following we will investigate a filamentation instability which can break up a large-amplitude magnetosonic wave into filaments. The magnetosonic wave is assumed to be initially uniform as described by (1) for simplicity. The filamentation instability results from small fluctuations in plasma density which lead to modulation of plasma dielectric constant and spatial wave distribution, which, in turn, enhance the plasma density fluctuations. Such a positive feedback process involves a four-wave coupling process: through the magnetosonic pump wave $(\omega_0,\vec{k}_0)$, two side-band perturbations $(\omega_\pm)$ are coupled with a purely growing density perturbation $(\omega,k\hat{z})$. The wave frequency and wave vector matching conditions, are $\omega_+-\omega=\omega_0=\omega_-+\omega^*$ and $\vec{k}_\pm=\vec{k}_0\pm\vec{k}$, are satisfied where the asterisk denotes the complex conjugate. Illustrated in Figure 1 is the wavevector matching condition, showing the relative orientation of these wave vectors. It will be sown that these perturbations can be excited simultaneously. In other words, they grow exponentially with the same growth rate, $\gamma=-i\omega$ at the expense of magnetosonic pump wave energy. This instability requires a threshold to occur, which is going to be determined later. In the analysis of filamentation instability, pump field intensity is assumed to be a constant maintained by a source. Pump depletion effect which may contribute to the saturation of filamentation instability is, therefore,ignored withia the present framework of instability analysis.

Our proposed theory is developed on the basis of the two-fluid plasma model. The fluid model is, in general, valid provided that the condition $k^2c_s^2/\Omega_i^2<<1$ is satisfied where k, c_s, and Ω_i are the wave number of the purely growing mode, the ion acoustic speed, and the ion gyrofrequency, respectively. Therefore, the analysis of filamentation instability is limited to the region of $k/k_0\lesssim 1.2$. To analyze the instability, the complete set of fluid equations will be linearized with respect to the first-order perturbations in physical quantities such as density (n), velocity (v), wave electric field $(\vec{E})$ and wave magnetic field $(\vec{B})$. These first-order physical quantities associated with the sideband modes are denoted by $\delta n_\pm$, $\delta\vec{v}_{ej\pm}$,$\delta\vec{E}_\pm$, and $\delta\vec{B}_\pm$ those associated with the purely growing mode n_s, $\vec{v}_{sej}$, $\vec{E}_s$, and $\vec{B}_s$. Thus, the total density is given by $n=n_0+n_0+(\delta n_+ +\delta n_- +\text{c.c.})$; similarly, $\vec{v}_{ej}=\vec{v}_{sej}+(\vec{v}_{pej}+\delta\vec{v}_{ej+}+\delta\vec{v}_{ej-}+\text{c.c.})$ $\vec{E}=\vec{E}_s+(\vec{E}_p+\delta\vec{E}_+ +\delta\vec{E}_- +\text{c.c.})$, and $\vec{B}=\vec{B}_0+(\vec{B}_p+\delta\vec{B}_+ +\delta\vec{B}_- +\text{c.c.})$ for the concerned four-wave interaction process.

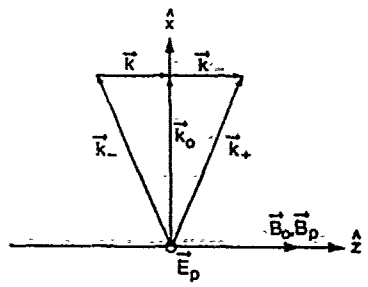

Fig. 1. The relative orientation and wave vector matching relation for the magnetosonic pump $(\omega_0,\vec{k}_0)$, two sidebands $(\omega_\pm,\vec{k}_\pm)$ and the purely growing mode $(\omega,\vec{k})$ as required in the proposed four-wave coupling process.

The purely growing mode is associated with electrostatic disturbances, varying spatially along the magnetic field, i.e., $\vec{k}=\hat{z}k$. The fluid equations used to derive the coupled mode equation for the purely growing mode include the linearized continuity equations for electrons and ions:

$$\frac{\partial n_s}{\partial t} + n_0\frac{\partial}{\partial z}v_{sez} = 0 = \frac{\partial}{\partial t}n_s + n_0\frac{\partial}{\partial z}v_{siz} \qquad (3)$$

and the combined linearized equations of motion for electrons and ions:

$$m_e\frac{\partial}{\partial t}v_{sez} + m_i\frac{\partial}{\partial t}v_{siz} + (F_{es} + F_{is}) = -m_i(c_s^2/n_0)\frac{\partial}{\partial t}n_s$$

In deriving the above equations, quasi-neutrality has been assumed. F_{es} and F_{is} represent the z components of the nonlinear Lorentz forces experienced by electrons and ions, respectively, namely, $F_{ejz}=<-m_{ej}(\vec{v}_{ej}\cdot\nabla\vec{v}_{ej}) + q_{ej}(\vec{v}_{ej}/c)x\vec{B}>_z$ where angle brackets denote the time average over the pump wave period. The explicit expressions of F_{ejz} are given by

$$F_{ejz}/m_{ej} = \frac{\partial}{\partial z}(\vec{v}_{pej}\cdot\delta\vec{v}_{ej}^*) + i\zeta_{ej}\left(\frac{\Omega_{ej}}{\omega_0}\right)\frac{\partial}{\partial z}[\delta v_{ejx}^* v_{pejy} - v_{pejx}\delta v_{ejy}^*] + \text{c.c.} \qquad (4)$$

where $\delta\vec{v}_{ej}=\delta\vec{v}_{ej+}+\delta\vec{v}_{ej-}$ is the velocity responses of electrons and ions to the combined sideband mode; $\zeta_e(\zeta_i)=+1(-1)$. The expression, (4) reduces to the form of ponderomotive force in an unmagnetized plasma. Without losing the generality, the density fluctuations of the purely growing mode can be expressed as

$$n_s = \tilde{n}_s\exp(\gamma t)\cos kz$$

where $\tilde{n}_s$ and γ are the real amplitude and the growth rate of the density fluctuations, respectively.

Combining the equations in (3) yields the coupled mode equation for the purely growing mode as

$$(\gamma^2+k^2c_s^2)(\tilde{n}_s/n_0) = (k/m_i)(\tilde{F}_{es}+\tilde{F}_{is}) \qquad (5)$$

where $F_{ejz}=\tilde{F}_{ejz}\exp(\gamma t)\sin kz$ is assumed. One can see from (4) and (5) that the density fluctuations associated with the purely growing mode stem from the differential interaction of the magnetosonic pump wave and sideband modes. Hence, expressions for the physical quantities of the combined sideband mode have to be determined in a self-consistent manner. The purely growing mode is realized to be a nonlinearly driven mode. However, in the absence of the nonlinear Lorentz force, (5) reduces to the linear dispersion relation of the ion acoustic wave.

The magnetosonic sideband modes are excited through the beating current driven by the magnetosonic pump wave field in the density fluctuations of the purely growing mode. It should be noted that, since the magnetosonic pump wave propagates perpendicularly across the magnetic field and the purely growing mode oscillates spatially along the magnetic field, two magnetosonic sidebands are excited symmetrically around the pump wave and they propagate obliquely across the magnetic field (see Figure 1). Thus, these two sideband modes propagate together in the propagation direction of the pump wave and form a standing wave pattern along the magnetic field. In the following derivation of the coupled mode equations for the two sideband modes, we can, therefore, combine them into a single coupled mode equation for the combined sideband mode.

This combined sideband mode is characterized by the following physical quantities with self-consistent expressions:

$$\delta n = \delta\tilde{n}\exp(\gamma t)\cos kz\exp[i(k_0x-\omega_0t)] + \text{c.c.}$$
$$\delta\vec{v}_{ej} = [(\hat{x}\delta\tilde{v}_{ejx} + i\hat{y}\delta\tilde{v}_{ejy})\cos kz + i\hat{z}\delta\tilde{v}_{ejz}\sin kz]\exp(\gamma t)\cdot\exp[i(k_0x-\omega_0t)] + \text{c.c.}$$
$$\delta\vec{B} = [(k/k_0)(-i\hat{x}+\alpha\hat{y})\sin kz + \hat{z}\cos kz]\delta\tilde{B}\exp(\gamma t)\cdot\exp[i(k_0x-\omega_0t)] + \text{c.c.} \quad (6)$$

where α, an unknown parameter defining the polarizations of the sideband modes, will be determined later on. The fluid equations, used to derive the coupled mode equation for the combined sideband mode, include the linearized continuity equations for electrons and ions:

$$\frac{\partial}{\partial t}(\delta n/n_0) + \nabla\cdot[\delta\vec{v}_e + (n_s/n_0)\vec{v}_{pe}] = 0 = \frac{\partial}{\partial t}(\delta n/n_0) + \nabla\cdot[\delta\vec{v}_i + (n_s/n_0)\vec{v}_{pi}] \quad (7)$$

the linearized Maxwell equation for induction law:

$$\frac{\partial}{\partial t}(\delta\vec{B}/B_0) = \nabla\times(\delta\vec{v}_e\times\hat{z}) \quad (8)$$

the combined equations of motion for electrons and ions:

$$\frac{\partial}{\partial t}\delta\vec{v}_i = -c_s^2\nabla(\delta n/n_0) + \Omega_i(\delta\vec{v}_i-\delta\vec{v}_e)\times\hat{z} \quad (9)$$

and the linearized Maxwell equation for Amperes' law:

$$\nabla\times(\delta\vec{B}/B_0) = (\Omega_i/v_A^2)[(\delta\vec{v}_i-\delta\vec{v}_e) + (n_s/n_0)(\vec{v}_{pi}-\vec{v}_{pe})] \quad (10)$$

Substituting (6) into equations (7)-(10), we obtain

$$\begin{aligned}
\delta\tilde{v}_{ex} &= (\omega_0/k_0)(\delta\tilde{B}/B_0)\\
\delta\tilde{v}_{ey} &= \alpha(\omega_0/k_0)(\delta\tilde{B}/B_0)\\
\delta\tilde{v}_{ix} &= -(\omega_0/k_0)[(k^2_0c^2_s/\Omega^2_i)(\delta\tilde{n}/n_0) - (1-\alpha\omega_0/\Omega_i)(\delta\tilde{B}/B_0)]/(1-\omega^2_0/\Omega^2_i)\\
\delta\tilde{v}_{iy} &= (\omega_0/\Omega_i)\{(k_0c^2_s/\omega_0)(\delta\tilde{n}/n_0) + [\alpha(\Omega_i/\omega_0)-1](\omega_o/k_0)(\delta\tilde{B}/B_0)\}/(1-\omega^2_0/\Omega^2_i)\\
\delta\tilde{v}_{iz} &= (kc^2_s/\omega_0)(\delta\tilde{n}/n_0)\\
\delta\tilde{v}_{ez} &= \delta\tilde{v}_{iz} + \alpha(kv^2_A/\Omega_i)(\delta\tilde{B}/B_0)\\
\delta\tilde{n}/n_0 &= \{[(1-\alpha\omega_0/\Omega_i)/(1-\omega^2_0/\Omega^2_i)](\delta\tilde{B}/B_0) + (\tilde{n}_s/n_0)(B_p/B_0)\}/[1-k^2c^2_s/\omega^2_0 + k^2_0c^2_s/(\Omega^2_i-\omega^2_0)] \quad (11)
\end{aligned}$$

Using the results in (11) together with the x and y components of (10), we can derive the following coupled mode equation for the combined sideband mode:

$$\begin{aligned}
&[\omega^2_0-(k^2+k^2_0)(v^2_A+c^2_s) + k^2(k^2+k^2_0)v^2_Ac^2_s/\omega^2_0\\
&+ \alpha(\omega_0/\Omega_i)[k^2_0c^2_s-\omega^2_0(1-k^2c^2_s/\omega^2_0)]](\delta\tilde{B}/B_0)\\
&= -k^2_0[v^2_A(1-k^2c^2_s/\omega^2_0) - c^2_s](\tilde{n}_s/n_0)(B_p/B_0) \quad (12)
\end{aligned}$$

as well as the expression for the parameter α:

$$\alpha = (\omega_0/\Omega_i)[1-2(k^2+k^2_0)c^2_s/\omega^2_0]/[1-c^2_s/v^2_A-(k^2v^2_A/\omega^2_0)(1-k^2c^2_s/\omega^2_0)] \quad (13)$$

In the derivation of (12) and (13), $\omega^2_0/\Omega^2_i \ll 1$ has been assumed. Equation (12) shows that the magnetosonic sideband fields are produced by the magnetosonic pump field in the density fluctuations of the purely growing mode. Equations (5) and (12) thus form the complete set of coupled mode equations, which can be based on to analyze the proposed filamentation instability of magnetosonic waves in the solar wind environment.

Analysis of the Proposed Instability

The dispersion relation of the concerned instability can be derived from the two coupled mode equations, (5) and (12). Its derivation is briefly described as follows. With the aid of (2), (4), (6), and (11), the coupling term on the right-hand side of (5) can be expressed as

$$\begin{aligned}
k(\tilde{F}_e+\tilde{F}_i)/m_i &= k^2[v^2_A-c^2_s(1-\alpha\omega_0/\Omega_i)/(1-k^2c^2_s/\omega^2_0)](B_p/B_0)(\delta\tilde{B}/B_0+\delta\tilde{B}^*/B_0)\\
&- 2[k^2c^2_s/(1-k^2c^2_s/\omega^2_0)](\tilde{n}_s/n_0)(B_p/B_0)^2 \quad (14)
\end{aligned}$$

Substituting (14) into (5) and combining it with (12) yield the dispersion relation

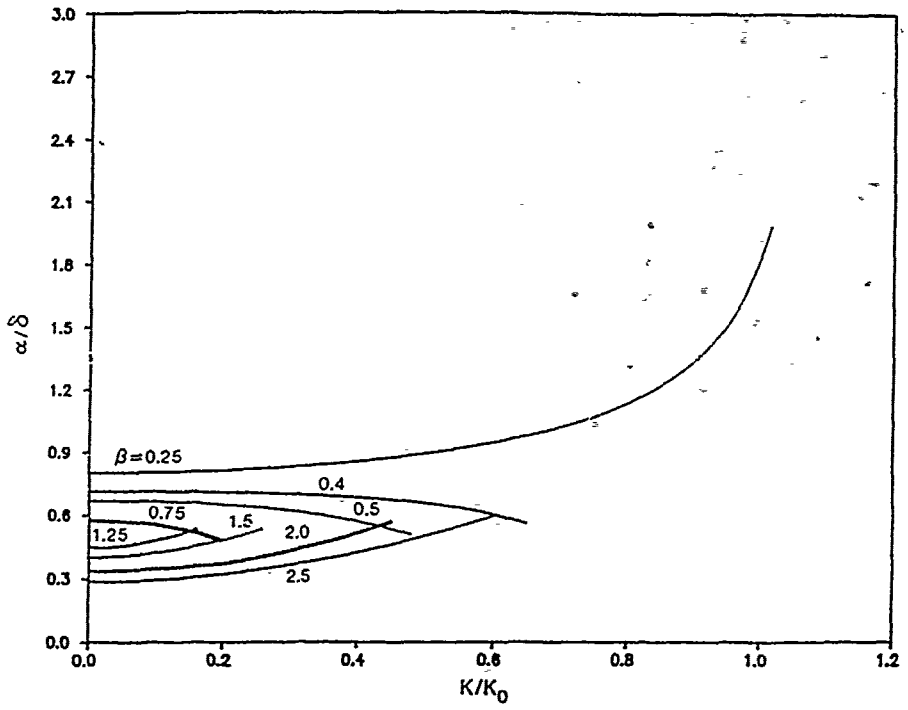

Fig. 2. α/δ versus k/k_0 for several selected values of β in the range of 0.25-2.5; it shows how the polarization of the excited magnetosonic sidebands is determined by the characteristics of the magnetosonic pump waves and the environmental plasmas.

$$\gamma^2+k^2c_s^2 = 2k_0^2v_A^2\{[1-\beta(1+\beta)/(\beta+1-\beta k^2/k_0^2)]$$
$$[1-\beta(1+\beta)(1-\alpha\delta)/(\beta+1-\beta k^2/k_0^2)]$$
$$(\beta+1-\beta k^2/k_0^2)/[(\beta+1)^2-\beta(1+k^2/k_0^2) + \alpha\delta(\beta+1)(k_0^2/k^2-\beta)]$$
$$-(k^2/k_0^2)\beta(\beta+1)/(\beta+1-\beta k^2/k_0^2))(B_p/B_0)^2 \qquad (15)$$

where $\beta=c_s^2/v_A^2$ is the ratio of the plasma kinetic pressure to the background magnetic pressure, and $\delta=\omega_0/\Omega_i$.

Setting $\gamma=0$ in (15) determines the threshold field of the filamentation instability

$$(B_{pth}/B_0)^2 = (k^2/2k_0^2)\beta(\beta+1)^2-\beta(1+k^2/k_0^2)$$
$$+ \alpha\delta(\beta+1)(k_0^2/k^2-\beta)]/\{1-\beta(\beta+1)/$$
$$(\beta+1-\beta k^2/k_0^2)[1-\beta(\beta+1)(1-\alpha\delta)/(\beta+1-\beta k^2/k_0^2)]$$
$$(\beta+1-\beta k^2/k_0^2)-(k^2/k_0^2)\beta(\beta+1)[(\beta+1)^2-\beta(1+k^2/k_0^2)$$
$$+ \alpha\delta(\beta+1)(k_0^2/k^2-\beta)]/(\beta+1-\beta k^2/k_0^2))\} \qquad (16)$$

In terms of (16), the growth rate of the instability derived from (15) is found to be

$$\gamma = [(B_p/B_{pth})^2-1]^{1/2}kc_s \qquad (17)$$

The threshold condition defined by (16) is conveniently expressed for the normalized threshold field intensity (B_{pth}/B_0) as a function of the normalized wave number (k/k_0). The parameters $\beta(=c_s^2/v_A^2)$, $\delta(=\omega_0/\Omega_i)$, and α (defined by (13)) characterize the solar wind plasmas and the propagating magnetosonic waves. In fact, the parameter α can also be expressed in terms of (k/k_0), δ, and β as follows:

$$\alpha = \delta\{1-2[1+(k/k_0)^2]\beta/(1+\beta)/(1-\beta-[(k/k_0)^2/$$
$$(1+\beta)][1-(k/k_0)^2\beta/(1+\beta)]\} \qquad (18)$$

Displayed in Figure 2 is (α/δ) as a function of (k/k_0) for several values of β chosen from the range of 0.25-2.5. The result shows that α is, in general, larger than one for $\delta\leq 0.3$ which is the region of practical interest. Especially, $\alpha\gg 1$ for $\beta<1$ and $\delta\ll 1$. In this parameter range, the decay sidebands become linear polarization on the y-z plane and are dominated in the nature of shear mode.

The threshold fields (B_{pth}/B_0) as a function of (k/k_0) are shown in Figures 3-6. For illustrative purposes, the values of β are again selected from the range of 0.25-2.5 and δ=0.01, 0.03, 0.06, or 0.3 is chosen. The corresponding growth rates, for $(B_p/B_0)^2$=0.05, as a function of k are given in Figures 7-10. Several outstanding features of the proposed instability can be seen from these figures. For instance, the threshold field generally increases with k, the wave number of the excited purely growing mode, and it finally reaches infinity at certain $k<k_0$. While the threshold field increases with β in the region $0<\beta<1$, it decreases with β for $\beta>1$. The growth rate has a peak value (denoted by γ_{max}) at certain k (denoted by k_m). We note that both γ_{max} and k_m decrease with β for $0<\beta<1$, but they increase with β for $\beta>1$. By contrast, while γ_{max} decreases with δ, k_m increases with δ. The thresholds and growth rates of the instability vary with the magnetosonic wave frequency.

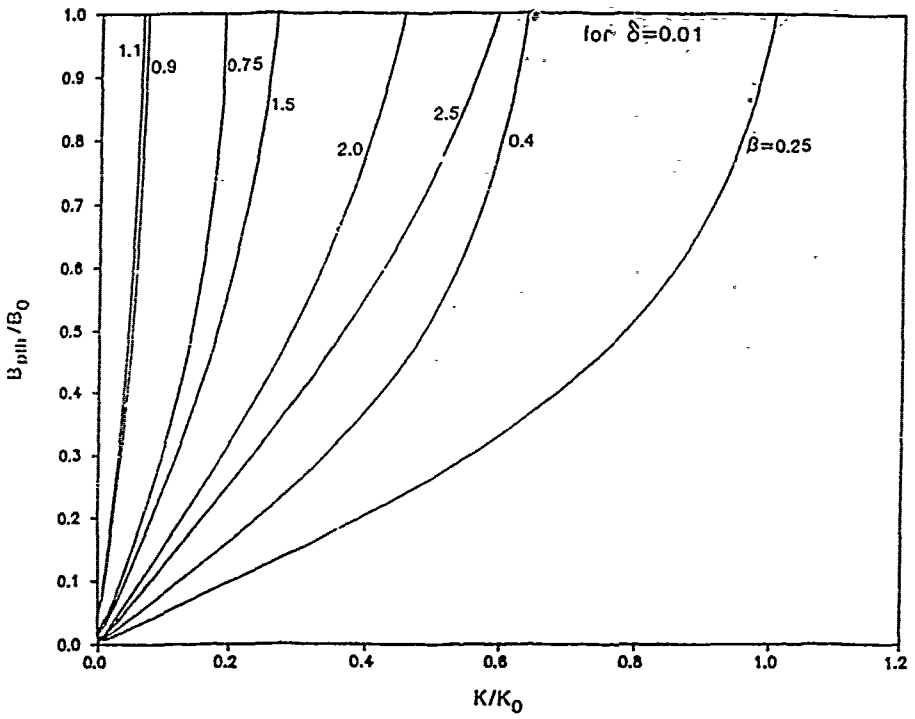

Fig. 3. The normalized threshold field intensity (B_p/B_0) versus (k/k_0) with several selected values of β in the range of 0.25-2.5 for δ=0.01.

It is found that the threshold fields (growth rates) increase (decrease) with the magnetosonic wave frequency.

Let us base upon the observed characteristics of magnetosonic waves [Hoppe and Russell, 1983; and references therein] to examine the excitation of the proposed filamentation instability. The magnetosonic waves observed by the ISEE 1 and 2 typically have low frequencies of order of 0.01 Hz, which is about 0.1 times the local proton gyrofrequency (i.e., $\delta=\omega_0/\Omega_i=0.1$).

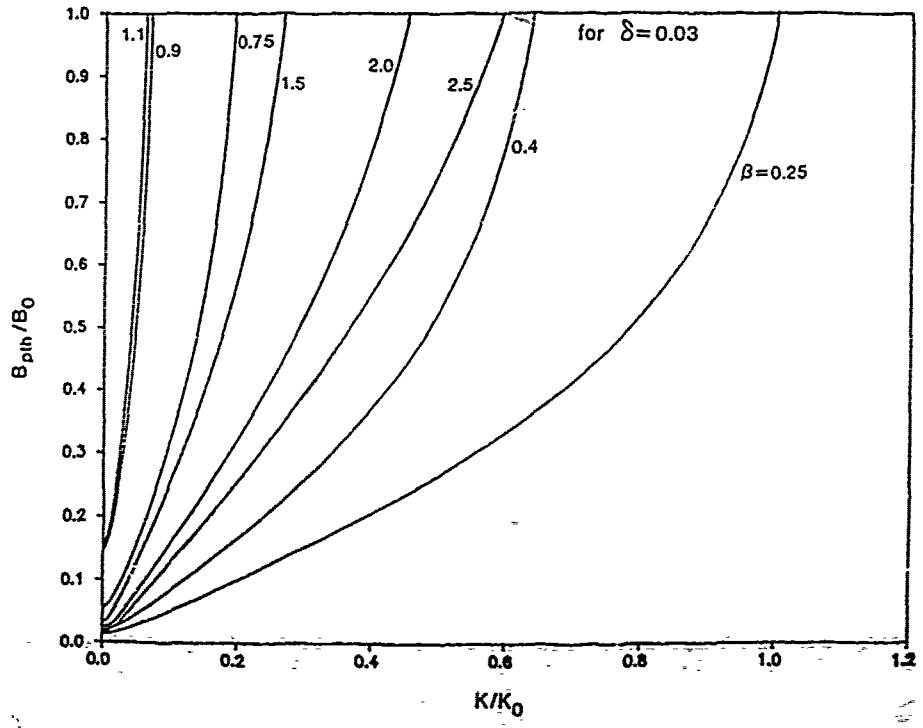

Fig. 4. (B_p/B_0) versus (k/k_0) for δ=0.03.

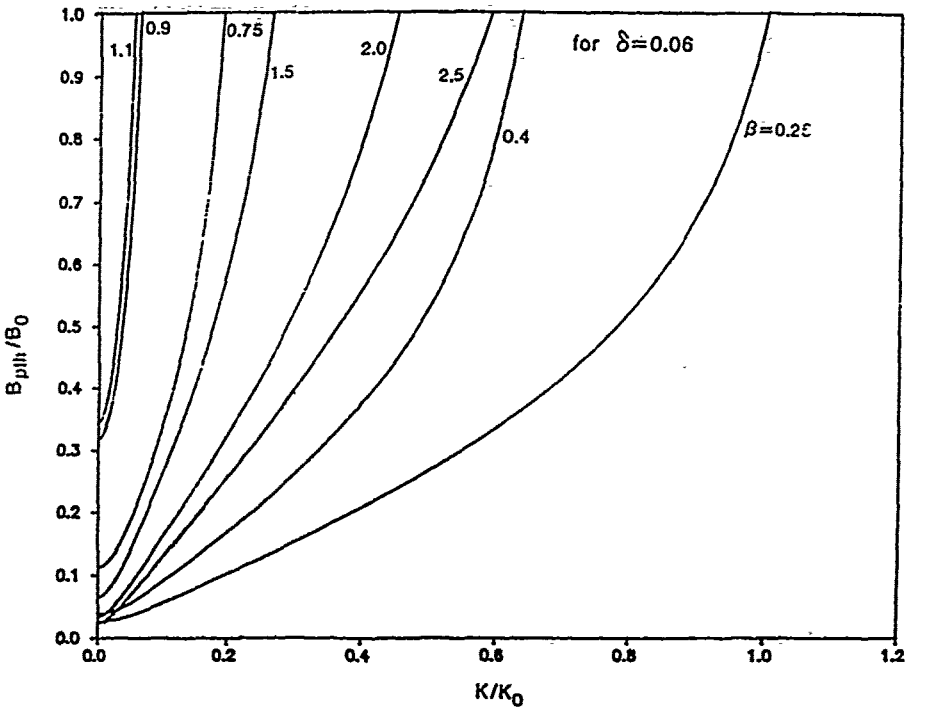

Fig. 5. (B_p/B_0) versus (k/k_0) for δ=0.06.

The local interplanetary magnetic field (B_0), therefore, is of order of 100 nT. The magnetosonic waves typically have amplitudes (B_p) of about 10 nT, namely, $B_p/B_0 \sim 0.1$ with wavelengths ~1 RE. The parameters adopted in the analysis of our proposed instability are generally in agreement with these observations. Under the condition of $B_p/B_0 \sim 0.1$, the thresholds of the proposed instability can be exceeded for k/k_0 $(=\lambda_0/\lambda)$ less than 0.1 or so, where λ_0 and λ are the wavelength of the magnetosonic wave and the scale length of the excited purely growing mode, respectively. An important prediction of the proposed process is that

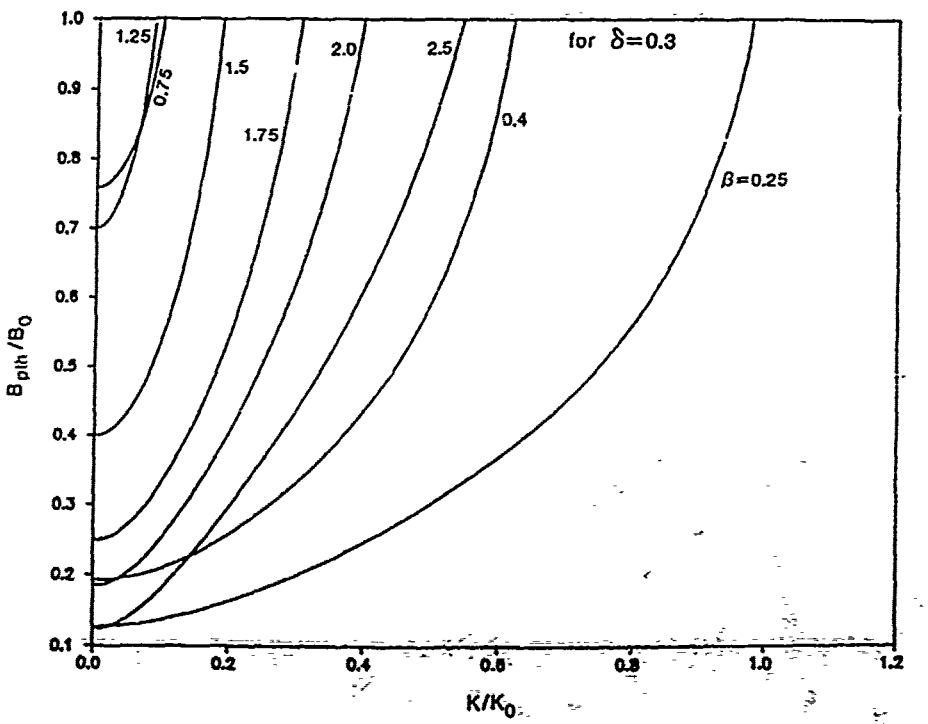

Fig. 6. (B_p/B_0) versus (k/k_0) for δ=0.3.

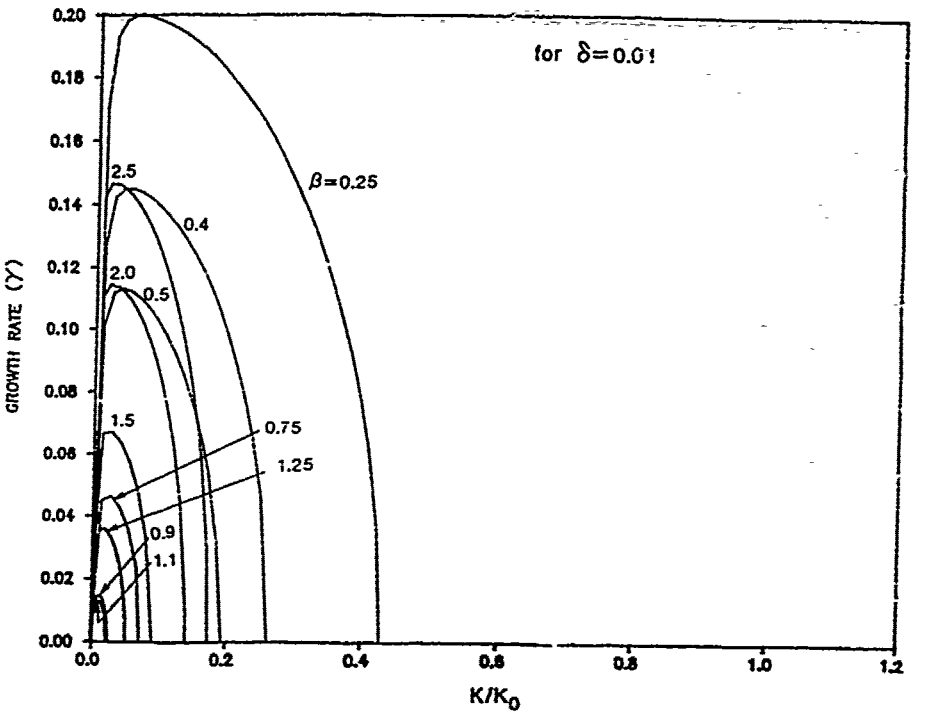

Fig. 7. The growth rate (γ), assuming $(B_p/B_0)^2=0.05$, as a function of k for δ=0.01.

plasma density fluctuations with scale lengths longer than at least, a few RE (Earth radius) can be generated along the magnetic field by magnetosonic waves. The polarization of the obliquely propagating magnetosonic waves is determined by the value of α which in turn, is a function of the characteristic parameters of the environment: δ, β, and k_0 (see equation (15)). However, we note that there seems to exist a discrepancy between the observed and the predicted propagation directions of magnetosonic waves. The waves upstream of Earth's bow shock with frequencies of 0.01 Hz were observed to propagate nearly parallel to the magnetic field, while the predicted magnetosonic waves propagate obliquely across the field. We suspect that this

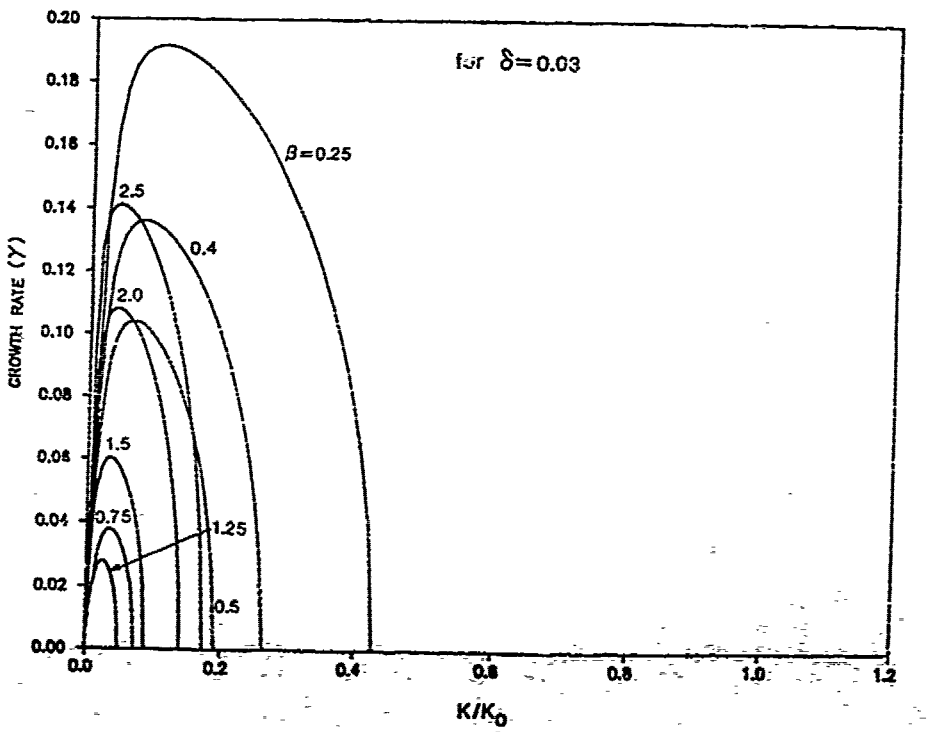

Fig. 8. γ versus (k/k_0) for δ=0.03.

734 Phys. Fluids B 1 (4), April 1989 0899-8221/89/040734-07$01.90 © 1989 American Institute of Physics 734

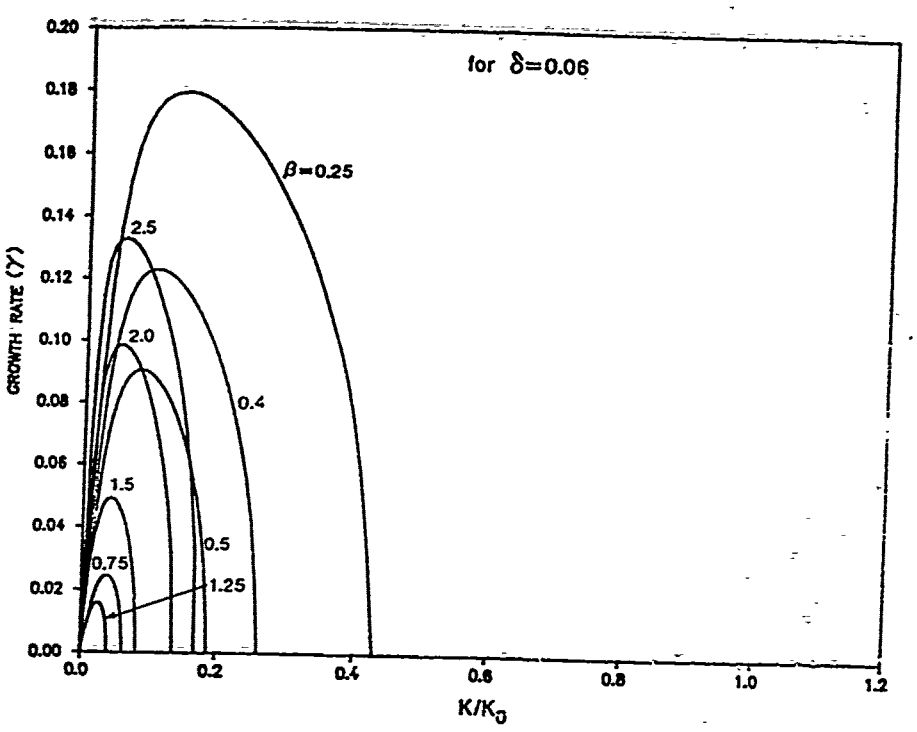

Fig. 9. γ versus (k/k_0) for δ=0.06.

discrepancy may arise from the intrinsic difficulty in the in situ measurements of upstream waves by satellites. Since the speed of solar wind is far greater than those of satellites, all measures waves appear to be nearly parallel propagating. The predicted oblique propagation of magnetosonic waves excited by filamentation instability awaits the corroboration of future observations.

4. Summary and Conclusions

The excitation of a parametric instability by magnetosonic waves in the solar wind environment is proposed. The magnetosonic pump wave originally propagates at the right angle with the magnetic field. This instability can excite a purely growing mode along

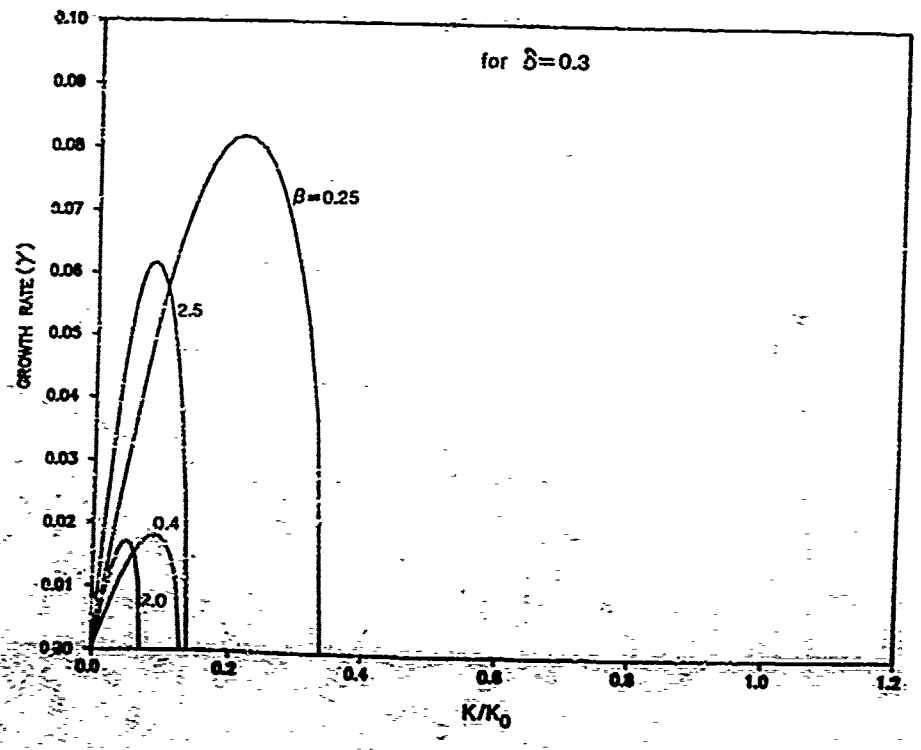

Fig. 10. γ versus (k/k_0) for δ=0.3.

the magnetic field together with two symmetric magnetosonic sidebands propagating obliquely across the magnetic field. These two sideband modes thus propagate together perpendicularly across the magnetic field and, meanwhile, form a standing wave pattern along the magnetic field. The physical process responsible for the instability can be described as the scattering of the magnetosonic pump wave into obliquely propagating sidebands by the simultaneously excited plasma density fluctuations, which are associated with a purely growing mode. This instability leads to the filamentation of the magnetosonic pump wave. The thresholds of this filamentation instability can, indeed, be exceeded in the solar wind environment. The density fluctuations produced by the filamentation instability along the magnetic field are predicted to have wavelengths greater than, at least, a few Earth radii. As shown in (18), the polarization of the obliquely propagating magnetosonic waves excited by the filamentation instability is determined by the environmental characteristic parameters: $\delta(=\omega_0/\Omega_i)$, $\beta(=c_s^2/v_A^2)$, and k_0. The predicted oblique propagation of magnetosonic waves, however, has not been confirmed by the available observations yet.

Acknowledgements. This work was supported by the Air Force Office of Scientific Research, grants AFOSR-88-0127 and AFOSR-85-0316, at Polytechnic University; the work was supported by NASA grant NAG5-1055 at the Massachusetts Institute of Technology. The numerical work was performed by M. H. Whang with the Pittsburgh Supercomputing Facility of NSF. The two referees' constructive comments are appreciated.

The Editor thanks S. R. Spangler and another referee for their assistance in evaluating this paper.

References

Abraham-Shranner, B., and W. C. Feldman, Nonlinear Alfven waves in high-speed solar wind streams, J. Geophys. Res., 82, 618, 1977.

Derby, N. F., Modulational instability of finite amplitude circularly polarized Alfven waves, Astrophys. J., 224, 1013, 1978.

Goldstein, M. L., An instability of finite amplitude circularly polarized Alfven waves, Astrophys. J., 219, 700, 1978.

Goldstein, M. L., H. K. Wong, A. F. Vinas, and C. W. Smith, Large-amplitude MHD waves upstream of Jovian bow shock: Reinterpretation, J. Geophys. Res., 90, 302, 1985.

Hada, T., C. F. Kennel, and B. Buti, Stationary nonlinear Alfven waves and solitons, J. Geophys. Res., 94, 65, 1989.

Hoppe, M. M. and C. T. Russell, Plasma rest frame frequencies and polarizations of the low-frequency upstream waves: ISEE 1 and 2 observations, J. Geophys. Res., 88, 2020, 1983.

Kuo, S. P., M. H. Whang, and M. C. Lee, Filamentation of large-amplitude Alfven waves, J. Geophys. Res., 93, 9621, 1985.

Kuo, S.P., M. H. Whang, and G. Schmidt, Convective filamentation instability of circularly polarized Alfven waves, Phys. Fluids B, 32, 734, 1989.

Lashmore-Davies, C.N., Modulation instability of a finite amplitude alfven wave, Phys. Fluids, 19, 587, 1976.

Longtin, M., and B.U.O. Sonnerup, Modulational instability of circularly polarized Alfven waves, J. Geophys. Res., 91, 3816, 1986.

Mjoehus, E., On the modulation instability of hydromagnetic waves parallel to the magnetic field, J. Plasma Phys., 16, 321, 1976.

Ovenden, C. R., H. A. Shah, and S. J. Schwartz, Alfven solitons in the solar sind, J. Geophys. Res., 88, 6095, 1983.

Spangler, S. R., Nonlinear astrophysical Alfven waves: Onset and outcome of the modulational instability, Astrophys. J., 299, 122, 1985.

Spangler, S. R., The evolution of nonlinear Alfven waves subject to growth and damping, Phys. Fluids, 29, 2535, 1986.

Terasawa, T., M. Hoshino, J. I. Sakai, and T. Hada, Decay instability of finite-amplitude circularly polarized Alfven waves: A numerical simulation of stimulated Brillouin scattering, J. Geophys. Res., 91, 4171, 1986.

Vinas, A. F., M. L. Goldstein, and M. H. Acuna, Spectral analysis of magnetohydrodynamic fluctuations near interplanetary shocks, J. Geophys. Res., 89, 6813, 1984.

Wong, H. K. and M. L. Goldstein, Parametric instabilities of circularly polarized Alfven waves including dispersion, J. Geophys. Res., 91, 5617, 1986.

S.P. Kuo, Weber Research Institute, Polytechnic University, Farmingdale, NY 11735.

M.C. Lee, Massachusetts Institute of Technology, Cambridge, MA 02139.

(Received December 5, 1988;
revised April 5, 1989;
accepted May 17, 1989.)

Journal of Atmospheric and Terrestrial Physics, Vol. 51, No. 9/10, pp. 727–731, 1989
Printed in Great Britain.

0021-9169/89 $3.00 + .00
Pergamon Press plc

Parametric excitation of whistler waves by HF heater

S. P. KUO
Weber Research Institute, Polytechnic University, Farmingdale, NY 11735, U.S.A.

and

M. C. LEE
Plasma Fusion Center, Massachusetts Institute of Technology, Cambridge, MA 02139, U.S.A.

(*Received in final form* 30 *April* 1989)

Abstract—Possible generation of whistler waves by Tromso HF heater is investigated. It is shown that the HF heater wave can parametrically decay into a whistler wave and a Langmuir wave. Since whistler waves may have a broad range of frequency, the simultaneously excited Langmuir waves can have a much broader frequency bandwidth than those excited by the parametric decay instability.

1. INTRODUCTION

There is considerable interest in investigating generation and amplification of VLF/ELF/ULF waves in the ionosphere by high power HF waves (see, e.g., STUBBE *et al.*, 1982; LUNNEN *et al.*, 1985). Several processes have been suggested as potential mechanisms causing them such as the modulation of electrojet current (STUBBE and KOPKA, 1981; FEJER and KRENZIEN, 1982), the thermal filamentation instability of HF heater (KUO and LEE, 1983) and parametric excitation of Alfven (ELF) waves (PAPADOPOULOS *et al.*, 1982). In this paper, we discuss a possible mechanism for VLF/LF wave generation in the ionosphere by HF heater.

As described in Sections 2 and 3, the proposed mechanism is the parametric excitation of whistler waves by HF heater. The concomitantly excited electrostatic waves are Langmuir waves. Thus, the considered process is the parametric decay of HF heater wave into a Langmuir wave and a whistler wave. This process is different from the so-called parametric decay instability of HF heater waves on two aspects. One is that the parametric decay instability generates a Langmuir wave and an ion acoustic wave; both of the excited waves are electrostatic mode waves. The other one is that the ion acoustic wave has a frequency of, typically, a few kHz in the ionosphere, while the whistler wave may have a broad range of frequency covering VLF, LF, and even MF bands. Therefore, Langmuir waves excited by the proposed mechanism can have a broader frequency bandwidth than those produced by the parametric decay instability.

Observations of the HF heater-produced VLF/ELF/ULF waves were constantly made at Tromso, Norway with the EISCAT heating facilities. Stimulated electromagnetic emissions with a broad frequency band of several tens of kHz were seen in the Tromso heating experiments (STUBBE *et al.*, 1984 and references therein). Hence, our proposed mechanism is specifically analyzed for high-latitude heating experiments with the intention to compare the theoretical results with observations made at Tromso, Norway. A brief discussion is finally given in Section 4.

2. THEORY

As mentioned earlier, the EISCAT heating facilities at Tromso, Norway were observed to produce VLF/ELF/ULF waves in the ionosphere. The Tromso HF transmitter is steerable to launch heater waves propagating along the earth's magnetic field. In view of these facts, we will present our theory as follows in a simple geometry of propagation, which is appropriate for describing the parametric excitation of whistler waves by HF heater at Tromso, Norway.

Consider a left-handed (L-H) circularly polarized heater wave propagating upward along a downward geomagnetic field in an overdense ionosphere. The ionospheric density (n) is assumed to have a linear profile, increasing with altitudes (z) as $n = n_0(1+z/L)$ where L is the scale size of the background ionospheric inhomogeneity. The heater wave is reflected at a critical height before reaching the ionospheric F peak and becomes a standing wave, whose energy follows an Airy function distribution illustrated in Fig. 1.

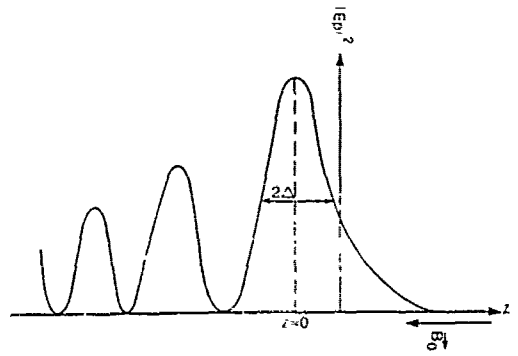

Fig. 1 Standing wave pattern of heater wave near the reflection height.

The first peak of the Airy function is located at $z = 0$ and its width is denoted by 2Δ. The heater wave field in this region is then modeled by $\mathbf{E}_p = (\hat{x} - i\hat{y})\varepsilon_p + c.c.$, where $\varepsilon_p = [\varepsilon_{0p}(1 - iz/\Delta)]\exp(-i\omega_0 t)$ whose phasor, $\varepsilon_{0p}(1 - iz/\Delta)$, is proportional to a complex Lorentzian function. The velocity response of electrons to the heater field is found to be

$$\mathbf{V}_p = -i(\hat{x} - i\hat{y})e\varepsilon_p/m[(\omega_0 - \Omega_e) + i\nu_e] + c.c. \quad (1)$$

where ν_e is the electron collision frequency.

We will show that the parametric decay of the heater wave $(\omega_0, \mathbf{k}_0)$ into a downgoing (or upgoing) whistler wave $(\omega, \mathbf{k})$ and an upgoing (or downgoing) Langmuir wave $(\omega_l, \mathbf{k}_l)$ can occur in the aforementioned peak region of heater wave field. The following wave frequency and wave vector relations, $\omega_0 = \omega + \omega_l$ and $\mathbf{k}(0) = -\mathbf{k}_l(0) = -\hat{z}k$, are satisfied. First derived is the coupled mode equation for the whistler wave, which is excited by the beating current driven by the pump field in the density perturbation associated with the excited Langmuir wave.

The density of beating current as the driving source of the whistler wave is given by $\delta\mathbf{J}_\omega^{NL} = -e\delta n_l^* \mathbf{V}_p$, where $\delta n_l (= \delta\tilde{n}_l \exp(-i\omega_l t) + c.c.)$ is the density perturbation associated with the Langmuir wave; $\mathbf{V}_p$, shown in (1), is the velocity response of electrons to the heater wave field. The density perturbation can be obtained from the Poisson's equation, $\delta n_l = -(1/4\pi e)(\partial\varepsilon_{ll}/\partial z)$, where ε_l is the amplitude of Langmuir wave field $\delta\mathbf{E}_l = \hat{z}\varepsilon_l = \hat{z}\tilde{\varepsilon}_l \exp(-i\omega_l t)$. In addition to the beating current, a linear current is caused by the whistler wave with the background plasma, $\delta\mathbf{J}_\omega^L = -en\delta\mathbf{V}_\omega$ where $\delta\mathbf{V}_\omega$ is the velocity response of electrons to the whistler field and n is the background electron density; $\delta\mathbf{V}_\omega$ has a similar form as $\delta\mathbf{V}_p$, namely,

$$\delta\mathbf{V}_\omega = -i(\hat{x} - i\hat{y})e\varepsilon_\omega/m[(\omega - \Omega_e) + i\nu_e] + c.c. \quad (2)$$

where ε_ω is the amplitude of the whistler wave field, $\delta\mathbf{E}_\omega = (\hat{x} - i\hat{y})\varepsilon_\omega + c.c. = (\hat{x} - i\hat{y})\tilde{\varepsilon}_\omega \exp(-i\omega t) + c.c.$ Substituting the respective expressions for $\delta\mathbf{J}_\omega^{NL}$ and $\delta\mathbf{J}_\omega^L$ into the whistler wave equation yields the coupled mode equation

$$\left\{\frac{\partial^2}{\partial t^2} + i[\omega_p^2(z)/(\omega - \Omega_e + i\nu_e)]\frac{\partial}{\partial t} - c^2\frac{\partial^2}{\partial z^2}\right\}\varepsilon_\omega = i[e/m(\omega_0 - \Omega_e + i\nu_e)]\frac{\partial}{\partial t}\left(\varepsilon_p\frac{\partial}{\partial z}\varepsilon_l^*\right) \quad (3)$$

where $\omega_p(z) = 4\pi e^2 n(z)/m$.

We next derive the coupled mode equation for the Langmuir wave. The driving force of the plasma oscillation is the Lorentz force experienced by the oscillating electrons in the wave magnetic fields. Responding to the electric fields of the heater wave and whistler wave, electrons oscillate, respectively, with velocities $\mathbf{V}_p$ and $\delta\mathbf{V}_\omega$, transverse to the background magnetic field. These cross-field motions interact with the wave magnetic fields, $\delta\mathbf{B}_\omega$ and $\delta\mathbf{B}_p$, and result in a longitudinal Lorentz force, $-(e/c)(\delta\mathbf{V}_\omega \times \mathbf{B}_p + \mathbf{V}_p \times \delta\mathbf{B}_\omega^*)$ which is responsible for the longitudinal plasma oscillation. Including this force in the electron momentum equation and combining this equation with the electron continuity equation, we obtain the following coupled mode equation for the Langmuir wave

$$\left[\frac{\partial^2}{\partial t^2} + \nu_e\frac{\partial}{\partial t} + \left(\omega_p^2 - V_t^2\frac{\partial^2}{\partial z^2}\right)\right]\varepsilon_l = -2(e\omega_p^2/m)\left[\varepsilon_p\frac{\partial}{\partial z}\varepsilon_\omega^*/\omega^*(\omega_0 - \Omega_e + i\nu_e) + \varepsilon_\omega^*\frac{\partial}{\partial z}\varepsilon_p/\omega_0(\omega^* - \Omega_e - i\nu_e)\right] \quad (4)$$

where V_t is the thermal velocity of electrons.

It is clear from the two coupled mode equations, (3) and (4), that the whistler wave and Langmuir wave are coupled through the HF heater wave, which acts as the pump of the concerned parametric instability. To proceed the instability analysis further, it is desirable to reduce these two equations into first-order differential equations. This can be done by introducing the transformations (Rosenbluth, 1972; White *et al.*, 1973),

$$\varepsilon_l = a_1 \exp\left\{i\left[k_1 z - \omega_1 t + \int_0^z \Delta k_1(z')\,dz'\right]\right\} \quad (5)$$

and

$$\varepsilon_2 = a_2 \exp\left\{i\left[k_2 z - \omega_2 t + \int_0^z \Delta k_2(z')\,dz'\right]\right\} \quad (6)$$

where $k_1 = k_1(0) = k = -k_2(0)$, $\omega_1^2 = \omega_l^2 = \omega_p^2(0) + k_1^2 V_l^2$ and $\omega_2 = \omega = \kappa_2^2 c^2 \Omega_e/\omega_p^2(0)$, $\Delta k_1 = [\omega_p^2(0) - \omega_p^2(z)]/2k_1 V^2$ and $\Delta k_2 = (\omega/2k_2\Omega_e c^2)[\omega_p^2(z) - \omega_p^2(0)]$. Note that $\omega_1 + \omega_2 - \omega_0 = \delta$ for a mismatch frequency and $\Delta k = \Delta k_1 + \Delta k_2 = k'z$, where $k' = -(\omega_p(0)/2kL)(\omega/\Omega_e c^2 + 1/V_l)$.

Substituting (5) and (6) into (3) and (4) and assuming that $|\partial a_1/\partial t| \ll \omega_l |a_1|$, $|\partial a_2/\partial t| \ll \omega |a_2|$, $|\partial a_1/\partial z| \ll |k_1||a_1|$, and $|\partial a_2/\partial z| \ll |k_2||a_2|$, we derive the following first-order differential equations for a_1 and a_2

$$\left(\frac{\partial}{\partial t} + V_1 \frac{\partial}{\partial z} + \nu_1\right) a_1 = (e/m)[\omega_p^2(z) k/\omega_l \omega(\omega_0 - \Omega_e)] \cdot a_p a_2^* \exp[-ik'z^2/2] \quad (7)$$

and

$$\left(\frac{\partial}{\partial t} - V_2 - \nu_2\right) a_2 = (e/m)[\Omega_e(\omega_2 - \delta) k/\omega_p^2(z)(\omega_0 - \Omega_e)] \cdot a_p a_1^* \exp[-ik'z^2/2] \quad (8)$$

where $V_1 = kV_l^2/\omega_1$ and $V_2 = 2kc^2\Omega_e/\omega_p^2(0)$ are the group velocities of Langmuir wave and whistler wave, respectively; $\nu_1 = \nu_e/2$ and $\nu_2 = \nu_e\omega/\Omega_e$. The simplified coupled mode equations, (7) and (8), will be analyzed in the next section for the parametric excitation of Langmuir wave and whistler wave by a nonuniform HF heater wave in a nonuniform ionospheric plasma.

3. ANALYSIS

After being Laplace-transformed in time, equations (7) and (8) can be written as

$$\left(p + \nu_1 + V_1 \frac{\partial}{\partial z}\right) A_1 = (e/m)[\omega_p^2(z) k/\omega_1 \omega_2(\omega_0 - \Omega_e)] \cdot a_p A_2^* \exp(-ik'z^2/2) + a_{10}(z) \quad (9)$$

$$\left(p^* + \nu_2 + i\delta - V_2 \frac{\partial}{\partial z}\right) A_2 = (e/m)[\Omega_e(\omega_2 - \delta) k/\omega_p^2(z)(\omega_0 - \Omega_e)] \cdot a_p A_1^* \exp(-ik'z^2/2) + a_{20}(z) \quad (10)$$

where p is the Laplace transform variable, $A_1 = \mathscr{L}[a_1]$ and $A_2 = \mathscr{L}[a_2]$, where $\mathscr{L}[\ ] = \int_0^\infty [\ ] \exp(-pt)\,dt$ represents the Laplace transform; $a_{10}(z)$ and $a_{20}(z)$ are the initial values of a_1 and a_2, respectively. In the following eigenmode analysis, $a_{10}(z)$ and $a_{20}(z)$ can be set to be zeros.

Combining (9) and (10) leads to a second-order differential equation for A_1:

$$\left[\frac{d^2}{dz^2} + f_1(z)\frac{d}{dz} + f_2(z)\right] A_1 = 0 \quad (11)$$

where

$$f_1(z) = (P + \nu_1)/V_1 - (p + \nu_2 - i\delta)/V_2 + [ik'z - 1/(L+z) - i/(\Delta - iz)] \quad (12)$$

and

$$f_2(z) = (e/m)^2[k^2\Omega_e(\omega_2 - \delta)/\omega_1\omega_2 \times (\omega_0 - \Omega_e)^2]\varepsilon_0^2/V_1V_2(1 + z^2/\Delta^2) + [(p + \nu_1)/V_1][ik'z - 1/(L+z) - i/(\Delta - iz)] - [(p + \nu_1)/V_1][(p + \nu_2 - i\delta)/V_2]. \quad (13)$$

Introducing that $f_1(z) = \Psi(z)\exp[-\frac{1}{2}\int_0^z f_1(z')\,dz']$, equation (11) can be further transformed into

$$\left[\frac{d^2}{dz^2} + f(z)\right]\Psi(z) = 0 \quad (14)$$

where $f(z) = f_2(z) - (1/2)[(1/2)f_1^2(z) + (d/dz)f_1(z)]$.

Both the effects of the background density inhomogeneity (i.e., $L \neq \infty$) and finite instability zone (i.e., $\Delta \neq \infty$) are taken into account and included in $f(z)$. However, since $L \gg \Delta$, the effect of background density inhomogeneity is negligible in comparison with that of the finite instability zone. Therefore, $f(z)$ can be approximately expressed as

$$f(z) \simeq \alpha^2/(1 + z^2/\Delta^2) - (1/4)[(p + \nu_1)/V_1 + (p + \nu_2 - i\delta)/V_2 - ik'z + 1/(\Delta - iz)]^2 - (1/2) \times [ik' + 1/(\Delta - iz)^2] \quad (15)$$

where

$$\alpha^2 = (e/m)^2[k^2\Omega_e(\omega_2 - \delta)/\omega_1\omega_2(\omega_0 - \Omega_e)^2]\varepsilon_0^2/V_1V_2.$$

The eigenvalue of (14) needs to be determined for finding the threshold fields of the heater wave and the growth rates of the instability. The requirement of threshold fields is, in general, imposed by two additive effects. They are the collisional loss of excited modes and the convective loss across the boundaries of finite instability zone. These two effects are evaluated separately as follows.

(a) *Collisional loss*

We first consider the damping of excited modes due to collisions by letting $\Delta \to \infty$. It is equivalent to the

study of instability in a uniform, unbounded ionospheric plasma. Then, A_1 and $f_2(z)$ become spatially independent functions; equation (13) reduces to

$$f_2 = \alpha^2 - [(p+\nu_1)/V_1][(p+\nu_2)/V_2]. \quad (16)$$

Note that $\delta = 0, k' = 0$ because of the neglect of background density inhomogeneity (i.e., $L \to \infty$).

The dispersion relation of the instability, determined from equation (11), is obtained by setting $f_2 = 0$ which leads to the growth rates (P) of the instability to be

$$p = (1/2)\{-(\nu_1+\nu_2)+[(\nu_1-\nu_2)^2+4\alpha^2 V_1 V_2]^{1/2}\}. \quad (17)$$

Taking $p = 0$ in (17), we derive the threshold condition for exciting the instability

$$\left[\frac{e\varepsilon_0}{m(\omega_0-\Omega_e)}\right]_{th} = (\nu_1\nu_2\omega_1/\Omega_e k^2)^{1/2}. \quad (18)$$

(b) Convective loss

We next examine the effect of the finite instability zone, namely, the convective loss of excited modes which is assumed to dominate over the collisional damping loss in determining the thresholds of the instability. In this case, equation (15) is simplified to be

$$f(z) = \alpha^2(1+z^2/\Delta^2) - (1/4) \times [p(\nu_1+\nu_2)/V_1V_2]^2 - (1/2\Delta^2). \quad (19)$$

In obtaining (19), we have also assumed that $\delta \simeq V_2/\Delta$.

The zeros of $f(z)$ are then found to be

$$z_{1,2} = \pm\Delta\{4\alpha^2 V_1^2 V_2^2/[p^2(V_1+V_2)^2 + 2(V_1V_2/\Delta)^2] - 1\}^{1/2} = \pm z_t. \quad (20)$$

These are the positions of two real turning points for equation (14), which has the following solutions:

$$\Psi^I(z) = f^{-1/4}(z)\exp\left[i\int_{z_1}^{z} f^{1/2}(z')\,dz'\right] \quad \text{for } z > z_1$$

$$\Psi^{II}(z) = f^{-1/4}(z)\exp\left[-i\int_{z_2}^{z} f^{1/2}(z')\,dz'\right] \quad \text{for } z < z_2$$

well behaved at $z \to \pm\infty$. Thus, spatially localized but temporally growing modes exist provided that a positive eigenvalue p can be found from the eigenvalue equation defined by the Bohr–Sommerfeld quantization condition (Landau and Lifshitz, 1965)

$$(m+\tfrac{1}{2})\pi = \int_{z_2}^{z_1} f^{1/2}(z)\,dz \quad (21)$$

where $m = 0, 1, 2, \ldots$ stands for the number of modes of the eigenfunction $\Psi(z)$ between the two turning points z_1 and z_2.

The integral in (21) can be expressed in terms of complete elliptic integral for numerical analysis. However, this integral can be much simplified for $z_t/\Delta \ll 1$, and a simple approximate form of (21) results as

$$z_t/\Delta \simeq [(2m+1)/\alpha\Delta]^{1/2}. \quad (22)$$

Substituting (20) into (22) to eliminate z_t and considering the $m = 0$ case for the requirement of lowest thresholds, we obtain the growth rate of the instability. It is

$$p = [2V_1V_2/\Delta(V_1+V_2)][(\alpha\Delta)^3/(1+\alpha\Delta) - 1/2]^{1/2}. \quad (23)$$

Setting $p = 0$ in (23) leads to the following expression for the threshold fields of heater wave

$$\left[\frac{e\varepsilon_0}{m(\omega_0-\Omega_e)}\right]_{th} = \frac{V_t c}{\omega_{p0}\Delta} \quad (24)$$

where $\omega_{p0} = (4\pi e^2 n_0/m)^{1/2}$.

4. DISCUSSION

We have formulated a mechanism whereby whistler wave and Langmuir wave can be parametrically excited by an HF heater in the overdense ionospheric heating experiments at Tromso, Norway. The required threshold fields of heater wave are derived and examined separately for two cases, wherein either the collisional loss or convective loss is considered to be the dominant damping process of the proposed instability. A quantitative analysis of the instability is carried out here with the following parameters: $\omega_0/2\pi = 4.04$ MHz, $\Omega_e/2\pi = 1.4$ MHz, $V_t = 1.3\times10^5\,\mathrm{m\,s^{-1}}$, $\Delta \sim 150$ m, $\nu_e \sim 500$ Hz, and $\omega_{p0} \simeq \omega_0$.

It is found that both calculations of the threshold fields from (18) and (24) have nearly the same magnitude, i.e. $1\,\mathrm{V\,m^{-1}}$. This indicates that the collisional loss and convective loss play equally important roles as the linear damping mechanisms of the proposed instability. The effective threshold field imposed by both damping mechanisms is, therefore, $\sqrt{2}\,\mathrm{V\,m^{-1}}$. The growth rate of the instability with the effective threshold field can be calculated from (23) with modified width (Δ') of the first peak of the heater wave energy distribution. The modified width is given by $\Delta' = \Delta[(1-x)/(1+x)]^{1/2}$ where $x = \varepsilon_{th}^2/\varepsilon_0^2$ and ε_{th} is the threshold field (given in (18)) imposed by the collisional loss as the dominant damping mechanism.

Conceptually, the width modification results from the reduction of heater wave energy by collisions.

The effective threshold fields ($\sim 1.4\,\mathrm{v\,m^{-1}}$) of the instability can be exceeded by the peak field intensity of pump waves transmitted from the Tromso HF heater, especially after the swelling effect on the wave field has been taken into account. If the effective field intensity of heater wave near the reflection height is assumed to be $3\,\mathrm{v\,m^{-1}}$, whistler waves with frequencies ranging from a few tens of kHz up to, say, several hundred kHz can be excited in a few seconds according to (23). The theory predicts that Langmuir waves excited concomitantly with whistler waves at Tromso may have a much broader frequency bandwidth than those excited by the parametric decay instability. The frequency bandwidth of excited Langmuir waves is determined by the wave frequency of excited whistler waves. Stimulated electromagnetic emissions with a broad frequency band were indeed observed in the Tromso heating experiments.

Acknowledgements—This work was supported by NSF grant ATM-8816467 and the AFOSR grant AFOSR 88-0127 at Polytechnic University, and by NASA grant NAG 5-1055 at Massachusetts Institute of Technology.

REFERENCES

Fejer J. A. and Krenzien E.	1982	*J. atmos. terr. Phys.* **44**, 1075.
Kuo S. P. and Lee M. C.	1983	*Geophys. Res. Lett.* **10**, 979.
Landau L. D. and Lifshitz E.	1965	*Quantum Mechanics*, Pergamon Press, Oxford.
Lunnen R. J., Ferraro A. J., Lee, H. S., Allshouse R., Carroll K., Werner D. and Collins T. W.	1985	*Radio Sci.* **20**, 553.
Papadopoulos K., Sharma R. R. and Tripathi V. K.	1982	*J. geophys. Res.* **87**, 1491.
Rosenbluth M. N.	1972	*Phys. Rev. Lett.* **29**, 565.
Stubbe P. and Kopka, H.	1981	*J. geophys. Res.* **86**, 1606.
Stubbe P., Kopka H., Lauche, H., Rietveld M. T., Brekke A., Holt O., Jones T. B., Robinson T., Hedberg A., Thide B., Crochet M. and Lotz H. J.	1982	*J. atmos. terr. Phys.* **44**, 1025.
Stubbe P., Kopka H., Thide B. and Derblom, H.	1984	*J. geophys. Res.* **89**, 7523.
White R. B., Liu C. S. and Rosenbluth M. N.	1973	*Phys. Rev. Lett.* **31**, 520.

NONLINEAR WORLD

PROCEEDINGS OF THE IV INTERNATIONAL
WORKSHOP ON NONLINEAR AND TURBULENT
PROCESSES IN PHYSICS

VOLUME 2

Nonlinear Wave-Particle Interaction in the Magnetosphere

S.P. Kuo
Polytechnic University, Route 110, Farmingdale, NY 11735 USA

M.C. Lee
Plasma Fusion Center, Massachusetts Institute of Technology, Cambridge, MA 02139 USA

ABSTRACT

The interaction between a bouncing proton and a kinetic Alfven wave in the magnetosphere is studied. It is shown that the trajectory of the proton becomes chaotic when the amplitude of the wave exceeds a threshold value. However, a further increase of wave amplitude to exceed a value of the trajectory becomes periodic and dominated by the wave.

I. INTRODUCTION

In the magnetosphere, energetic protons (order of keV) can be trapped by the earth's dipole magnetic field. These protons execute simple harmonic motion along the line of force in the equatorial region where a symmetric mirror field can be assumed. When a kinetic Alfven wave is present,[1] the motion of protons is expected to be perturbed, in particular, as the wave frequency becomes close to the bouncing frequency of protons. This is because the kinetic Alfven wave has a sizable component of electric field parallel to the direction of background magnetic field.

The nonlinear dynamics of such bouncing protons in the presence of a kinetic Alfven wave has been studied recently by Prakash.[2] Including only the parallel component of the wave electric field in the analysis, the threshold field amplitude for the onset of chaos has been computed. It is shown that the threshold value can be marginally exceeded by the kinetic Alfven wave in the magnetosphere. However, the analysis has neglected the effect of the transverse component of the wave electric field on the proton trajectory. Such an approximation is, in fact, not justifiable, since the transverse component of the wave electric field is about an order of magnitude larger than that of the parallel component.[1]

In this work, both transverse and parallel components of the wave electric field will be included in determining the proton trajectory. The particle dynamics will be studied in four-dimensional phase space (x, z, v_z, t) by solving two coupled nonlinear equations (one first order, and one second order differential equation) numerically, where z and v_z are the coordinate and velocity component of the proton along the magnetic field, x is the transverse coordinate along the direction of transverse component of the wave vector. Nonlinearity arises due to the spatial dependence of the field quantities. The stochastic aspects are studied in the surface of section plot.

II. GOVERNING EQUATIONS

Geomagnetic micropulsations (PC3-PC5) are usually explained by field line resonance with the externally excited Alfven waves. Moreover, the field line resonance can excite a kinetic Alfven wave with a perpendicular wavelength comparable to the gyro radius of the ion. The kinetic Alfven wave is accompanied by a sizable parallel component of the electric field. We choose a coordinate system with the z axis parallel to the magnetic field at equator and wavevector $\vec{k}$ on the x-z plane. The origin of the coordinate system is fixed at the center of the local mirror field which coincide with the location of the equator. The total wave electric field is then expressed as

$$\vec{E}(x,z,t) = (\eta\hat{x} + \hat{z})E_0\cos(k_x x + k_z z - \omega t) \tag{1}$$

where $\eta=(k_x/k_z)(k_x\rho_i)^{-2}$ and ρ_i is the ion Larmour radius.

The wave magnetic field is a few nanotesias and, hence, plays an insignificant role in comparison to the restoring field (magnetic mirror) and the wave electric field. Therefore, the guiding center motion of a proton can be described by

$$\frac{d^2}{dt^2}z = -\omega_b^2 z + \frac{e}{m}E_0\cos(k_x x + k_z z - \omega t) \tag{2}$$

and

$$v_y = -c(\eta E_0/B_0)\cos(k_x x + k_z z - \omega t) \tag{3}$$

where $\omega_b^2=(2\mu\alpha B_0/m)^{1/2}$ is the bouncing frequency of a proton with magnetic moment μ in a parabolic mirror $B_0(1+\alpha z^2)$; v_y is the result of $\vec{E}\times\vec{B}$ drift.

Substituting (3) into the y component of the momentum equation, $\frac{d}{dt}v_y = -\Omega_i v_x$, leads to

$$\frac{d}{dt}x = (\omega - k_z v_z)(c\eta E_0/B_0)\sin(k_x x + k_z z - \omega t)/[\Omega_i + (k_x c\eta E_0/B_0)\sin(k_x x + k_z z - \omega t)] \tag{4}$$

where $\Omega_i=eB_0/mc$ is the ion gyrofrequency; $|\alpha z^2|<<1$ has been assumed.

In the following, the nonlinear dynamics of particle motion will be studied by solving (2) and (4) together with $\frac{d}{dt}z=v_z$ numerically. In the numerical analysis, the dimensionless quantities are employed. Replacing $\omega t\to 2\pi t$, $k_z z\to 2\pi z$, $k_x x\to 2\pi x$, and $k_z v_z/\omega\to v_z$, (2) and (4) become

$$\frac{d^2}{dt^2}z = -(2\pi/q)^2 z + (2\pi/q^2)\epsilon\cos 2\pi(x+z-t) \tag{5}$$

$$\frac{d}{dt}x = (\alpha/k_z^2)(1-v_z/\epsilon)\sin 2\pi(x+z-t)/[1+(\alpha/k_z^2)\epsilon\sin 2\pi(x+z-t)] \tag{6}$$

where $\epsilon=k_z e E_0/m\omega_b^2$ is a dimensionless parameter characterizing the strength of the ac

field; $q=\omega/\omega_{ci}$ is a winding number.

III. RESULTS AND DISCUSSION

We adopt the parameters used in the work of Prakash, in which the interaction occurs along the $L=6$ field line with $k_z=\pi/3R_E$. Thus, $\alpha/k_z^2=0.1$ and $q=0.8$ are used. Starting with small ϵ and increasing its value gradually, the approach to chaos is thus studied by examining the surface of section plot on $z-v_z$ plane. For very small ϵ, e.g., $\epsilon=0.01$, the particle trajectory is bounded and integrable. The motion of the integrable orbit is constrained to the surface of an invariant torus whose intersection with the $z-v_z$ plane is a closed curve. As ϵ is increased to 0.05, the trajectory in the phase space is confined to what appears to be a "ribbon," i.e., the solution manifold is confined to the surface of a two-torus. If ϵ is increased further, the particle motion becomes strongly coupled to the wave. Shown in Fig. 1(a) is the surface of section plot for $\epsilon=0.25$ and the initial conditions $x(o)=0$, $z(o)=0.015$ and $v_z(o)=0$. A series of bifurcation from an ellipse is observed. However, the plot has a regular pattern. The trajectories are still in the regular regime. The phase space gradually becomes a mixture of regular and irregular regimes as ϵ increases. Figure 1(b) is the surface of section plot for $\epsilon=0.35$ case with the same initial conditions as Fig. 1(a). It shows that the center region of the plot displays irregular pattern. With further increase in ϵ, the irregular region extends outward continuously. As shown in Fig. 1(c) for the $\epsilon=0.65$ case, the particle motion is predominantly irregular. In Fig. 1(d), results are shown for the onset of chaos which takes place for $\epsilon_c=0.8$. Nearby initial conditions reproduce the pattern of particle chaos in the surface of section plot. This implies that nearby trajectories diverge exponentially. For $\epsilon>\epsilon_c$, the salient features of particle dynamics do not change. However, the amplitude of motion in phase space increases.

In the magnetosphere, kinetic Alfven waves can be excited with amplitude as large as giving $\epsilon=1.2$ during the geomagnetic pulsation events. Therefore, the value $\epsilon_c=0.8$ for the onset of stochastic motion can be easily exceeded. Since the irregular motion leads to particle diffusion near the equatorial region, this suggests that proton precipitation can occur in the equatorial region during the geomagnetic pulsation events.

ACKNOWLEDGEMENT

This work is supported by the Air Force Office of Scientific Research, Grant No. AFOSR 88-0127.

REFERENCES

Hasegawa, A., Geophys. Res. Lett., 1979, 6, 664.

Prakash, M., J. Geophys. Res., 1980, 94, 2487, and the references therein.

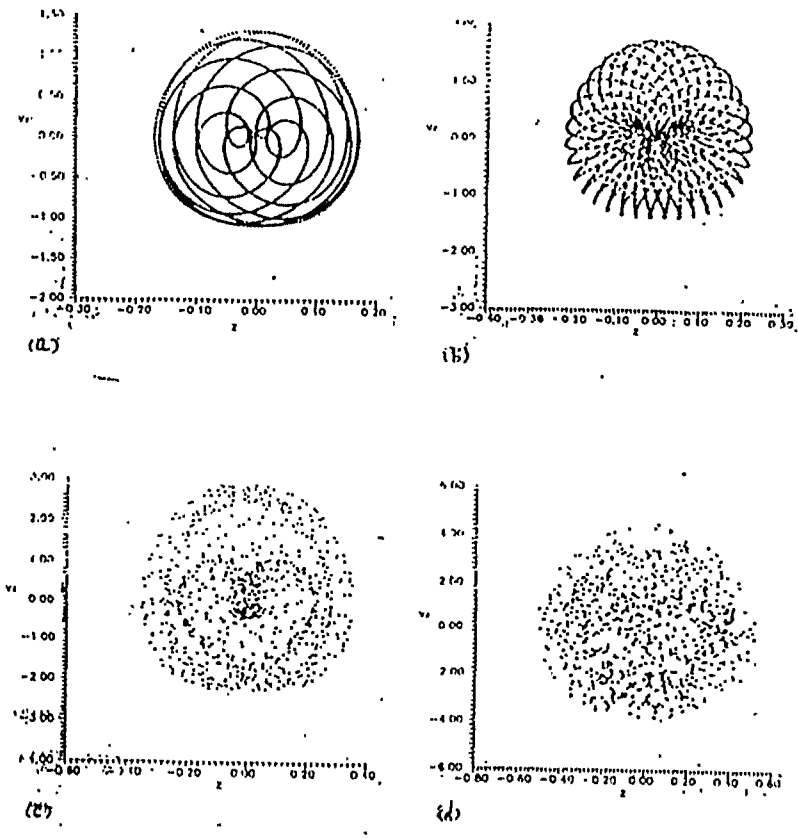

Fig. 1 Surface of section plots for (a) $\epsilon=0.25$, (b) $\epsilon=0.35$, (c) $\epsilon=0.65$, and (d) $\epsilon=0.8$

GEOPHYSICAL RESEARCH LETTERS, VOL. 17, NO. 12, PAGES 2209-2212, NOVEMBER 1990

TEMPORAL EVOLUTION OF HF-ENHANCED PLASMA LINES

S. P. Kuo and A. Y. Ho

Weber Research Institute, Polytechnic University

M. C. Lee

Plasma Fusion Center, Massachusetts Institute of Technology

Abstract The temporal evolution of HF-enhanced plasma lines (HFPLs) is investigated theoretically. The HFPLs refer to the radar echoes at frequencies near the sum and difference of the radar frequency and the HF heater wave frequency. These enhanced spectral lines are caused by backscatter of radar signals from plasma waves having a wavenumber of 18 m^{-1}. A nonlinear theory has been developed to explain both the intensity overshoot and altitude expansion of HFPLs observed at Arecibo, Puerto Rico [Djuth and Sulzer, 1989] with good agreement.

Introduction

Parametric instability plays an important role in ionospheric HF heating experiments to produce various nonlinear plasma phenomena. One of the most pronounced signature of this instability is the constant observation of HF-enhanced plasma lines (HFPLs) at Arecibo, Puerto Rico, which refer to the enhanced backscatter spectrum of the Arecibo 430 MHz radar signals at frequencies near 430 MHz $\pm f_{HF}$ [e.g. Carlson et al., 1972]. Here f_{HF} is the frequency of the HF heater wave. The enhanced radar echoes at these two sidebands provide useful information on the characteristic features of those parametrically excited upgoing and downgoing plasma waves. One of the interesting characteristics of the observed HFPLs at Arecibo is the plasma line overshoot phenomenon [Showen and Behnke, 1978; Showen and Kim, 1978].

This overshoot phenomenon was further investigated in recent experiments on the temporal evolution of HFPLs by Djuth et al. [1986]. The experimental results at high HF power (80 MW ERP) showed that the HFPLs exhibited an initial growth for a few tens of milliseconds before reaching a maximum intensity, and then drastically reduced their strength in a time period of a second. An interpretation of this phenomenon has been offered in Kuo et al. [1987], suggesting that anomalous damping introduced by incoherent scattering of electron orbits by the excited plasma waves results in a mode competition process. It is found that anomalous damping is generally larger for plasma waves with greater propagation angles with respect to the geomagnetic field. Hence, the plasma waves picked up by the Arecibo 430 MHz radar at the propagation angle of, approximately, 40° can be suppressed by those propagating at smaller angles after the heater is on for about a second. Similar mode competition process leading to plasma line overshoot has also been considered in the early work by Perkins et al. [1974]. In their formulation of the nonlinear damping rate, the effect of geomagnetic field is neglected. Their nonlinear damping mechanism is based on resonant velocity diffusion of charged particles in the beat wave fields (i.e. nonlinear Landau damping), which becomes much less effective than that caused by orbit (spatial) diffusion mechanism [Dum and Dupree, 1970] in the magnetized plasma if there is no specific cyclotron resonance involved.

In the heating experiments conducted by Djuth and Sulzer at Arecibo in April, 1988, the HF heater was operated in a pulse mode of 1 minute on and 9 minutes off. During these observations, the HF heater was operated at 5.1 MHz and approximately 80 MW effective radiated power was transmitted. Radar measurements with improved altitude and temporal resolution were made in the experiments to investigate the time evolution of both the intensity and location of HFPLs. The observations showed that, after the HF heater was turned on, the intensity of HFPLs exhibited overshoots. During the same time period, the altitude interval of HFPLs also expanded to an extent greater than that predicted by a linear theory. The upper cutoff altitude (~ 275.8 Km) was very close to the reflection point of HF waves in the ionospheric plasma. While the location of HFPLs never exceeded the HF reflection height, it could generally extend downward over 1 to 2 kilometers within 30 - 50 milliseconds after the HF heater was turned on [see Figure 1 of Djuth and Sulzer, 1989].

A theory is offered in the present paper to explain this newly observed downward extension of altitude interval of the HFPLs. The proposed theory is based on the "fake" heating of the bulk plasma by excited Langmuir waves [e.g. Segdeev and Galeev, 1969, pp 63-64]. In addition to parametric instabilities, strong turbulence processes involving the production of cavitons/solitons have been suggested as possible sources of HF-enhanced plasma waves in the Arecibo ionosphere [e.g. DuBois et al., 1990; Payne et al., 1984]. The "fake heating" should occur regardless of the source of induced Langmuir waves. To illustrate the effect, we will use parametric instability theory so that Langmuir wave intensities can be more readily calculated and the modal equations derived in our previous work addressing the plasma line overshoot phenomenon [Kuo et al., 1987] can be directly incorporated in the present study. An "apparent" increase in the plasma temperature, which is proportional to the energy density of excited Langmuir waves, can cause the lowering of the resonant location of HFPLs picked up by the radar. Thus, following the growth and saturation of Langmuir waves, an expansion of the originating altitude interval of HFPLs is detected.

Theory and Numerical Results

As Langmuir waves are excited by HF heater via parametric decay instability, their wave fields can affect electron motion

Paper number 90GL02070
0094-8276/90/90GL-02070$03.00

and cause diffusion in the velocity space. Such a diffusion process can be described by a quasilinear equation wherein the diffusion coefficient can be separated into two parts. One part arises from the resonant interaction of waves with electrons and only very few electrons contribute to this part of the diffusion coefficient. By contrast, the nonresonant (or adiabatic) wave-electron interaction involves the main body of the plasma distribution in the plasma oscillations.

The oscillatory kinetic energy associated with the excited Langmuir waves increases with the field intensity of the waves and the main body of the plasma appears to be heated. This effective heating of electrons by Langmuir waves leads to the apparent increment in the electron temperature by $\tau = \Sigma_k E_k^2/4\pi n_e$, where E_k^2 is the spectral intensity of Langmuir waves and n_e is the background electron density [e. g. Sagdeev and Galeev, 1969]. Consequently, the dispersion relation of Langmuir waves has the following modified form: $\omega_\ell^2 = \omega_{pe}^2+\Omega_e^2\sin^2\theta+3k_\ell^2(T_e+\tau)/m_e$ where ω_ℓ, ω_{pe}, k_ℓ, Ω_e, m_e and T_e have the standard meaning and θ is the propagation angle of Langmuir wave with respect to the geomagnetic field. Note that $\vec{k}_{\ell\pm}$ and ω_ℓ are fixed by the relations $\vec{k}_{\ell\pm} = +(2\vec{k}_R \pm \vec{k}_{HF})$ [Showen, 1979] for the radar detected HFPLs, where $\vec{k}_R$ is the wavevector of the radar signal and $\omega_\ell \approx \omega_{HF}$ from the frequency matching condition of the parametric instability. In order to maintain the maximum growth rate of the parametric decay instability, it requires that $\omega_{pe}^2+3k_\ell^2\tau/m_e$ remain a constant so that the sideband of the instability process can always satisfy the dispersion relation. Consequently, the matching altitude of the radar detected HFPLs has to move downward for a smaller ω_{pe} because plasma heating occurs at altitudes below the F peak. The instability of Langmuir waves associated with HFPLs in the original height will, however, continue to grow as long as the instability thresholds are still exceeded by the heater wave field. Then, the lowering of the HFPLs' matching altitude actually represents the expansion of the originating altitude interval of the detected HFPLs. This process of lowering the matching altitude of HFPLs can be described by $d\omega_{pe}^2/dt = -3(k_\ell^2/m_e)\, d\tau/dt$.

A linear density profile is assumed for the heated ionosphere, i.e., $\omega_{pe}^2 = \omega_{peo}^2(1+x/L)$, where L is the linear scale height of the ionospheric density and ω_{pe}^2 is the electron plasma frequency at the initial location of the concerned HFPLs. Then, the above equation can be written as

$$dx/dt = -(3k_\ell^2 L/m_e\omega_{peo}^2)d\tau/dt \qquad (1)$$

showing the temporal change of the height of the detected HFPLs. Let $I_\theta = 4\pi\sin\theta\int dk k^2 E_{k\theta}^2$ represent the spectral intensity of Langmuir waves propagating at the same angle θ with respect to the geomagnetic field. Thus, τ is defined to be $\int_o^{\theta_o} I_\theta d\theta/4\pi n_e$, where θ_o is the averaged maximum spectral angle of the excited Langmuir waves [Kuo et al., 1987]. Substituting this expression for τ into (1) yields

$$dx/dt = -(3k_\ell^2 L/4\pi n_e m_e\omega_{peo}^2)[I_{\theta_o} d\theta_o/dt+\int_o^{\theta_o} dI_\theta/dt\, d\theta] \qquad (2)$$

where θ_o and I_θ are governed by the rate equations derived in our earlier work [Kuo et al., 1987] on the study of HFPLs overshoot phenomenon. They are

$$dI_\theta/dt = [\bar{\alpha}_\theta\cos\theta - \bar{\beta}_\theta - 2\bar{d}_\theta - \bar{\eta}I_\theta^{1/2}]I_\theta \qquad (3)$$

and

$$d\theta_o/dt = -\{b\sin^3\theta_o\cos^4\theta_o/[\bar{\alpha}\sin^3\theta_o + bI_{\theta_o}\sin^5\theta_o\cos^5\theta_o$$

$$+ (2 - 5\sin^2\theta_o/\cos^2\theta_o)(\bar{\alpha}_{\theta_o}\cos\theta_o - \bar{\beta}_{\theta_o} - \bar{\eta}_{\theta_o}I_{\theta_o}^{1/2}]\}$$

$$\int_o^{\theta_o}[\bar{\alpha}_\theta\cos\theta - \bar{\beta}_\theta - 2\bar{d}_\theta - \bar{\eta}I_\theta^{1/2}]I_\theta\sin^2\theta\cos^2\theta d\theta \qquad (4)$$

where $b = \alpha^6c^2/32\beta_1^5B_o^2\omega_o^2$, $\bar{\alpha} = \alpha^2/\beta_1$, $\bar{\alpha}_\theta = 2\alpha\sqrt{k_o}$, $\bar{\beta}_\theta = 2(\beta_o+\beta_1k_o)$, $\bar{\eta}_\theta = (\Delta k/k_o)^{3/2}ek_o^{1/2}/(4\pi\sin\theta m_e m_i\omega_o c_s)^{1/2}$, and $\bar{d}_\theta = [h\alpha c^2k_o^2\sin^2\theta/2B_o^2\omega_o^2]\int_o^{\theta_o} I_{\theta'}\sin^2\theta'\cos\theta' d\theta'$; θ_o is determined via $\bar{\alpha}_{\theta_o}\cos\theta_o - \bar{\beta}_{\theta_o} - 2\bar{d}_{\theta_o} - \bar{\eta}_{\theta_o}I_{\theta_o} = 0$ in equation (3) because plasma waves with this propagation angle have zero nonlinear growth rate; $\alpha = eE_o/2(m_e m_i\omega_o c_s)^{1/2}$, $k_o = \alpha^2\cos^2\theta/4\beta_1^2$ and $\beta_o = \nu_{ei}/4$; $2E_o$, ω_o, c_s, and ν_{ei} are the amplitude of the HF heater wave, the heater wave frequency, the ion acoustic speed, and the electron-ion collision frequency, respectively; β_i defined by $(c_s/4)(\pi/8)^{1/2}(T_e/T_i)^{3/2}\exp[-T_e/2T_i - 3/2]$ is proportional to the ion Landau damping rate ; $\Delta k/k_o$ given by $(\sqrt{2})\omega_o\beta_o/k_o v_{te}^2$ is the bandwidth of spectral lines contributing to the anomalous damping rate of the Langmuir cascading process ; $h = 2k_o/\Delta k_{\theta=0}$ and v_{te} is the electron thermal speed defined by $(T_e/m_e)^{1/2}$.

The three coupled equations (2)-(4) describe the temporal evolution of x, I_θ and θ_o which correspond to the altitude of HFPLs, the spectral intensity of excited plasma waves, and the maximum propagation angle of plasma waves, respectively. For a numerical analysis, we rewrite these equations in terms of the dimensionless variables $\bar{x} = x/L$, $\xi = 2\beta_o t$, and $\bar{I}_\theta = I_\theta/4\pi n_e T_e$ as follows:

$$d\bar{x}/d\xi = -A[\bar{I}_{\theta_o}(d\theta_o/dt)+\int_o^{\theta_o}(dI_\theta/dt)d\theta \qquad (5)$$

$$d\bar{I}_\theta/d\xi = [\alpha_1^2\cos^2\theta - 1 - B\cos^5\theta\sin^2\theta\int_o^{\theta_o}\bar{I}_\theta\sin^2\theta'$$

$$\cos\theta' d\theta' - C\cos^2\theta\sin^{-1/2}\theta\bar{I}_\theta^{1/2}]\bar{I}_\theta \qquad (6)$$

$$d\theta_o/d\xi = -\{B\sin^3\theta_o\cos^4\theta_o/[2\alpha_1^2\sin^2\theta_o + B\bar{I}_{\theta_o}$$

$$\sin^2\theta_o\cos^5\theta_o + (2 - 5\sin^2\theta_o/\cos^2\theta_o)$$

$$(\alpha_1^2\cos^2\theta - 1) - C(5/2 - 7\sin^2\theta_o/\cos^2\theta_o)$$

$$\cos^{-2}\theta_o\sin^{-1/2}\theta_o\bar{I}_{\theta_o}^{1/2}]\}\int_o^{\theta_o}(d\bar{I}_\theta/d\xi)\sin^2\theta\cos\theta d\theta \qquad (7)$$

where $\alpha_1 = \alpha/\alpha_{th}$, $\alpha_{th} = 2(\beta_o\beta_1)^{1/2}$, $A = 3k_\ell^2 v_{te}^2/\omega_{peo}^2$, $B = (\sqrt{2})\alpha_1^3\beta_o^3 v_{te}^4\omega_{peo}^2/\beta_1^4\Omega_e^2\omega_o^3$, and $C = \beta_1^2\omega_o\omega_{pi}/20\alpha_1^2\beta_o^2 v_{te}^2$. Using the parameters relevant to the Arecibo heating experiments: $v_{te} = 1.3\times10^5$ m/sec, $c_s = 1.5\times10^3$ m/sec, $T_e = T_i = 1100$°K, $\omega_o/2\pi = 5.1$ MHz, $\lambda_\ell = 2\pi/k_\ell = 35$ cm (for the plasma mode detected by the 430 MHz radar), $\nu_{ei} = 500$ Hz

and $\alpha_1 \approx 2.0$, we then have $\beta_0 = 125$ Hz, $\beta_1 = 31.8$ n/sec, A = 1/50, B = 120 and C = 0.325. Thus, the time dependence of the matching altitude and intensity of HFPLs can be determined by integrating equations (5)-(7).

Shown in Figure 1 is the numerical result of temporal evolution of the spectral intensity I_{40o} of the Langmuir waves simulating that detected by the Arecibo 430 MHz radar at the angle of 40° with respect to the geomagnetic field. The observed overshoot phenomenon of HFPLs is successfully reproduced by our model. Further, the calculated evolution of the HFPLs' height is presented in Figure 2, showing that the matching altitude of HFPLs moves downward as the instability grows. The evolution of the "fake" temperature increment τ is also shown in the same figure. As mentioned before, this represents the expansion of the originating region of the HFPLs because the Langmuir waves responsible for HFPLs are excited not only from their original location but also extending to a lower altitude due to "fake heating" of electrons by the Langmuir waves. The calculated distance of lowering is 0.05 times of the ionospheric scale height (L) after the HF heater is turned on for 50 milliseconds. The ionospheric scale height, L, deduced from the experiments is about 22 kilometers, leading to the expansion of originating altitude interval of HFPLs to be 1.1 kilometers. These theoretical results agree well both qualitatively and quantitatively with the observations [Djuth and Sulzer, 1990].

In the formulation of present theory, mode competition mechanism is included for overshoot while cascading mechanism is included for the saturation of the plasma lines. Only when the first mechanism dominates over the second mechanism, overshoot can occur. Therefore, it is useful to find out the relationship between overshoot phenomenon and the HF intensity. The dependence of the overshoot intensity and overshoot time on the pump intensity are concerned.

Let t_1, t_2 and t_3 represent the times for the plasma line intensity to reach its peak, then drop to one-half and then one-tenth of its peak value, respectively. Note that t_1 approaches infinity if this plasma line does not overshoot. The dependence of these characteristic times on the heater intensity is displayed in Figures 3(a) and 3(b). Shown in Figure 4 is the dependence of the peak intensity of HFPLs on the heater intensity. The results show that both overshoot times and peak intensity of HFPLs decrease generally with the heater intensity. It is also shown that the overshoot phenomenon occurs only when the heater intensity exceeds the threshold of the parametric decay instability by a value $\alpha_1 \sim 1.42$. These predictions await to be corroborated in the future experiments.

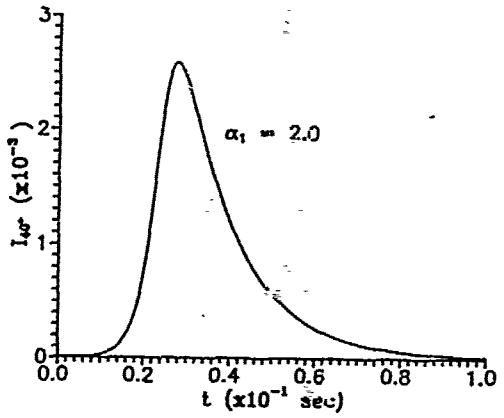

Fig. 1 Temporal evolution of the intensity I_{40}° of HFPLs detected by Arecibo's 430 MHz radar.

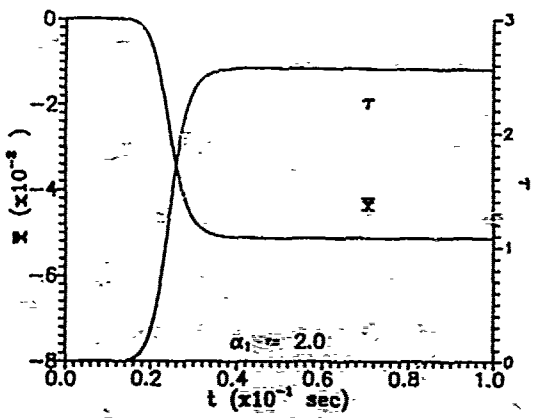

Fig. 2 Normalized matching altitude x and the fake temperature τ vs. time t.

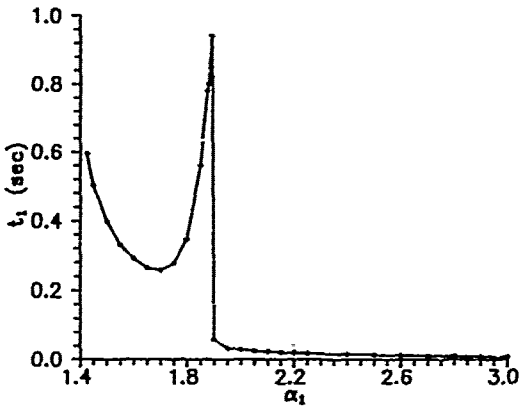

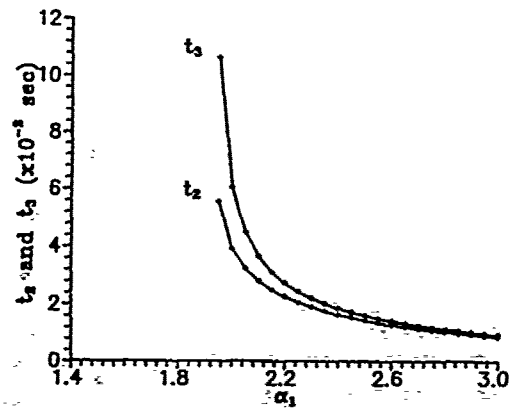

Fig. 3 Funtional dependence of the times (t_1,t_2,t_3) for HFPLs' intensity to reach its peak (t_1), to drop to one-half (t_2) and one-tenth (t_3) of its peak value on the normalized pump intensity α_1.

(a) t_1 vs α_1.

(b) t_2 and t_3 vs α_1.

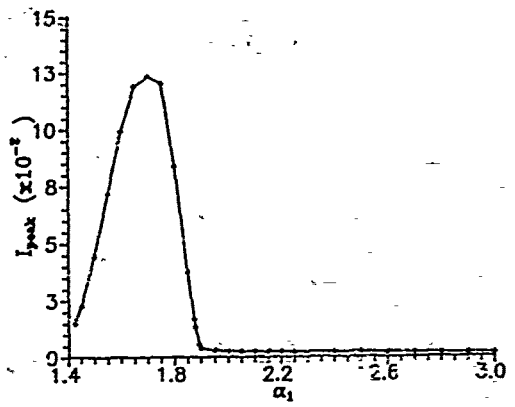

Fig. 4 The peak value of I_{40}° vs α_1.

Summary

Our theoretical model [Kuo et al., 1987] developed originally for explaining the intensity overshoot of the HFPLs has been extended. The extension of the model is based on the fact that nonresonant heating of plasma electrons by the parametrically excited Langmuir waves can yield an apparent increment in electron temperature. This fake heating of electrons introduces an extra term into the dispersion relation of Langmuir waves. The modification of the dispersion relation moves the matching location of the HFPLs to a lower altitude where the plasma density is less than that at their initial location. This model has successfully reproduced both phenomena of the intensity overshoot and the downward expansion of the originating altitude interval of HFPLs in good agreement with the observations. The numerical results also show that both the overshoot time and peak intensity decrease generally with the pump intensity and overshoot occurs only when the pump intensity exceeds the threshold intensity of the parametric decay instability by a factor $\alpha_1 \sim 1.42$.

It is noted that thermal filamentation instability can generate large scale density perturbation (> 1 Km scale length) which may also cause the shift of the plasma line altitude. However, two facts stand on the way to rule out the possibility of such a cause mechanism for the observed phenomena. One is its growth time. It takes at least a few seconds for the development of large scale density irregularities through thermal filamentation instability [Kuo and Schmidt, 1983]. The other one is the filamentation direction which is perpendicular to rather than within the magnetic meridian plane for an O-mode pump wave [Kuo and Schmidt, 1983].

Acknowledgements: We appreaciate useful comments and discussions with Dr. F. T. Djuth and Dr. R. L. Showen. This work was supported by the National Science Foundation Grant No. ATM-8816467 and by the Air Force Office of Scientific Research Grant No. AFOSR-88-0127 at the Polytechnic University, and by the NASA Grant No. NAG5-1055 at the Massachusetts Institute of Technology. The numerical work was performed at the Pittsburgh Supercomputing Center which is supported by the National Science Foundation.

References

Carlson, H. C., Gordon, W. E., and Showen, R. C., High frequency induced enhancements of the incoherent scatter spectrum at Arecibo, *J. Geophys. Res.*, *77*, 1242-1250, 1972.

Djuth, F. T., Gonzales, C. A., and Ierkic, H. M., Temporal evolution of HF-enhanced plasma line in the Arecibo F region, *J. Geophys. Res.*, *93*, 12089-12107, 1986.

Djuth, F. T., and Sulzer, M. P., High-resolution observations of HF-enhanced plasma waves at Arecibo, *Geophys. Res. Lett.*, September, 1990.

DuBois, D. F., Rose, H. A. , and Russel, D., Excitation of strong Langmuir turbulence in plasmas near critical density : Application to HF heating of the ionosphere, *J. Geophys. Res.*, to be published.

Dum, C. T. and Dupree, T. H., Nonlinear stabilization of high frequency instabilities in a magnetized field, *Phys. Fluids*, *13*, 2064-2081, 1970.

Kuo, S. P. and Schmidt, G., Filamentation instability in magnetized plasmas, *Phys. Fluids*. *26*, 2529-2536, 1983.

Kuo, S. P., Lee, M. C., and Djuth, F. T., A new interpretation of plasma-line overshoot phenomena, *Geophys. Res. Lett.*, *14*, 961-964, 1987.

Payne, G. L., Nicholson, D. R., Downie, R. M., and Sheerin, J. P., Modulation instability and soliton formation during ionospheric heating, *J. Geophys. Res.*, *89*, 10921-10928, 1984.

Perkins, F. W., Oberman, C. and Valso, Parametric instabilities and ionospheric modification, *J. Geophys. Res.*, *79*, 1478-1496, 1974.

Sagdeev, R. Z., and Galeev, A. A., *Nonlinear plasma theory*, edited by T. M. O'Neil and D. L. Book, Bejamin Publications, New York, 1969.

Showen, R. L. and Behnke, R. A., The effect of HF-induced plasma instabilities on ionospheric electron temperatures, *J. Geophys. Res.*, *83*, 207-209, 1978.

Showen, R. L., and Kim, D. M., Time variations of HF-enhanced plasma waves, *J. Geophys. Res.*, *83*, 623-628, 1978.

Showen, R. L., The spectral measurement of plasma lines, *Radio Sci.*, *14*, 503-508, 1979.

S.P. Kuo and A.Y. Ho, Weber Research Institute, Polytechnic University, Farmingdale, NY 11735.
M.C. Lee, Plasma Fusion Center, Massachusetts Institute of Technology, Cambridge, MA 02139.

(Received December 1, 1989;
revised July, 16, 1990;
Accepted September 10, 1990)

J. Plasma Physics (1991), *vol.* 45, *part* 2, *pp.* 159–172
Printed in Great Britain

Reconstruction of global micropulsations in the magnetosphere

M. H. WHANG, S. P. KUO
Department of Electrical Engineering/Computer Science. Weber Research Institute. Polytechnic University. Farmingdale. New York 11735. U.S.A.

AND M. C. LEE
Plasma Fusion Center. Massachusetts Institute of Technology. Cambridge. Massachusetts 02139. U.S.A.

(Received 31 August 1990 and in revised form 15 December 1990)

The coupling of hydromagnetic Alfvén waves is studied numerically in a dipole-field model of the magnetosphere. The two coupled hydromagnetic equations derived by Radoski are solved as an implicit boundary-value problem, namely the boundary conditions at the magnetopause are determined self-consistently. Thus the calculated wave-field distribution inside the magnetosphere can match all known linear characteristic features of the stormtime Pc5 waves observed on 14/15 November 1979 from satellites. A set of proper boundary conditions is found, excellent agreement between the numerical results and observations is demonstrated. Based on the very limited spatial coverage ($L \approx 6{\cdot}6$ and within a latitudinal region $(-10°, 10°)$), of the data provided by the satellites, the theoretical model can successfully reconstruct the global micropulsations in the magnetosphere and identify the source regions of hydromagnetic waves.

1. Introduction

Recent observations of a stormtime Pc5 event during 14/15 November 1979, near geosynchronous orbit (Higbie *et al.* 1982; Takahashi, Higbie & Baker 1985) provide comprehensive data on the characteristic features of the stormtime Pc5 waves, where Pc5 waves appear as geomagnetic fluctuations having their oscillation periods in the range from 150 to 600 s. This event was characterized by long-duration (50 h) highly compressional magnetic perturbation, and modulation in energetic particle fluxes. The azimuthal phase velocity $|V_\phi| =$ 4–14 km s^{-1} and azimuthal wavenumber $m = 20$–120 were measured. However, the field-aligned structure of the stormtime Pc5 waves was not reported until recently by Takahashi *et al.* (1987). Magnetic field data from the four satellites SCATHA (P78-2), GOES2, GOES3 and GEOS2 have been analysed to examine the wave structure along the ambient magnetic field line ($L \approx 6{\cdot}6$) within a latitudinal region $(-10°, 10°)$. Five distinct features have been identified. It has been observed that the compressional component of the wave has a node near the equator, offering evidence of an antisymmetric standing-wave structure, while the transverse component has a symmetric standing-wave structure with an antinode near the equator. Moreover, nodes for the transverse components at several degrees off the dipole equator have also been observed. They indicate

that these components of the magnetic perturbation have a very short parallel wavelength about $3R_e$, which is much shorter than $30R_e$ for the fundamental mode of the shear wave at $L \approx 6{\cdot}6$. For the wave frequency of 0·002 Hz, the field-aligned phase speed of the Pc5 wave is estimated to be about 40 km s^{-1}, an order of magnitude lower than the estimated Alfvén speed (Takahashi *et al.* 1985). It has been shown that the two transverse components of the wave have different wavelengths, as evidenced by the result that their nodes are located at different magnetic latitudes. One possible cause leading to this result, suggested by Takahashi *et al.* (1987), is the inhomogeneity of the magnetosphere along the field line. The relative phase among the magnetic field components is either 0°, $\pm 90°$ or 180°, and changes by 180° as the observing satellites move across the nodes of the wave. The compressional component oscillates 90° out of phase with the azimuthal component. It oscillates, however, either in phase or 180° out of phase with the radial component. An interpretation of these relationships based on wave propagation in an inhomogeneous medium is also provided. The last of the identified features is the presence of harmonics. This is manifested by the wave form of the compressional magnetic field component, which oscillates in time with different heights for two consecutive peaks. This feature is associated with the nonlinearity of the plasma.

Many mechanisms have been suggested to explain the excitation of the stormtime Pc5 waves. These include the drift mirror instability (Hasegawa 1960), bounce drift resonance excitation of ULF waves (Southwood 1976), drift compressional instability (Hasegawa 1971; Ng, Patel & Chan 1984) and coupling between a drift mirror wave and a shear Alfvén wave (Walker *et al.* 1982). Recently, Cheng & Lin (1987) performed a comprehensive eigenmode analysis for both the drift mirror and drift compressional instabilities. The results show that two of the five features deduced from the observations, the antisymmetric standing-wave structure and the phase relations among the field components, can be explained by the eigenmode structures of the drift mirror instability in the dipole magnetic field configuration. However, the difficulty in using the drift mirror instability to interpret stormtime Pc5 waves comes from the instability condition. Using the SCATHA ion data (17 eV–300 keV), Takahashi *et al.* (1987) have shown that the instability condition cannot be satisfied. They have also shown that all the existing theories have limited success in explaining the results of the event. It is therefore recognized that a new theoretical development to explain the excitation mechanism of stormtime Pc5 waves is desirable.

Information on the spatial structure of the waves, both radial and latitudinal variations, seems to play a key role in guiding the theoretical development. However, only very limited spatial coverage of the data provided by the satellites is available. In the present work we study theoretically the coupling and propagation of hydromagnetic waves in the dipole-field model of the magnetosphere. The set of coupled hydromagnetic wave equations (Radoski 1967) is solved numerically. The solution satisfies the perfect-conductor boundary conditions at the ionosphere, together with the imposed wave structures drawn by Takahashi *et al.* (1987) from the magnetospheric storm events during 14/15 November 1979. The local data obtained by satellites are then used to reconstruct the global wave structures of the event in terms of hydromagnetic waves in the magnetosphere. The boundary conditions at the

magnetopause are determined self-consistently so that the spatial dependence of the solutions along the $L = 6{\cdot}6$ line matches all four linear features drawn from the satellite data (Takahashi *et al.* 1987).

Section 2 describes the dipole-field model of the magnetosphere and the coupled hydromagnetic wave equations used in the following numerical analysis. The numerical results and a comparison with the satellite data are presented in §3. A summary of the present work and conclusions are given in §4. The method of numerical analysis is briefly described in an Appendix.

2. Governing equations

It is generally believed that geomagnetic micropulsations are associated with hydromagnetic waves that can be excited through different types of plasma instabilities in the magnetosphere or on its boundary, or in the solar wind. In general, the sources of these plasma instabilities can be considered to be localized in comparison with the range of the magnetosphere. Therefore only a source-free hydromagnetic wave equation will be used in the following to study the propagation of hydromagnetic waves in the magnetosphere. The MHD equations are used for the analysis of hydromagnetic perturbations in the magnetosphere, which can be considered to be an ideal MHD system. It is then straightforward to convert the MHD equations into the ideal MHD wave equation, which is a single second-order time-derivative equation for the wave electric field $\mathbf{E}$:

$$\frac{\partial^2 \mathbf{E}}{\partial t^2} = \mathbf{A} \times \{\mathbf{A} \times [\nabla \times (\nabla \times \mathbf{E})]\}, \tag{1}$$

where $\mathbf{A} = \mathbf{B}_0/(4\pi\rho)$ is the Alfvén-wave velocity.

An orthogonal dipole co-ordinate system is employed to describe the wave propagation in the magnetosphere. The unit vectors are along the principal normal to the field line ($\hat{\nu}$), parallel to the field line ($\hat{\mu}$) and in the azimuthal direction ($\hat{\psi}$) respectively. More specifically, the co-ordinates are given by $\nu = (\sin^2\theta)/\bar{r}$, which is constant along a dipole field line, $\mu = (\cos\theta)/\bar{r}^2$, which is constant along an orthogonal trajectory of the dipole field lines, and ψ, which is the ordinary azimuthal spherical polar co-ordinate; $\bar{r} = r/R_e$ is the normalized radius in spherical co-ordinates.

Having a time-harmonic dependence of the form $e^{-i\omega t}$, and an oscillating longitudinal variation of the form $e^{im\psi}$, the two scalar components of (1) in the dipole model of the magnetosphere become (Radoski 1967)

$$H_1\left[\frac{\partial}{\partial\mu}\left(H_2\frac{\partial}{\partial\mu}\epsilon_\nu\right) - m^2\epsilon_\nu\right] + \frac{\omega^2}{A^2}\epsilon_\nu = imH_1\frac{\partial}{\partial\nu}\epsilon_\psi, \tag{2}$$

$$H_2\left[\frac{\partial}{\partial\mu}\left(H_1\frac{\partial}{\partial\mu}\epsilon_\psi\right) + \frac{\partial^2}{\partial\nu^2}\epsilon_\psi\right] + \frac{\omega^2}{A^2}\epsilon_\psi = imH_2\frac{\partial}{\partial\nu}\epsilon_\nu. \tag{3}$$

Here $\bar{r}$ is related to ν and μ through the relation $\nu\bar{r} + \mu^2\bar{r}^4 = 1$,

$$H_1 = \frac{1}{\nu\bar{r}^3}, \quad H_2 = \frac{\nu(\nu + 4\mu^2\bar{r}^3)}{\bar{r}^2},$$

$$\epsilon_\nu = \frac{\bar{r}}{[(\nu + 4\mu^2\bar{r}^3)\,\nu]^{\frac{1}{2}}}E_\nu,$$

with E_ν the toroidal component of the wave electric field.

$$\epsilon_\psi = (\bar{r}^3\nu)^{\frac{1}{2}} E_\psi,$$

with E_ψ the poloidal component of the wave electric field, and ρ is the plasma mass density, with the spatial dependence $\rho = \rho_0(1/\bar{r})^n$, where ρ_0 is the plasma mass density on the earth and n is an adjustable positive density index. Since a dipole magnetic field

$$\mathbf{B}_0 = \hat{\mu}\frac{M_0}{R_e^3}\left(\frac{\nu + 4\mu^2\bar{r}^3}{\bar{r}^5}\right)^{\frac{1}{2}}$$

is assumed,

$$\frac{\omega^2}{A^2} = \left(\frac{\omega R_e^3}{M_0}\right)^2 \frac{4\pi\rho_0 \bar{r}^{5-n}}{\nu + 4\mu^2\bar{r}^3}.$$

Equations (2) and (3) describe two basic types of hydromagnetic waves. One is called the guided or toroidal mode; it channels its energy only along the magnetic field lines of forces. The other, called the isotropic or poloidal mode, propagates equally in all directions at the Alfvén speed (Radoski 1976). In general, these two modes are coupled to each other through the inhomogeneities, as shown by the coupling terms on the right-hand sides of (2) and (3). However, for the special case of axial symmetry, $m = 0$, (2) and (3) become decoupled, and thus these two modes are separate. In this case (2) and (3) represent the eigenequations of the toroidal and poloidal modes respectively. Along the magnetic field line ($\hat{\mu}$), the phase velocity of the toroidal mode has magnitude equal to the local Alfvén speed. Hence the toroidal mode is sometimes also called the Alfvén mode. On the other hand, the poloidal mode propagates isotropically, with total phase speed equal to the Alfvén speed. While (B_ψ, E_ν) represent the field components of the toroidal mode, (B_μ, B_ν, E_ψ) represent those of the poloidal mode. The corresponding fluid velocity perturbations are found to be in the $\hat{\psi}$ and $\hat{\nu}$ directions respectively. $\mathbf{V}_\psi$, the response of E_ν, is perpendicular to the wave propagation direction, which is in the $(\hat{\mu}, \hat{\psi})$ plane (for the $m = 0$ case), while $\mathbf{V}_\nu$, the response of E_ψ, has a component along the propagation direction. On the basis of the shear compressional features of the velocity responses, the shear (or slow) and the compressional (or fast) modes are also called the toroidal and poloidal modes respectively.

Since the toroidal mode only channels its energy along the magnetic field, it resonates only with the local field line, and its oscillating frequency is, in general, characterized by the length of the associated geomagnetic field line. Hence periods of geomagnetic micropulsations associated with such field-line resonant modes vary with the L value of the field line. It is believed that such field-line resonant modes are directly responsible for the geomagnetic micropulsations (Dungey 1954; Chen & Hasegawa 1974; Radoski 1974; Chen & Cowley 1989). On the other hand, the energy of the poloidal mode can flow across the field line and fill the volume of the magnetosphere. The characteristics of the poloidal mode depend on the size of the magnetosphere, which is a feature of the cavity mode (see e.g. Kuo, Lee & Wolfe 1987). Without coupling ($m = 0$), the field-line resonant mode (toroidal mode) will not respond to perturbations starting outside the field-line resonance region. However, perturbations in the magnetosphere, in general, stem from the solar wind, which is outside the magnetosphere. Therefore the study of the general case ($m \neq 0$), with coupling between toroidal and poloidal modes, is clearly crucial

to the understanding of dynamical processes such as magnetospheric substorms resulting from the solar-wind–magnetosphere interaction.

For solving (2) and (3), the boundary conditions must be specified. We assume that the magnetosphere extends from $L = 2$ to $L = 10$, the ionosphere is a perfect conductor, and the tangential components of the electric field at the inner boundary are zero. These assumptions lead to the fixed boundary conditions $P(\nu, \mu = \pm 0{\cdot}25) = 0 = T(\nu, \mu = \pm 0{\cdot}25)$, where $P = ie_\varphi$ and $T = e_r$. The boundary conditions at the magnetopause, $P(\nu = 0{\cdot}1, \mu)$ and $T(\nu = 0{\cdot}1, \mu)$, are generally imposed by an external source such as the solar wind. They can thus be assumed to be any functions of μ varying with the physical situation. For good agreement between numerical results and recently reported observational data (Takahashi *et al.* 1987), the boundary conditions at $\nu = 0{\cdot}1$ are found to be of the form

$$P(\nu = 0{\cdot}1, \mu) = P_0(\mu) = \sin\left[k\pi\left(\frac{\mu}{0{\cdot}25}\right)^{\frac{1}{2}q}\right], \tag{4}$$

$$T(\nu = 0{\cdot}1, \mu) = 0, \tag{5}$$

where $P_0(\mu)$ is a spatially distributed sinusoidal perturbation, q is an odd integer less than nine, and k is the harmonic number of the sinusoidal perturbation. For practical reasons, the toroidal mode at the outer boundary is cut-off, i.e. $T = 0$ in the frequency range of the observed perturbations. Using the relations derived from Faraday's law,

$$B_r = \frac{1}{\omega}\left(\frac{1+3\mu^2\bar{r}^4}{\bar{r}^9\nu}\right)^{\frac{1}{2}}\frac{\partial P}{\partial \mu}, \tag{6}$$

$$B_\varphi = -\frac{i}{\omega}\left(\frac{1+3\mu^2\bar{r}^4}{\bar{r}^7}\right)^{\frac{1}{2}}\frac{\partial T}{\partial \mu}, \tag{7}$$

$$B_\mu = -\frac{1}{\omega}\frac{(1+3\mu^2\bar{r}^4)^{\frac{1}{2}}}{\bar{r}^8}\left(\frac{\partial P}{\partial \nu} + mT\right), \tag{8}$$

the numerical solutions for the magnetic field can be determined from the solutions for the electric field.

3. Numerical results and comparison with observations

In the appendix our numerical method is described and the coupled equations (2) and (3) are converted into two difference equations (A 1) and (A 2) for numerical analysis. Equations (A 1) and (A 2) are then solved to obtain the numerical solutions of the coupled hydromagnetic wave equations (2) and (3). The local data acquired by four satellites during the occurrence of the magnetic substorm event on 14/15 November 1979 will be used to prescribe conditions to be matched by the numerical solutions. These data on magnetic fluctuations were recorded with flux-gate magnetometers. The geostationary satellites GOES2, GOES3 and GEOS2 were located at the geographic equator, with geographic longitudes of 107° W, 135° W and 15° E, which correspond to magnetic latitudes of 9° N, 5° N and 1° N, by taking centred dipole graphic coordinates. SCATHA had an elliptical orbit with an orbital period of 23·6 h. The apogee and perigee were $7{\cdot}8R_e$ and $5{\cdot}3R_e$ respectively, and the inclination of the

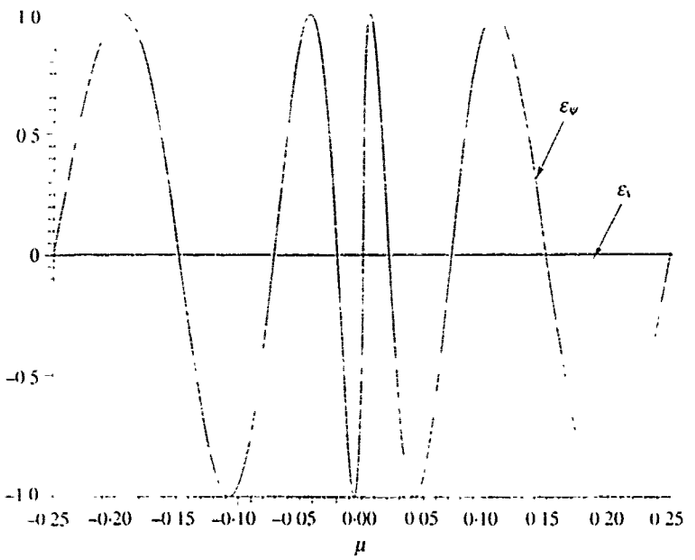

FIGURE 1. Normalized electric fields ϵ_ψ and ϵ_ν at the magnetopause with $k = 4$ and $q = 5$.

orbit was 7·8°. During the course of the 14/15 November event, its magnetic latitude varied between −7° and 0°. The details of the experiments were described by Fennell (1982) with SCATHA, by Grubb (1975) with GOES2 and GOES3, and by Knott (1982) with GEOS2.

A normalized quantity

$$\hat{B}_\alpha \equiv \left(\frac{\langle B_\alpha^2 \rangle}{\langle B_\nu^2 \rangle + \langle B_\psi^2 \rangle + \langle B_\mu^2 \rangle} \right)^{\frac{1}{2}} \tag{9}$$

was introduced in Takahashi *et al.* (1987) to describe the relative amplitudes of each component of the magnetic field, which varies with magnetic latitude. Here $\alpha = \nu, \psi$ or μ, and $\langle B_\alpha^2 \rangle$ is the mean-square amplitude of the magnetic field component, which was obtained by integrating its power-spectral density over the frequency range of the wave. In the same spectral analysis the relative phase of the magnetic field components was also calculated. The relative phase of component α with respect to component β is denoted by $\phi_{\alpha\beta}$.

The best match of numerical results with observational data is found when the harmonic numbers of the sinusoidal perturbation of the poloidal mode at the magnetopause as given by (4) are $M = 20$, $k = 4$ and $q = 5$. The normalized wave electric field at the magnetopause with the boundary condition (4) has the form shown in figure 1. Equations (A 1) and (A 2) are then solved to obtain the field distributions in the entire magnetosphere. The consistency of the numerical results with observations is checked as follows. The numerical results for the magnetic field around the equator in the magnetic latitudinal range $-11° \leqslant \lambda \leqslant 11°$ at a radial distance $L \approx 6{\cdot}6$, i.e. $\nu = 0{\cdot}1515$, are extracted for comparison. The ionospheric boundary is chosen to be about $1{\cdot}84R_e$ in our model. Following the same procedure as Takahashi *et al.* (1987) for data analysis, the normalized amplitude and the relative phase are determined by the numerical solutions of the coupled hydromagnetic wave equations as shown in figures 2 and 3. These results can now be compared directly with the observational data summarized

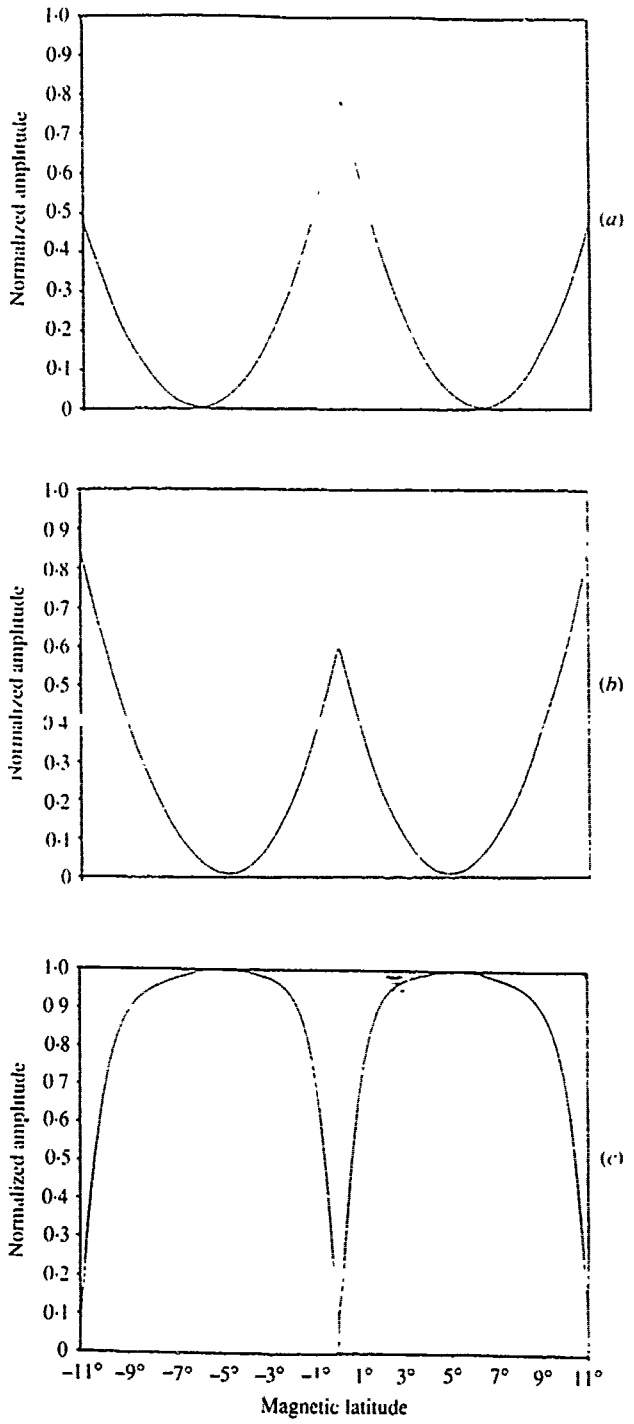

FIGURE 2. Normalized amplitude of the waves as a function of magnetic latitude given from numerical calculations: (*a*) component of outward direction of field line: (*b*) component of east–west direction: (*c*) component of field-line direction.

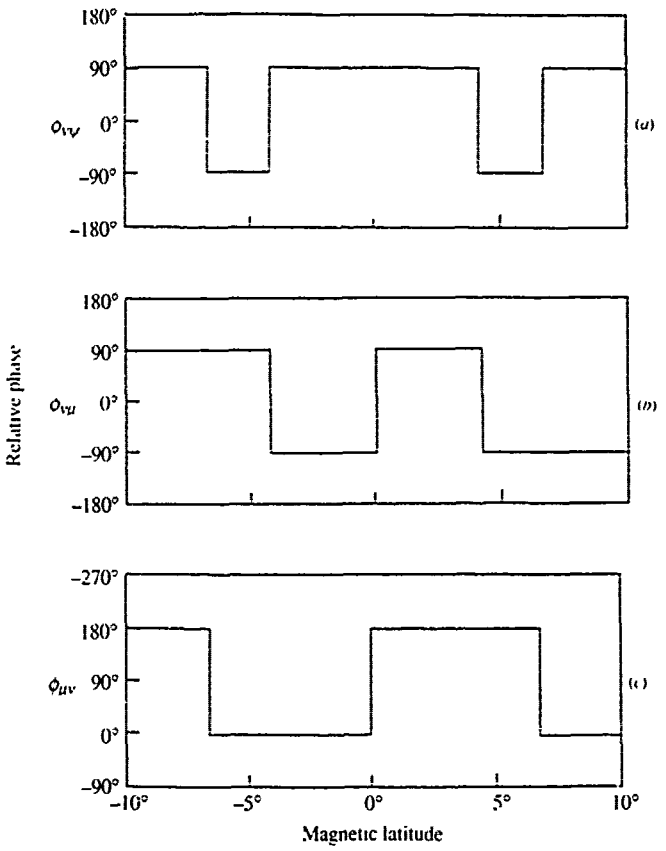

FIGURE 3. Intercomponent cross-phase of the wave given from numerical calculations.

in figures 5 and 6 of Takahashi *et al.* (1987. hereinafter referred to as ref. 1). Excellent agreement is found between our numerical results (i.e. figures 2 and 3) and the observations (i.e. figures 5 and 6 of ref. 1).

As stated in §1, five distinct features have been identified from the observational data. These features are the basis for the further test of the theoretical results. First, the property of $\hat{B}_z$ having short parallel wavelength of a few earth radii (about $3R_e$) as shown in figure 5(*c*) of ref. 1 is reproduced by the numerical result shown in figure 3(*c*) for $\hat{B}_\mu$. As shown in figures 5(*a*) and (*b*) of ref. 1, the nodes of $\hat{B}_x$ and $\hat{B}_y$ appear at different locations, indicating that these two wave components have different parallel wavelengths. Such a multiple-wavelength phenomenon also appears in the numerical results as can be seen from figures 2(*a*) and (*b*) on comparing the locations of the nodes of $\hat{B}_v$ and $\hat{B}_\psi$. The antisymmetric standing-wave structure found in figure 5(*c*) of ref. 1 is also reproduced by the numerical results shown in figure 2(*c*).

The relative phases between each pair of magnetic field components are obtained by calculating the latitude dependence of the relative amplitude of the pair. The relative amplitude between the ν and ψ components. for example. is defined as

$$\hat{B}_\alpha^* \equiv \left(\frac{\langle B_\alpha^2 \rangle}{\langle B_\nu^2 \rangle + \langle B_\psi^2 \rangle} \right)^{\frac{1}{2}}, \tag{10}$$

where $\alpha = \nu$ or ψ. The relative phases for the three different components are evaluated and displayed in figure 3. They agree quite well with the observational

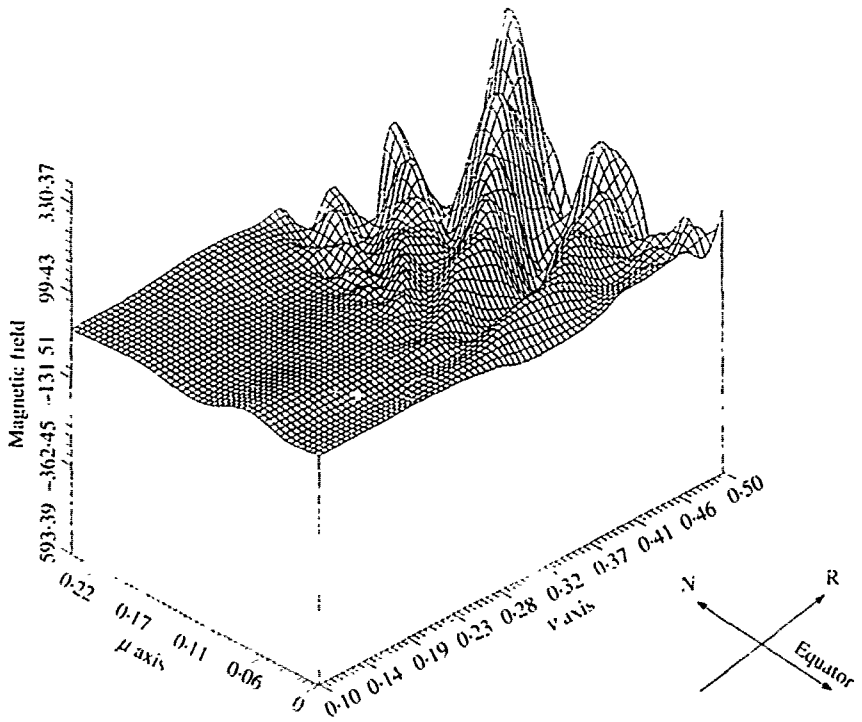

FIGURE 4. Normalized magnetic field of radial component ($m = 20$, $k = 4$, $q = 5$).

results shown in figure 6 of ref. 1. Both the numerical and observational results show that $\hat{B}_\mu$ and $\hat{B}_\nu$ oscillate 180° out of phase for $\theta > 5°$ and in phase for $\theta < 5°$: $\hat{B}_\mu$ and $\hat{B}_\psi$ are out of phase by $\pm 90°$.

The last feature deduced from the satellite data is the frequency doubling often observed near the magnetic equator. The second-harmonic waves observed by GEOS2 and GEOS3 appear along the field-line direction near magnetic latitude $\lambda \approx 0{\cdot}5°$ and along the azimuthal direction at magnetic latitude $\lambda \approx 4{\cdot}7°$ respectively. It is generally believed that the harmonic is due to the nonlinear effect of the plasma. The present study only considers MHD waves in a linear magnetospheric plasma, so the nonlinear harmonic generation process cannot be revealed in the numerical results. Since the nonlinearity of the magnetospheric plasma is weak because of the low plasma density, its effect on the results of the presently extrapolated global reconstruction is expected to be small.

As mentioned in §1, the satellites' orbits cover only a small and specific region of the magnetosphere. Hence the collection of the data by them is bounded in a local region. By contrast, our numerical results are applicable to the entire magnetosphere. Therefore the present work provides a way to use local information to reconstruct the global hydromagnetic waves in the magnetosphere. Consequently, detailed information on the coupling between the toroidal and poloidal modes of hydromagnetic waves can be extracted. Figures 4–6 show the global structure of the three magnetic field components. Their local values at $L = 6{\cdot}6$ and $-11° \leqslant \lambda \leqslant 11°$ lead to the results shown in figures 2 and 3. The μ axis (from 0 to 0·25) is directed along the magnetic field line and covers the region from the equator to the north pole. The other half of the field distributions can be obtained by its symmetrical counterpart. The ν axis

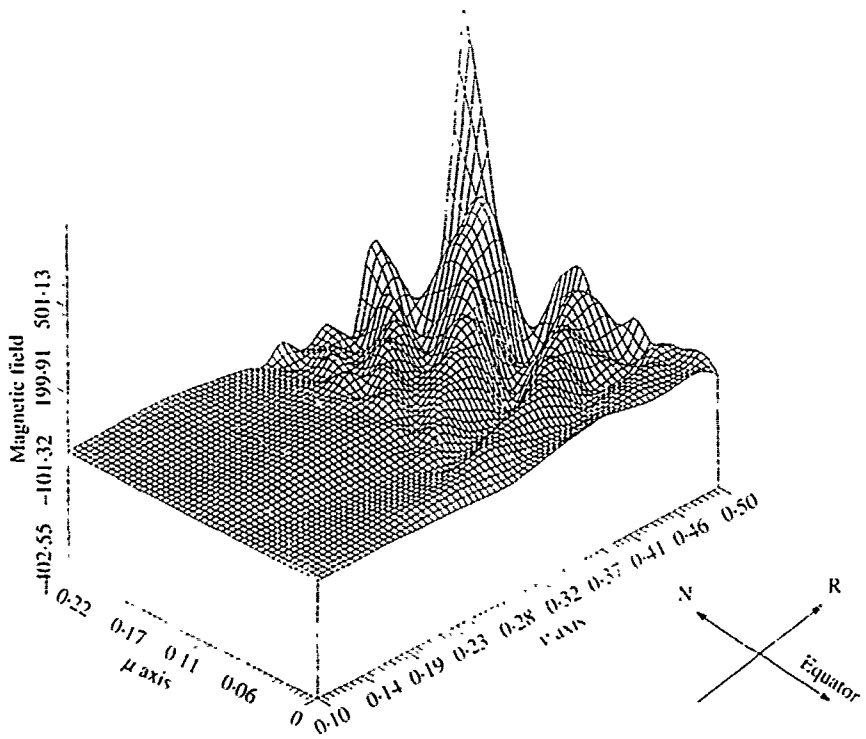

FIGURE 5. Normalized magnetic field of east–west component ($m = 20$, $k = 4$, $q = 5$).

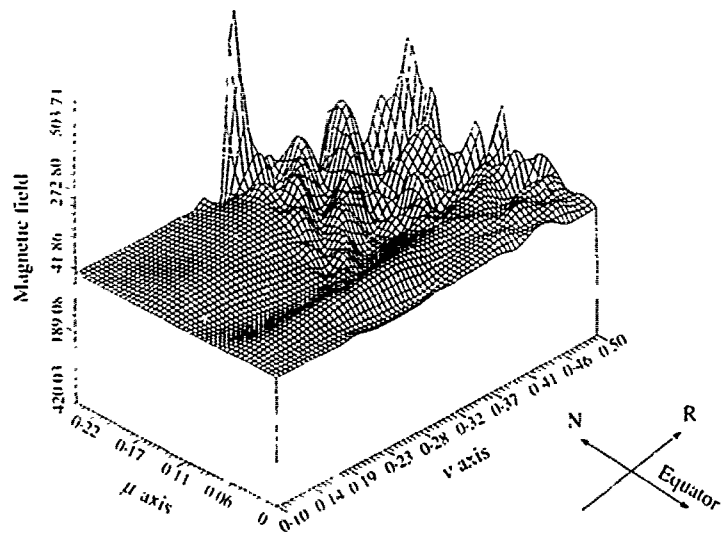

FIGURE 6. Normalized magnetic field of north–south component ($m = 20$, $k = 4$, $q = 5$).

represents the outward direction of the field line: $\nu = 0{\cdot}1$ ($r = 10R_e$) is at the magnetopause, while $\nu = 0{\cdot}5$ ($r = 2R_e$) is at the ionosphere.

The global structure of the field components presented in figures 4–6 shows that the dominant regions of the wave field in terms of its amplitude and spatial variation are somewhere near the inner boundaries of the region inside $L = 6{\cdot}6$. This suggests that the location of the source of the instability responsible for the observed Pc5 wave at $L = 6{\cdot}6$ may not be at $L = 6{\cdot}6$. Therefore the use of the

SCATHA ion data to deduce if the drift mirror instability is the cause of the observed Pc5 wave may not be conclusive. Although Takahashi *et al.* (1987) have shown that the instability condition cannot be satisfied at $L = 6{\cdot}6$, it is, in fact, possible that the condition for drift mirror instability may be satisfied at the actual location of the source of instability, which is near the inner boundary of the magnetosphere as indicated in our theoretical analysis.

5. Summary and conclusion

We have investigated hydromagnetic oscillations of the geomagnetic field in the earth's magnetosphere to explain low-frequency geomagnetic pulsations. A dipole-field model of the magnetosphere is adopted for the analyses of the problems, whereas the plasma density distribution is matched to *in situ* measurements with satellites. Considering an ideal MHD plasma, a hydromagnetic wave equation for the vector wave field is derived. In terms of the dipole co-ordinates, this equation is then decomposed into two mixed-type coupled partial differential equations with variable coefficients for two coupled hydromagnetic wave modes. A numerical code has been developed for solving these two equations using a finite-difference technique. The stability of the numerical scheme is examined by both the Fourier and matrix methods, using the following procedure: the stability conditions are first determined by the Fourier method and then checked by the matrix method. Since two different methods are used, one can be sure that the stability conditions are determined consistently. This code is employed to study an implicit boundary-value problem, namely finding the self-consistent boundary conditions at the magnetopause so that the wave field distribution inside the magnetosphere matches the characteristic features drawn from the data information obtained by the satellites. Then, on the basis of local data, we can reconstruct the global structure of the stormtime Pc5 waves in the magnetosphere.

The characteristic features of the hydromagnetic waves derived from our theoretical model are found to be consistent with those of the observed stormtime Pc5 waves. For instance, the compressional component of the waves has an antisymmetric standing-wave structure evidenced by a node near the equator, while the transverse component exhibits a symmetric standing-wave structure with an antinode near the equator. That the two wave components have different parallel wavelengths (referred as the multiple-wavelength phenomenon) is also seen in our numerical results. The calculated relative phases for the three wave components agree quite well with observations. The appearance of a harmonic wave, which, however, cannot be reproduced by the present model, is believed to originate from nonlinear effects of the magnetoplasma.

The reconstructed global structure of the micropulsations can provide useful information on the mechanism(s) generating the stormtime Pc5 waves. Our numerical results show that strong variation and large wave structure occur near the boundary of the magnetoplasmas spanning the magnetosphere and ionosphere. This suggests that the source(s) of instability mechanisms responsible for the observed Pc5 waves are located in that region, namely near either the magnetopause or the ionosphere.

In conclusion, the global micropulsations in the magnetosphere can be reconstructed by the present model. The success of this theoretical model has

been demonstrated by comparing the numerical results with a 1979 event (Takahashi *et al.* 1987) for which the stormtime Pc5 waves were measured by the four geosynchronous satellites SCHATHA, GOES2, GOES3 and GEOS2. This model has also identified the source regions of micropulsations to be at either the magnetopause or the ionosphere. Moreover, it can correlate geomagnetic activities inside the magnetosphere with solar wind activity in the neighbourhood of the magnetopause. The present model has neglected possible wave dissipation processes. We have assumed that the dissipation of waves in the magnetosphere has been compensated by sources located at the boundaries. This is realized by the fact that the observed waves were last for a long duration of about 50 h.

This work was supported by the Air Force Office of Scientific Research Grant No. AFOSR-88-0127. The numerical work was performed at the Pittsburgh Supercomputing Center, supported by the National Science Foundation. The authors wish to thank Professor Jerry Shmoys for critical comments on the original manuscript.

Appendix. Numerical methods

The governing equations (2) and (3) constitute a set of mixed-type coupled partial differential equations (PDEs) with variable coefficients. Equation (2) is a parabolic type of PDE, while (3) is of elliptic type. The two equations are first converted into difference equations for numerical analysis. This is done by a finite-difference technique using a staggered grid with grid increments $\Delta\mu$ and $\Delta\nu$. Both of the employed computational grids are carefully chosen to ensure second-order accuracy in the resulting system of algebraic equations. A fully implicit scheme is used for this numerical algorithm. The resulting finite-difference equations are

$$P_i^{j-1}-\left(\frac{2\Delta\nu}{\Delta\mu^2}a_{1_{i+1}}^j+\frac{\Delta\nu}{\Delta\mu}a_{2_i}^j\right)T_{i-1}^{j-1}+\left(\frac{4\Delta\nu}{\Delta\mu^2}a_{1_i}^j-2\Delta\nu\,a_{3_i}^j\right)T_i^{j-1}$$
$$-\left(\frac{2\Delta\nu}{\Delta\mu^2}a_{1_i}^j-\frac{\Delta\nu}{\Delta\mu}\right)T_{i-1}^{j+1}=P_i^{j-1}. \quad \text{(A 1)}$$

$$\left(1-a_{3_i}^j b_4-2\Delta\nu\,a_{3_i}^j b_4+\frac{2}{\Delta\mu^2}a_{1_i}^j b_4+4\frac{\Delta\nu}{\Delta\mu^2}a_{1_{ri}}^j b_4\right)T_i^{j-1}$$
$$-\left(\frac{1}{\Delta\mu^2}a_{1_i}^j b_4+\frac{1}{2\Delta\mu}a_{2_i}^j b_4+2\frac{\Delta\nu}{\Delta\mu^2}a_{1_{ri}}^j b_4+\frac{\Delta\nu}{\Delta\mu}a_{2_{ri}}^j b_4\right)T_{i+1}^{j+1}$$
$$-\left(\frac{1}{\Delta\mu^2}a_{1_i}^j b_4-\frac{1}{2\Delta\mu}a_{2_i}^j b_4+2\frac{\Delta\nu}{\Delta\mu^2}a_{1_{ri}}^j b_4-\frac{\Delta\nu}{\Delta\mu}a_{2_{ri}}^j b_4\right)T_{i-1}^{j-1}$$
$$-\left(\frac{2\Delta\nu}{\Delta\mu^2}b_{1_{i+1}}^j+\frac{\Delta\nu}{\Delta\mu}b_{2_i}^j\right)P_{i+1}^{j+1}+\left(\frac{4\Delta\nu}{\Delta\mu^2}b_{1_i}^j-2\Delta\nu\,b_{3_i}^j\right)P_i^{j-1}-\left(\frac{2\Delta\nu}{\Delta\mu^2}b_{1_i}^j-\frac{\Delta\nu}{\Delta\mu}b_{2_i}^j\right)P_{i-1}^{j+1}$$
$$=\left(1+\frac{2}{\Delta\mu^2}a_{1_i}^j b_4-a_{3_i}^j b_4\right)T_i^{j-1}-\left(\frac{1}{\Delta\mu^2}a_{1_i}^j b_4+\frac{1}{2\Delta\mu}a_{2_i}^j b_4\right)T_{i+1}^{j-1}$$
$$-\left(\frac{1}{\Delta\mu^2}a_{1_i}^j b_4-\frac{1}{2\Delta\mu}a_{2_i}^j b_4\right)T_{i-1}^{j-1}. \quad \text{(A 2)}$$

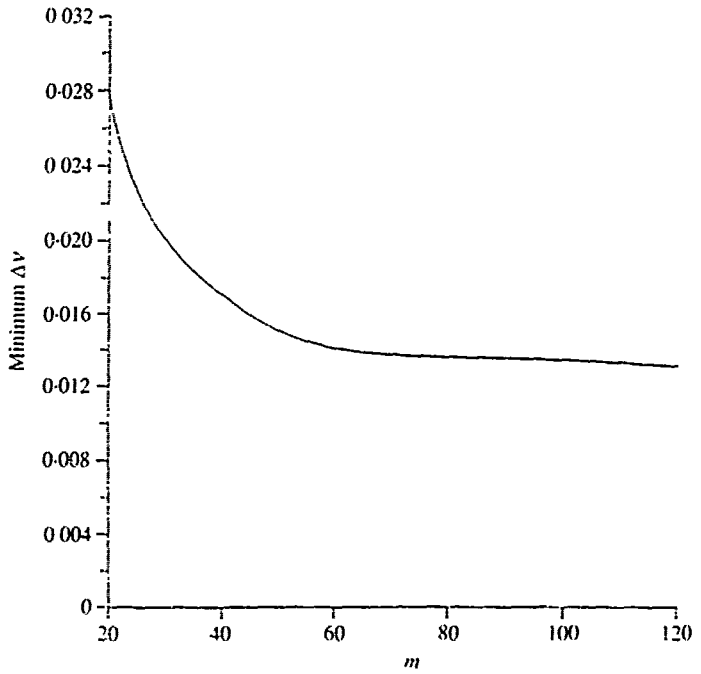

FIGURE 7. Dependence of the minimum $\Delta\nu$ on m, with $\Delta\mu = 0{\cdot}004$.

where $1 \leqslant i \leqslant I-1$ and $1 \leqslant j \leqslant J-1$.

$$P \to i\epsilon_{\psi}, \quad T \to \epsilon_{\nu}.$$

$$a_1 = \frac{H_2}{m}, \quad a_2 = \frac{G_2}{m}, \quad a_3 = \frac{1}{mH_1}\left(\frac{\omega^2}{A^2} - m^2 H_1\right).$$

$$b_1 = -\frac{H_1}{m}, \quad b_2 = -\frac{G_1}{m}, \quad b_3 = -\frac{1}{mH_2}\frac{\omega^2}{A^2}, \quad b_4 = -\frac{1}{m}.$$

$$G_1 = \frac{\hat{c}H_1}{\hat{c}\mu}, \quad G_2 = \frac{\hat{c}H_2}{\hat{c}\mu}.$$

$$X_{\mu} = \frac{\hat{c}X}{\hat{c}\mu}, \quad X_{\nu} = \frac{\hat{c}X}{\hat{c}\nu}, \quad X = P, T, a_1, a_2, a_3.$$

Methods are adopted to establish the stability conditions of the finite difference scheme numerically. The Fourier method (Potter 1972) is first used to examine parametrically the stability conditions of the designed numerical scheme. These conditions are then incorporated by applying the matrix method (Ames 1977). This method is used to exemplify the validity of these stability conditions. Since the designed algorithm is effective for a parametric study of the stability conditions, the optimum parameters, which can increase the accuracy of the numerical solution, can be determined together with the stability analysis. For instance, considering the case of longitudinal mode number $m = 100$, we find that the stability conditions of both methods are satisfied for $\Delta\mu = 0{\cdot}004$ and $\Delta\nu \geqslant 0{\cdot}01334$. Hence the minimum $\Delta\nu = 0{\cdot}01334$ is used in the numerical analysis. The numerical programs for the coupled equations (2) and (3) and the stability analysis have been executed on the Cray X-MP/48 of the Pittsburgh Supercomputing Center.

Using the same procedure to perform the stability analysis for different m values, the dependence of the minimum $\Delta\nu$ on m can be determined. The result is shown in figure 7, which shows that the minimum $\Delta\nu$ decreases rapidly with m for $20 \leqslant m \leqslant 40$ and approach a constant value for $m > 40$. Since the minimum $\Delta\nu$ is smaller for larger m, the numerical solution is expected to achieve better accuracy for the case of layer m.

REFERENCES

Ames, W. F. 1977 *Numerical Methods for Partial Differential Equations*, p. 56. Academic.

Chen, L. & Cowley, S. C. 1989 *Geophys. Res. Lett.* **16**, 895.

Chen, L. & Hasegawa, A. 1974 *J. Geophys. Res.* **79**, 1024 and 1033.

Cheng, C. Z. & Lin, C. S. 1987 *Geophys. Res. Lett.* **14**, 884.

Dungey, J. W. 1954 *Electrodynamics of the Outer Atmosphere, Scientific Report* 69. *Pennsylvania State University.*

Fennel, J. F. 1982 *The IMS Source Book, Guide to the International Magnetospheric Study Data Analysis* (ed. C. T. Russel & D. J. Southwood), p. 65. American Geophysical Union.

Grobb, R. N. 1975 *NOAA Technical Memorandum* SEL-42. *Space Environment Laboratory. National Oceanic and Atmospheric Administration*, Boulder.

Hasegawa, A. 1969 *Phys. Fluids.* **12**, 2642.

Hasegawa, A. 1971 *Phys. Rev. Lett.* **27**, 11.

Knott, K 1982 *The IMS Source Book, Guide to the International Magnetospheric Study Data Analysis* (ed. C. T. Russel & D. J. Southwood), p. 43. American Geophysical Union.

Kuo, S. P., Lee, M. C & Wolfe, A. 1987 *J. Plasma Phys.* **38**, 235.

Ng, P. H., Patel, V. L. & Chan, S. 1984 *J. Geophys. Res.* **89**, 10763.

Potter, D. 1972 *Computational Physics*, p. 13. Wiley-Interscience.

Radoski, H. 1967 *J. Geophys. Res.* **72**, 418.

Radoski, H. 1974 *J. Geophys. Res.* **79**, 595.

Radoski, H. 1976 *Hydromagnetic Waves, Temporal Development of Coupled Modes*. AFGL-TR-76-0104.

Southwood, D. J. 1976 *J. Geophys. Res.* **81**, 3340.

Takahashi, K., Fennel, J. F., Arnata, E. & Higbie, P. R. 1987 *J. Geophys. Res.* **92**, 5857.

Takahashi, K., Higbie, P. R. & Baber, D. N. 1985 *J. Geophys. Res.* **90**, 1473.

Walker, A. D. M., Greenwald, R., Korth, A. & Kremser, G. 1982 *J. Geophys. Res.* **87**, 9135.